The Development of Subsynoptic and Mesoscale Cyclones in a Tornado Outbreak

by
Joseph A. Rogash

Department of Atmospheric Science
Colorado State University
Fort Collins, Colorado

December 1982

Colorado State University

Department of Atmospheric Science

Paper No. 362

THE DEVELOPMENT OF SUBSYNOPTIC AND MESOSCALE CYCLONES IN A TORNADO OUTBREAK

by

Joseph A. Rogash

Atmospheric Science Department

Colorado State University

Fort Collins, Colorado

December 1982

Atmospheric Science Paper No. 362

ABSTRACT

On May 2, 1979, a small tornado outbreak occurred in northwest Oklahoma. Remote sensing instruments revealed that these intense cyclonic disturbances developed within counterclockwise rotating systems a scale of magnitude larger, mesocyclones. In turn, the mesocyclones evolved within a frontal wave or subsynoptic low pressure system.

By combining surface, satellite, radar, and photographic data each scale of cyclone is investigated with emphasis on determining mechanisms by which they intensify or evolve, especially through scale interactions. Since cyclonic disturbances have anomalously low pressure and positive relative vorticity, intensification mechanisms are defined as those factors which contribute to falling pressures and positive vorticity production.

The subsynoptic scale low had negative vorticity advection or neutral advection superimposed at mid-levels during the morning and afternoon hours, yet it experienced falling pressures and an increase in circulation. Using satellite and surface data it was determined that localized warm advection and solar heating were the primary mechanisms for this wave cyclone's intensification.

Convergence within the subsynoptic low triggered convective cells in the potentially unstable air mass occupying its southeast quadrant. It is surmised that the resulting updrafts converged the large ambient vorticity already existing within the frontal wave plus tilted

horizontal vortex tubes formed by the ambient shear into the vertical. Vorticity production rates from these processes are estimated to be sufficient to produce mesocyclones.

Finally, the mesocyclones produced tornados after they became two celled structures with the circulation cores divided between an updraft and rear flank downdraft. Photographs of one of the tornados show that tornadogenesis occurred within the portion of the updraft almost immediately bounded by a downdraft. Doppler radar shows that vorticity and convergence have maximum values within the mesocyclone at the updraft-downdraft interface making this sector a favorable zone for tornado production.

The results of this study should prove useful for severe weather forecasting in that it stresses more attention being placed on localized lower tropospheric warming as a factor which will strengthen sub-synoptic lows despite an absence of favorable dynamical features such as 500 mb positive vorticity advection. A quantitative method of determining the potential of mesocyclogenesis within the subsynoptic low is also introduced.

ACKNOWLEDGEMENTS

The author would like to express deep appreciation to Dr. Thomas H. Vonder Haar for both his advice and guidance throughout this project. The input provided by Dr. Richard Johnson concerning mesoscale dynamics is also deeply appreciated. The author also wishes to thank Dr. David Krueger for his review of the manuscript.

The author are extremely grateful to John Weaver of NOAA-NESS for his assistance and instruction in mesoscale weather analyses and severe local storm nowcasting. James Purdom of NOAA-NESS and Andrew Negri of the Goddard Space Flight Center provided valuable satellite data. Edward Brandes of the National Severe Storms Laboratory provided the Doppler wind data. Invaluable assistance was also rendered by Ms. Judy Sorbie for her meticulous drafting of the many figures in this project, Dwayne Barnhart for the intricate photograhic processing that was required, and Ms. Robin Wilson for her expert typing. And finally, Dr. Howard Bluestein supplied photographs of the Onienta tornado.

This research was supported by the National Science Foundation under grant number ATM-7918513.

TABLE OF CONTENTS

LIST OF TABLES

LIST OF FIGURES

Page

LIST OF FIGURES (cont'd)

LIST OF FIGURES (cont'd)

LIST OF FIGURES (cont'd)

Page

CHAPTER I

INTRODUCTION

Cyclonically rotating low pressure disturbances are associated with adverse weather phenomena such as destructive winds, hail, and floods. These systems however may have at least three orders of magnitude of size and circulation such that smaller scales of cyclones are embedded within the larger ones.

This is best demonstrated during a tornado outbreak. The tornado is an example of the atmosphere's most concentrated and destructive cyclonically rotating low pressure area (although a tiny fraction spin anticyclonically). Major tornadoes usually form within rotating thunderstorms an order of magnitude larger but not as intense. Such thunderstorms have been classified as mesocyclones (Fujita, 1963).* In turn, mesocyclones commonly originate in warm sectors of baroclinic low pressure fontal wave cyclones.

It has long been observed that smaller scale cyclones can be embedded within those of a larger scale but past studies have dealt mainly with the characteristics of the individual disturbances. Petterson (1956) and Palmen and Newton (1969) are among many scientists

---

*Orlanski (1975) categorizes certain horizontal scales of weather systems as meso γ (2-20 km), meso β (20-200 km), and meso α (200-2000~km). For this project mesoscale will refer to meso γ sized features such as rotating thunderstorms. References to the synoptic or sub-synoptic scale will include features with horizontal dimensions greater than 100 km.

who have described the three dimensional structure and genesis of synoptic scale cylcones. The recent advances in multiple Doppler radar has allowed severe weather research scientists to obtain much information on the airflow and structure of the mesocyclone (Brandes, 1977, 1978, 1981, Heymsfield, 1978). Using advanced photogrametric techniques, Golden and Purcel (1978) and Forbes (1978) have discovered important circulation characteristics of the tornado.

Though there have been attempts to explain the interaction between the mesoscale and tornado scale (Barnes, 1978b; Forbes, 1978; Brandes, 1977, Lemon and Doswell, 1979), less effort has been made in determining how the synoptic scale environment can influence mesoscyclogenesis. Specifically, quantitative methods are lacking which could specify if a region will be conducive to convection which will develop large rotating updrafts.

Some deficiencies also remain in the investigation of smaller frontal wave cyclones. These so-called subsynoptic low pressure systems (SSL) were investigated by Tetgmeir (1974) who found them to often be associated with severe storms. These systems, usually between 80 and 200 miles in diameter, have been connected with tornado outbreaks which occur in short narrow paths instead of broad areas (Moller, 1979). Thus the severe weather associated with these lows are especially difficult to forecast. Yet, little research has been done on the intensification mechanisms of the SSL outside of that done by Tetgmeir. He attributed SSL deepening to mid-level positive vorticity advection associated with an approaching short wave trough.

With these problems in mind this project analyzed a tornado outbreak which occurred in northwest Oklahoma on May 2, 1979. During

the afternoon a SSL developed near the intersection of a stationary front and dry line despite an absence of supporting upper tropospheric dynamics. At least three mesocyclones evolved within the warm sector which were to produce hail, straight line wind damage and tornadoes, one of which had an F-4 (Fujita 1973) intensity (Figure 1.1). Because this occurred during the Severe Environmental Storms and Mesoscale Experiment (SESAME), rapid scan satellite images, multiple Doppler radar, aircraft, and special photographic teams monitored mesoscale and tornado scale aspects of the storms. Thus a rare opportunity was afforded to observe the subsynoptic low, the mesoscylones embedded within it, and the resulting tornadoes.

In observing the development of the different scales of cyclones, the following objectives were accomplished:

1. Determining the mechanism responsible for the development of the SSL;
2. Investigating the role of the SSL in triggering convection;
3. Examining factors within the environment of the SSL which will encourage mesocyclongesis;
4. Observing and analyzing the growth and structure of the mesocyclones, especially during the tornadic phase.

To complete this study characteristics of the tornadoes will be briefly described. It is ultimately hoped that the results of this project will prove useful in improving severe weather nowcasting as well as explain some of the dependencies smaller cyclones have on the larger ones in which they are embedded.

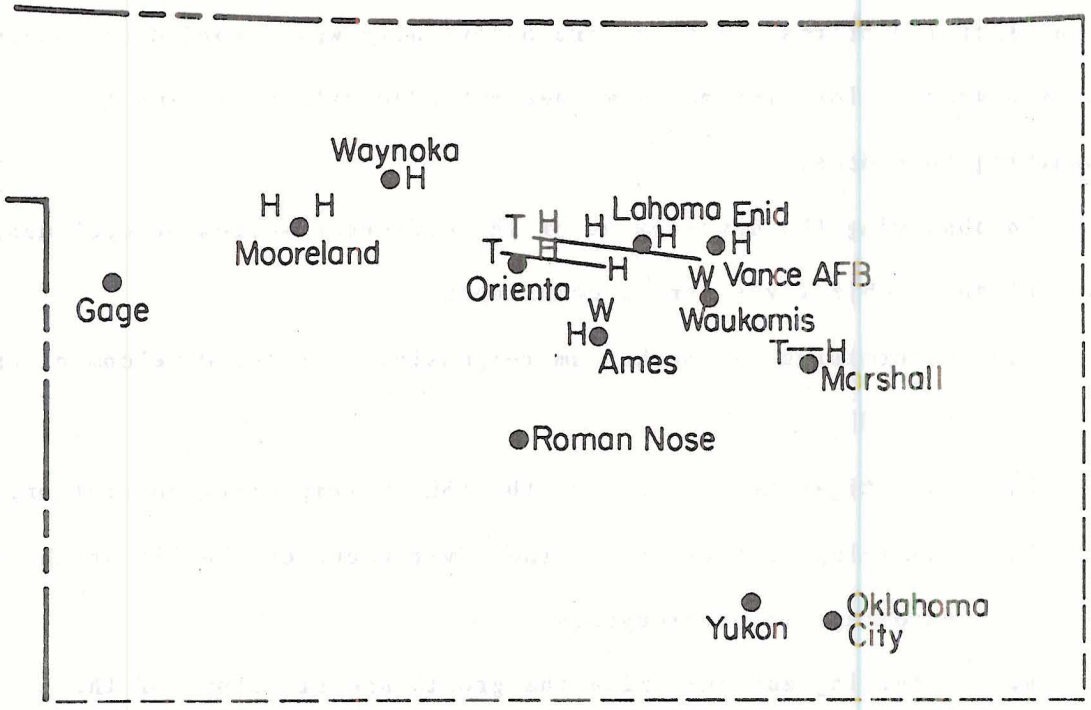

Figure 1.1. Map of Oklahoma showing severe weather events for May 2, 1979 from 2100Z to 2345Z. H designates large hail, W damaging straight line winds and T tornado. Paths of tornados are also given.

CHAPTER II

A BRIEF REVIEW OF THREE SCALES OF CYCLONIC DISTURBANCES

The subsynoptic low, mesocyclone and tornado have important differences and similarities both in structure and in the dynamics of genesis and intensification. It is important to understand the properties of each of these scales of cyclones so to first become aware of factors conducive to their growth and second, to help determine how smaller scale cyclones are dependent upon the larger ones in which they are are embedded.

2.1 Positive Vorticity and Low Pressure

Significant cyclonic disturbances, whether they be synoptic scale, mesoscale, or tornadic scale are distinguished by counterclockwise wind flow (for the northern hemisphere) and anomalously low-pressure. Thus, to predict genesis or intensification, mechanisms responsible for vorticity generation or pressure falls must be detected and analyzed. A general equation for the production of the vertical component of vorticity that includes diffusion by vorticity by either boundary layer or cloud processes is given by:

$$\frac{d\xi}{dt} = \underbrace{-\underset{\sim}{V} \cdot \nabla f}_{A} \underbrace{-(\xi+f)\nabla \cdot \underset{\sim}{V}}_{B} + \underbrace{\frac{\partial w}{\partial y}\frac{\partial u}{\partial z} - \frac{\partial w}{\partial x}\frac{\partial v}{\partial z}}_{C}$$

$$+ \underbrace{\frac{1}{\rho^2}\left(\frac{\partial \rho}{\partial x}\frac{\partial p}{\partial y} - \frac{\partial \rho}{\partial y}\frac{\partial p}{\partial x}\right)}_{D} \underbrace{- K_H \nabla^2 \xi}_{E} \underbrace{- \frac{\partial}{\partial z}\left(K_z \frac{\partial \xi}{\partial z}\right)}_{F} \qquad (2.1.1)$$

For the above equation, $\underset{\sim}{V}$ represents the horizontal wind velocity with u and v the respective x and y components of $\underset{\sim}{V}$ with respect to a cartesian coordinate system. The letter ''f'' designates the Coriolis parameter, p the pressure and ρ the density of the atmosphere (see Appendix A). Finally, w represents the vertical velocity. Term A represents the horizontal advection of absolute vorticity. For the scales of motion in this study, ∇f is very small so that term A can be neglected. Term B represents vorticity produced by horizontal convergence. If a chain of fluid is rotating and the area enclosed by the chain is decreased, then the rate of rotation must increase much like an ice skater who increases her spin by pulling her arms inward (Holton, 1979). Term C, commonly known as the tilting term, indicates vertical vorticity production from horizontal vortex tubes tilted into the vertical by differential vertical motion (Holton, 1979), (see Figure 2.1.1). Term D, the solenoid term, shows resultant vorticity production which arises from the solenoid circulation along thermal boundaries (Petterson, 1956). Terms E and F represent vorticity production by turbulent diffusion with K_H and K_Z the horizontal and vertical eddy exchange coefficients, respectively. The form terms E and F take may depend on the horizontal scale to which 2.1.1 is applied. In subsequent sections, scaling of this equation for the various scales of phenomena under study will be given.

Mechanisms for pressure falls at the surface associated with cyclonic storms may be determined from the pressure tendency equation in the form:

$$\frac{\partial p}{\partial t} = -g\int_{\infty}^{o}\rho\nabla_H \cdot V dZ - g\int_{\infty}^{o} V \cdot \nabla_H \rho dz \qquad (2.1.2)$$

A B

Term A of Equation 2.1.2 denotes net horizontal divergence while term B is the change in pressure due to density advection. Pressure falls (rises) result if there is mass divergence (convergence) in an atmospheric column plus warm (cold) advection (Palmen and Newton, 1969). Implicit in this relation are hydrostatic changes (Austin, 1951) which cause surface pressures to decrease (increase) if there is net diabatic heating (cooling) over a specified area with respect to adjacent regions. The desert heat lows are an example of a semipermanent low pressure system caused by nonadvective diabatic heating.

The pressure tendency equation assumes a hydrostatic atmosphere. For smaller scale disturbances, such as mesocyclones associated with rotating thunderstorms, nonhydrostatic, i.e., dynamic, processes also contribute to falling barometers. For example, dynamic pressure effects can result from an accelerating updraft interacting with the ambient wind flow (Alberty, 1969). These nonhydrostatic factors play an important role in updraft enhancement and storm propagation and may result in surface pressure perturbations of several mb's. (Newton, 1963; Barnes, 1970).

2.2 The Synoptic Scale Baroclinic Low

Baroclinic disturbances, as addressed here, are hydrostatic quasi-geostrophic weather systems ranging in size from the SSL to larger heavy precipitation producing winter cyclones. Since they are baroclinic they are most common along thermal boundaries such as fronts.

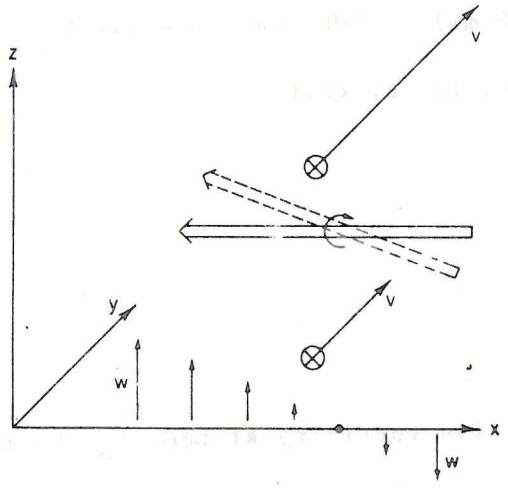

Figure 2.1. Vorticity generation by the tilting of a horizontal vorticity vector (double arrow).

Scale analyses of the vorticity equation (assuming no deep convection) for this scale of cyclone leaves only the divergence and advective terms (Petterson, 1956).

$$\frac{\partial \xi}{\partial t} = \underset{\sim}{V} \cdot \nabla(\xi + f) - \nabla \cdot \underset{\sim}{V}(\xi + f) \tag{2.2.1}$$

At the level of nondivergence (LND) this equation reduces to

$$\frac{\partial \xi_L}{\partial t} = -\underset{\sim}{V}_L \cdot \nabla(\xi_L + f) \tag{2.2.2}$$

where $\underset{\sim}{V}_L$ is the horizontal wind velocity at LND. If $\underset{\sim}{V}_o$ is the horizontal wind near the surface and $\underset{\sim}{V}_T$ is the thermal wind from near the surface (or 1000 mb) to LND, we may write $\underset{\sim}{V}_L = \underset{\sim}{V}_o + \underset{\sim}{V}_T$. This expression enables us to say that

$\xi_L = \xi_o + \xi_T$ and

$$\frac{\partial \xi_L}{\partial t} = \frac{\partial \xi_o}{\partial t} + \frac{\partial \xi_T}{\partial t} \tag{2.2.3}$$

where ξ_L is the relative vorticity at LND, ξ_o the relative vorticity near the surface, and ξ_T the vorticity from the thermal wind.

By the thermal wind relation (Holton, 1979)

$$u_T = \frac{-g}{f} \frac{\partial Z}{\partial y} \ln \frac{p_o}{p_L} \text{ and } v_T = \frac{g}{f} \frac{\partial Z}{\partial y} \ln \frac{p_o}{p_L}.$$

Z represents the thickness in meters between the surface pressure p_o and the pressure at LND p_L. Therefore,

$$\xi_T = \frac{\partial v_T}{\partial y} - \frac{\partial u_T}{\partial x} = \frac{g}{f} \nabla^2 Z \text{ and } \frac{\partial \xi_T}{\partial t} = \frac{g}{f} \nabla^2 \frac{\partial Z}{\partial t}$$

By the first law of thermodynamics

$$\frac{\partial \bar{T}}{\partial t} = \overline{-\underset{\sim}{V}} \cdot \nabla \bar{T} + \left[\overline{\Gamma_a} - \Gamma\right]\bar{\omega} + \frac{1}{C_p}\frac{\partial h}{\partial t}$$

For the above relation $\bar{T}$ is the mean temperature of a tropospheric layer, Γ_a is the dry adiabotic lapse rate with respect to pressure, $\bar{\omega}$ the mean vertical motion (dp/dt) of the layer, C_p the specific heat of dry air at a constant pressure (1004 $J^{o}K^{-1}kg^{-1}$) and h the diabatic heating. By the thickness equation $\bar{T} = \frac{g}{R} Z \ln \frac{p_o}{p_L}$ between the surface and LND where g is the accelleration due to gravity and R is the gas constant for dry air (287 $J^{o}K^{-1}kg^{-1}$).

Therefore,

$$\frac{\partial \xi_T}{\partial t} = \nabla^2\left[\frac{g}{R} A_T + \ln \frac{p_o}{p_L}\left[\omega\overline{\Gamma_a} - \Gamma\right] + \frac{1}{C_p}\frac{d\bar{h}}{dt}\right]$$

Substituting this relation into equation 2.2.3 we have an expression for vorticity production near the surface (Petterson, 1956).

$$\frac{\partial \xi_o}{\partial t} = -(\xi_o + f)\nabla \cdot \underset{\sim}{V}_o - \underset{\sim}{V}_o \nabla(\xi + f) =$$

$$A_Q - \underset{\sim}{V}_o \nabla(\xi_o + f) - \frac{R}{f}\nabla^2(A_T + S + H) \qquad (2.2.4)$$

A_Q is the vorticity advection at LND which is often taken to be between 500 and 600 mb. The expression $V_o \nabla(\xi + f)$ is the vorticity advection near the surface. It is usually very small and can be neglected. A_T is the thickness advection between the surface and LND. Since thermal advection diminishes toward the midtropophere, A_T is mainly a result of thermal advection in the lower layers of the atmosphere (Palmen and Newton, 1969).

In 2.2.3, $H = \log \frac{p_o}{p} \frac{1}{C_p} \frac{\partial \bar{h}}{\partial t}$ where $\bar{h}$ represents diabatic heating of the atmosphere. An example of this is when cold polar air in winter moves over warmer ocean water so that it is heated from below. $S = \log \frac{p_o}{p_L} \bar{\omega} (\overline{\Gamma_a - \Gamma})$. This stability or buoyancy term represents adiabatic temperature changes due to vertical motion.

Although these terms cannot be accurately evaluated for smaller scales such as that in this case study, qualitative features related to this equation can be very useful to a forecaster. For example, 500 mb positive vorticity advection is often a reliable indicator of surface cyclonic vorticity spin up. Similarly, heating effects must be taken into account. A body of land which is warmed relative to surrounding areas will experience an increase in vorticity as its pressure falls and air converges toward its center (like a desert heat low). One can also assume over land that the lower troposphere will acquire greater amounts of diabatic heating from solar radiation in an area of clear skies as opposed to a cloud covered region and thus experience an increase in circulation provided there will be an absence of strong cold advection. The thickness advection likewise implies that an intrusion of warmer air into a cooler environment either encourages surface cyclogenesis or maintains an already existing storm system. Thus the development of such low pressure areas is most favorable when mid-level PVA (positive vorticity advection) becomes superimposed over a baroclinic boundary such as a front and moves toward a region of warm advection and/or warm surface temperature. Note that vorticity generation is dependent on the Laplacian of warm advection and heating. These elements should occur in a localized or relatively narrow zone.

Term S, the stability factor, represents vorticity changes due to the adiabatic cooling caused by the vertical motion ω. Since vertical motion is upward ($\omega < 0$) ahead of cyclonic storms and since the atmosphere is almost always stable ($\Gamma_a > \Gamma$), this term tends to oppose vorticity production. In other words, while heating and warm advection contribute to vorticity increases, the resultant vertical motion associated with term S causes adiabatic cooling which partially offsets the advective and diabatic warming. High moisture contents may counteract some of this cooling as greater amounts of latent heat will be released through condensation. This explains why the strongest cyclones have air with high dewpoints in their warm sectors.

From the above discussion it becomes apparent that vorticity production and falling pressures are related to one another for lower tropospheric synoptic cyclones. Both are highly dependent on advective and diabatic heating processes. Divergence, an important mechanism for pressure falls, also correlates to regions of strong mid level PVA (Palmen and Newton, 1969). Usually, with the approach of a 500 mb trough, there is PVA, upper tropospheric divergence, and because of Dines compensation, ascending motion to about 200 mb. It is this divergence with a resulting lowering of the tropopause (Petterson, 1956) which contributes to surface pressure falls.

Relevant to this case study is the difference between warm and cold core lows. Briefly, extratropical cold core lows become more intense with height above the ground and thus are associated with strong 500 mb mid-level PVA and upper tropospheric divergence (Petterson, 1956). Most of the large scale severe weather outbreaks are associated with such dynamically intense systems. Warm core extratropical lows are most

intense near the surface and diminish in strength with height. Usually there is little evidence of their existence above 700 mb. Since they are caused by differential heating, the resultant thickness changes do result in divergence aloft and pressure falls. Often, these systems occur over relatively small areas such that the weak divergence cannot be detected through rawinsondes. Lacking strong mid level PVA, these lows are considerably less intense than cold core ones and thus, are often overlooked as severe weather producers by forecasters.

2.3 The Mesocyclone

Brooks (1949) described a low pressure area associated with tornadoes which is an order of magnitude larger than the tornado but at least an order of magnitude smaller than the synoptic scale cyclone. Such a phenomena has since been defined the mesocyclone or tornadocyclone. At the present the former usually refers to any severe cyclonically rotating thunderstorm while the latter is applied to a mesocyclone which produces a tornado.

Under certain conditions (discussed in section 4) supercell thunderstorms evolve from weaker convective activity in which they consist one large updraft up to 10 km in diameter which may attain maximum vertical velocities of over 40 m sec^{-1} near their centers or cores (Marwitz, 1972). These updrafts frequently develop cyclonic rotation and thus become mesocylones (Lemon and Doswell, 1979). A favored location for such storms is at thermal boundary intersections (Magor, 1959; Miller, 1972; Maddox, et al., 1979), such as an old squall line and a warm front, and near the location of the low level jet (Bonner, 1966). The mesocyclone initially spins up in the sector of the moist potentially unstable air. Besides causing flash flooding, hail,

and destructive straight lined winds (Burgess, 1976), mesocyclones are associated with most significant tornadoes (Lemon and Doswell, 1979).

Figure 2.3-1, taken from Lemon and Doswell (1979), summarizes the evolution of a mesocyclone. As the rotating updraft intensifies, dry air at mid levels (Figure 2.3-1a) intrudes into the boundary of its rear flank where it entrains precipitation particles, cools, and sinks to the surface (Figure 2.3-1b). This cooler air forms a small cold front or outflow boundary on the rear flank of the updraft while the secondary cool air downdraft often exists on the forward flank due to previously existing storms (Miller, 1972) or from rain cooled air sinking ahead of the primary updraft itself (Lemon and Doswell, 1979).

It is during the development of the rear flank downdraft that the mesocyclone undergoes a significant transition. Recent dual Doppler radar studies show conclusive evidence that the most intense and organized mesocyclones cease to become warm core updrafts but instead are transformed into two-cell structures (Brandes, 1978, 1981) with the cold rear flank downdraft cyclonically wrapping around and occluding the warm updraft (Figure 2.3-1c). Thus, despite being an order of magnitude smaller than the synoptic scale cyclone, the mesocyclone resembles it in that it consists of a sector of cyclonically turning rising warm humid air interposed in regions of cool sinking air which will eventually occlude it(Figure 2.3-1d). And it is during the two-cell structure stage that tornadoes appear to form within the larger circulation of the mesocyclone.

Vorticity production for a mesocyclone is initially very much dependent on updraft strength, and later on, both updraft and downdraft intensity and position. A vigorous updraft with a diameter of between 3

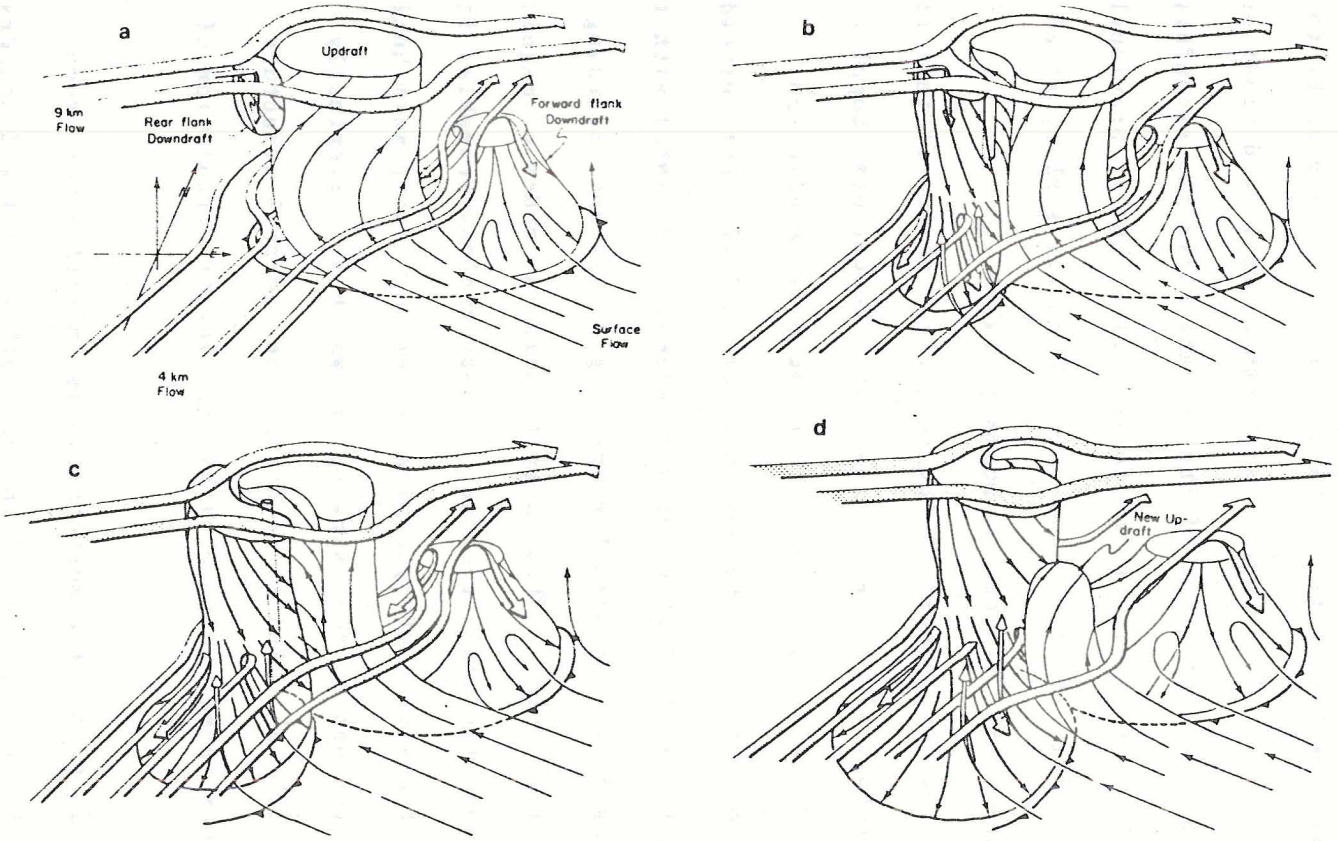

Figure 2.3-1. Schematic three-dimensional depiction of evolution of the drafts, tornado and mesocyclone in an evolving supercell storm. The stippled flow line suggesting descent of air from the 9 km stagnation point has been omitted from (c) and (d), for simplicity. Fine stippling denotes the TVS. Flow lines throughout the figure are storm relative and conceptual only, not intended to represent flux, streamlines, or trajectories. Conventional frontal symbols are used to denote outflow boundaries at the surface. Salient features are labeled on the figure.

to 10 km will tilt horizontal vortex tubes produced by low level wind shear into the vertical while the updraft further spins itself up by converging ambient vorticity as it draws surrounding air toward its center. An adjacent downdraft further accentuates these processes by increasing the vertical velocity gradient and thus intensifying the tilting effect, and by further increasing convergence as its gust front forces more air into the updraft.

Numerical model results (Wilhelmson and Klemp, 1978; Rotunno, 1981) as well as observational studies (Ray, 1976; Heymsfield, 1978; Brandes, 1978) indicate that at levels near 3 km above the ground, tilting is the dominant mechanism for thunderstorm rotation while at levels below 1 km, updraft convergence is significant if not dominant. For mesocyclone scale disturbances, the solenoidal and turbulent diffusion terms of equation 2.1.1 have been estimated to be at least two orders of magnitude smaller than the tilting and divergence terms. Solenoidal effects may become important along the boundary separating the cool downdraft induced outflow from the warm inflow (Heymsfield, 1978; Lemon and Doswell, 1979). As yet, no effective ways have been found to measure this.

Pressure fall mechanisms within the mesocyclone are both hydrostatic and dynamic. Since the updraft must be warmer than the surrounding atmosphere, pressures beneath its column should be lower in comparison to that in an adjacent undisturbed environment. Upward acceleration of air parcels in the updraft also result in dynamic pressure falls (Newton, 1963) which can be ignored for synoptic scale motions. Finally, rotation in the updraft may enhance upper tropospheric divergence (Davies-Jones and Kessler, 1974). Pressure

falls for a mesocyclone have been measured up to 9 mb near the period of tornadogenesis (Forbes, 1978).

2.4 Tornadogenesis and the Tornado

Doppler derived wind fields indicate that beginning at mid-levels within the mesocyclone core, a circulation evolves with vorticity and horizontal wind shear values of an order of 10^{-2} sec^{-1}. Such radar detected circulations are referred to as tornado vortex signatures (TVS) and designate not the actual tornado (which is too small to be detected) but that the mesocyclone has strengthened into a tornado cyclone (Brown, et al., 1978). Tornado vortex signatures are almost always located near the updraft-downdraft interface (Figure 2.3-1c) and apparently descend to the surface with the rear flank downdraft. They indicate an immediate threat of a tornado.

The key element to tornadogenesis appears to be the rear flank downdraft. Observations (Lemon, et al., 1978; Barnes, 1978a; Brandes, 1978) reveal that the strongest tornadoes coincide with the lowering of the mesocyclones rear flank downdraft to the surface. Numerical (Davies-Jones, 1982) and laboratory (Tidwell, 1982) simulations support these observations by suggesting that downdrafts with speeds 20 m sec^{-1} being adjacent to an updraft of similar magnitude greatly increase the vertical velocity gradient and shearing deformation within the mesocyclone core thus contributing to concentrated vorticity production due to tilting. As it descends, the downdraft advects this enhanced midlevel vorticity to the surface where the updraft-gust front flow fields further converge it to values of up to 10 sec^{-1} over diameters of the order of 100 m. Turbulent diffusion (Heymsfield, 1978) and solenoidal effects (Bluestein, personal communication) could also play

an important role in vorticity production on the tornado scale. In addition, since tornadoes are not always vertical, production of vorticity in the horizontal can be significant and equation 2.1.1 may be inapproporiate. As yet, no effective ways have been found to measure these parameters and the exact mechanisms of vorticity production in tornadoes is not clearly understood.

Finally, the tornado itself must be considered. No accurate pressure deficits have been measured within the tornado due to its destruction of weather instruments. However, engineering surveys of tornado structural damage plus photogrametric analysis indicate wind speeds can be over 200 M.P.H. or 100 m sec^{-1}. (Davies-Jones and Kessler, 1974).

Because of the tornado's relatively small size, Corioles effects can be neglected (Holton, 1979) and crude estimates of the tornadoes tangential velocity may be obtained by the cyclostrophic relation:

$$\frac{\partial p}{\partial r} = \frac{\rho V\theta^2}{r} \qquad (2.4.1)$$

in a Rankine vortex where:

$$V\theta = V\theta_{max} \frac{r}{r_c} \text{ for } r < r_c \qquad (2.4.2)$$

and

$$V\theta = V\theta_{MAX} \frac{r_c}{r} \text{ for } r > r_c \qquad (2.4.3)$$

(Forbes, 1978) where r_c is the radius of maximum winds and $V\theta$ is the tangential wind speed.

Pressure falls in a tornado are attributed to hydrostatic warming due to its vortex consisting of a bouyant updraft, plus a possible

secondary downward flow within the tornado core causing adiabatic compressional heating (Davies-Jones and Kessler, 1974). Mass divergence aloft may also be a contributing factor. As with vorticity production, the violent and transient nature of the tornado, combined with its relatively small size, has made it impossible to accurately determine the origins of its extremely large pressure falls.

Some tornadoes contain multiple suction vortices (Fujita, et al.; 1976, Forbes, 1978) less than 50m wide which orbit the core of the parent tornado. Such vortices account for the irregular pattern of devastation associated with some tornadoes, especially the Xenia, Ohio tornado of April 4, 1974 (Forbes, 1978).

CHAPTER III

DATA

The primary emphasis of this project was to analyze the development of three scales of cyclones which occurred on the case study day. Thus the available data were used to detect mechanisms which generate and/or intensify the cyclones, especially through pressure reduction and vorticity increase. While it was possible to obtain quantitative values of such parameters as surface temperatures advection and convergence as applied to equations 2.1.2 and 2.2.4, the problem of obtaining measurements of heating due to solar radiation is quite complex and beyond the scope of this project. Qualitatively it can be confidently stated that solar heating near the boundary layer will certainly be greater in a region of scattered clouds as opposed to regions where the skies are overcast. (See Appendix B.)

3.1 Satellite

Rapid scan three-minute images were received at the Colorado State University ground station on the case study day at one km resolution from the eastern Geostationary Operational Environmental Satellite (GOES East) (Maddox et. al., 1979). The rapid scan period coincided with mesocyclone and tornadogenesis thus providing an excellent detailed record of cloud characteristics during the storm. The data were stored on magnetic tape and subsequently navigated (Pelsen 1977) using an algorithm on the VAX (virtual address extension) Computer. A second

program on the VAX, NVPLT uses the navigation information to assign state borders on the image.

The actual pictures for the project were taken from the COMTOL graphics display system which enables a user to first display the image on a screen and then to magnify it through the ZOOM function. Since in the magnification process, much of the original picture cannot be seen on the viewing screen, the ROAM command is utilized, enabling the user to see selected portions of the image.

To determine vertical subcloud wind shear in real time, it was necessary to obtain wind vectors derived from low level cumulus cloud tracking. These vectors were provided by the Laboratory for Atmospheric Science at the Goddard Space Flight Center. Clouds were tracked for at three-minute intervals over the period of time between 2113 and 2122Z, on the case study day. Cloud vectors were selected from the total data file only if their wind speed varied by less than ten percent and their direction deviated by less than 10 degrees over the selected time interval. Detailed accounts of cloud tracking procedures and data editing for other severe weather outbreaks are described by Pelson (1977) Houghton and Wilson (1979), and Negri and Vonder Haar (1980).

Height assignments to the clouds being used were based on stereographic studies of this day (Hasler, 1981) and rawinsonde data at OKC Oklahoma City, Oklahoma (Negri and Vonder Haar, 1980) which gave cloud base elevations of 1.5 km and 1.6 km respectively (just above the convective condensation level). The former value was used since it was obtained during the earliest stages of deep convection.

3.2 Radar

Noncoherent 10 cm WSR-57 radar reflectivity data was taken this day at Oklahoma City, Oklahoma (OKC) and is used in this study to determine storm movement and intensity relative to surface weather features such as fronts. These radar echoes are composited with hourly weather station data whenever possible.

NCAR CP3 3cm Doppler radar, located at Roman Nose, Oklahoma, provides a finer detail of the storm due to its shorter wavelength and is used to observe smaller scale features such as reflectivity cores and hook or pedant echoes.

The CP3 Doppler data was combined with the National Severe Storms Laboratory (NSSL) 10.9cm Doppler radar at Yukon, Oklahoma to extract horizontal wind fields for the storm complex for the period after 2230Z. Using the Barnes (Barnes, 1974) objectives analysis techniques the field of wind vectors was interpolated over a grid with a 1 km interval between points (Brandes, 1977). Two-dimensional wind vectors are available, courtesy of N.S.S.L. at certain times for 2, 4, 6, 8, and 14 km elevations while vertical velocity fields are available (courtesy of N.S.S.L.) at 2, 8, and 14 km for 2258Z.

Using centered finite differencing (see below), fields of vorticity and divergence were calculated from the wind component at 2 km for 2258Z. The quantitative results for all kinematic and dynamical fields should not be applied too rigorously due to errors inherent in the acquisition and processing of this type of data (Brandes, 1977 and Brown, et al., 1981). Nevertheless, by accepting even the order of magnitude of the results and the qualitative nature of the wind fields, one can gain valuable information about mesocyclone structure.

3.3 Analyses of Surface Data

Unfortunately this storm system occurred north of the SESAME Portable Automated Mesonetwork (PAM) instruments in Central Oklahoma and the surface data is restricted to Service A hourly airway reports. Simularly, upper air data is based on the synoptically spaced conventional rawinsonde network which takes readings from balloons launched daily at 1200Z and 0000Z.

Certain surface or lower tropospheric meteorological parameters have proven useful in determining probability and severity of severe weather in the United States (discussed in detail in section 4).

These include:

A. Divergence,

$$D = \nabla \cdot \underset{\sim}{V}_s = \frac{\partial u}{\partial x} + \frac{\partial v}{\partial y} \qquad (3.3.1)$$

(Scoggins and Wood, 1971) B. Moisture Convergence,

$$(\nabla \cdot \underset{\sim}{V}_s q) = \frac{\partial (uq)}{\partial x} + \frac{\partial (vq)}{\partial y} \qquad (3.3.2)$$

(Negri and Vonder Haar, 1982)

C. Relative Vorticity

$$\xi = \frac{\partial v}{\partial x} - \frac{\partial u}{\partial y} \qquad (3.3.3)$$

(Weaver and Safford, 1977; Maddox, et al., 1979)

D. Synoptic Scale Vorticity production

$$\frac{d\xi}{dt} = \nabla \cdot \underset{\sim}{V}_s (\xi + f) \qquad (3.3.4)$$

(Negri, 1976, Maddox et al., 1979)

E. Lower tropospheric (including surface) warm advection

$$\underset{\sim}{V}_s \cdot \nabla_H T = u\frac{\partial T}{\partial x} + v\frac{\partial T}{\partial y} \qquad (3.3.5)$$

(Maddox and Doswell, 1982)

For the above equations, u and v are the x and y components respectively of the horizontal surface wind velocity $\underset{\sim}{V}_s$ (with respect to the Cartesian coordinate system), T is the temperature in degrees Fahrenheit, q is the surface mixing ratio and ξ is the vertical component of earth relative vorticity near the surface. Raw wind and temperature data were obtained from hourly station observations. Mixing ratios were obtained by using station dewpoints, surface elevations with respect to sea level, and skew T/log p diagrams as described in the AWS Manual 105-124 (1969).

The above parameters were calculated via a centered finite differencing method with:

$$\frac{\partial M}{\partial r} \sim \frac{\Delta M}{\Delta r}$$

where M represents any meteorological parameter and r the length in meters between data points. Applying a Barnes objective analysis technique (Barnes, 1973) to the raw weather station data, a 29 by 29 grid was interpolated with points 36 km apart. The center coordinated was latitude 35^{o}N, longitude 100^{o}W.

The weighting function which determines the influence the raw data has on values on surrounding grid points was subjectively determined by two considerations. First, objectively analyzed data were compared to actual raw input data as measured at a weather station at the same location. Second, hand calculations using only raw station data

approximated divergence and vorticity values in a given sector. These values were then compared with the computer generated fields, based on the Barnes scheme. The weighting function which produced an objectively analyzed field most compatible with values determined using only the raw data, was subsequently used. No analyzed fields are plotted along the outer 150 km of the grid perimeter due to the sparcity of raw data in these regions. Such areas lie well beyond our zone of interest however, and need not concern us meteorologically.

Finally, N.S.S.L. photographers took motion pictures of the tornado cyclone and its respective tornado (hereafter referred to as the Orienta tornado). Selected stills will be presented and important features are identified based on observations of the movie from which they were taken.

CHAPTER IV

THE OKLAHOMA TORNADIC STORMS OF MAY 2, 1979

Strongly baroclinic low pressure systems do cause most large scale tornado outbreaks. However such systems are well defined with pronounced middle and upper tropospheric PVA superimposed over a broad area of marked cyclonic flow near the surface. Thus, classical severe weather forecasting procedures are generally successful with such disturbances (Maddox and Doswell, 1982).

More understanding is needed of severe weather producing systems where there is little dynamic support aloft and weak synoptic features at the surface. As will be demonstrated in this section, such an envirement can, through certain processes in the lower troposphere, trigger convection which can become intense enough to produce tornadoes.

With the exception of Bluestein et. al., (1980), little research has been published analyzing the synoptic or mesoscale weather features on this day. Various studies have been done on the satellite observations of this storm system, including one by Hasler (1981) who used stereographic techniques to determine such features as cloud heights.

4.1 The Prestorm Environment

4.1.1 Morning Surface and Upper Air Features.

The 1200Z surface map for this day (Figure 4.1-1) depicts four distinct air masses covering the case study region. (Pressures are given in altimeter settings since these are available for all service A stations whereas conventional pressure readings are not.) In west central Texas and eastern New Mexico is a layer of warm dry continental tropical (CT) air represented by the Midland Texas (MAF) 1200Z sounding (Figure 4.1-2). Notice that high surface dewponts reported at stations within the CT air indicates it has not mixed out at the boundary layer yet.

Through central Kansas and into the Texas panhandle, a quasi-staionary front separates cool moist continental polar (CP) air to the north from warm moist maritime tropical (MT) air streaming from the Gulf of Mexico into central Texas and western Oklahoma. The 1200Z sounding (Figure 4.1-3) for Dodge City, Kansas (DDC) represents the former air mass while rawinsonde data from OKC and Stephenville, Texas (SEP) characterize the MT air (Figures 4.4-4.5).

Not so apparent, but to prove extremely important, is the fourth air mass over northeast Oklahoma including the towns of Enid (END), Ponca City (PNC) and Bartlesville (BVO). Originally MT air, it was subsequently made cooler and dryer by early morning thundershower activity (which at 1200Z is occurring at END). Notice that it is still distinctly warmer and more moist than the CP air to its north, while winds within its sector are from a southerly quadrant as opposed to northerly north of the stationary front. There should be little doubt

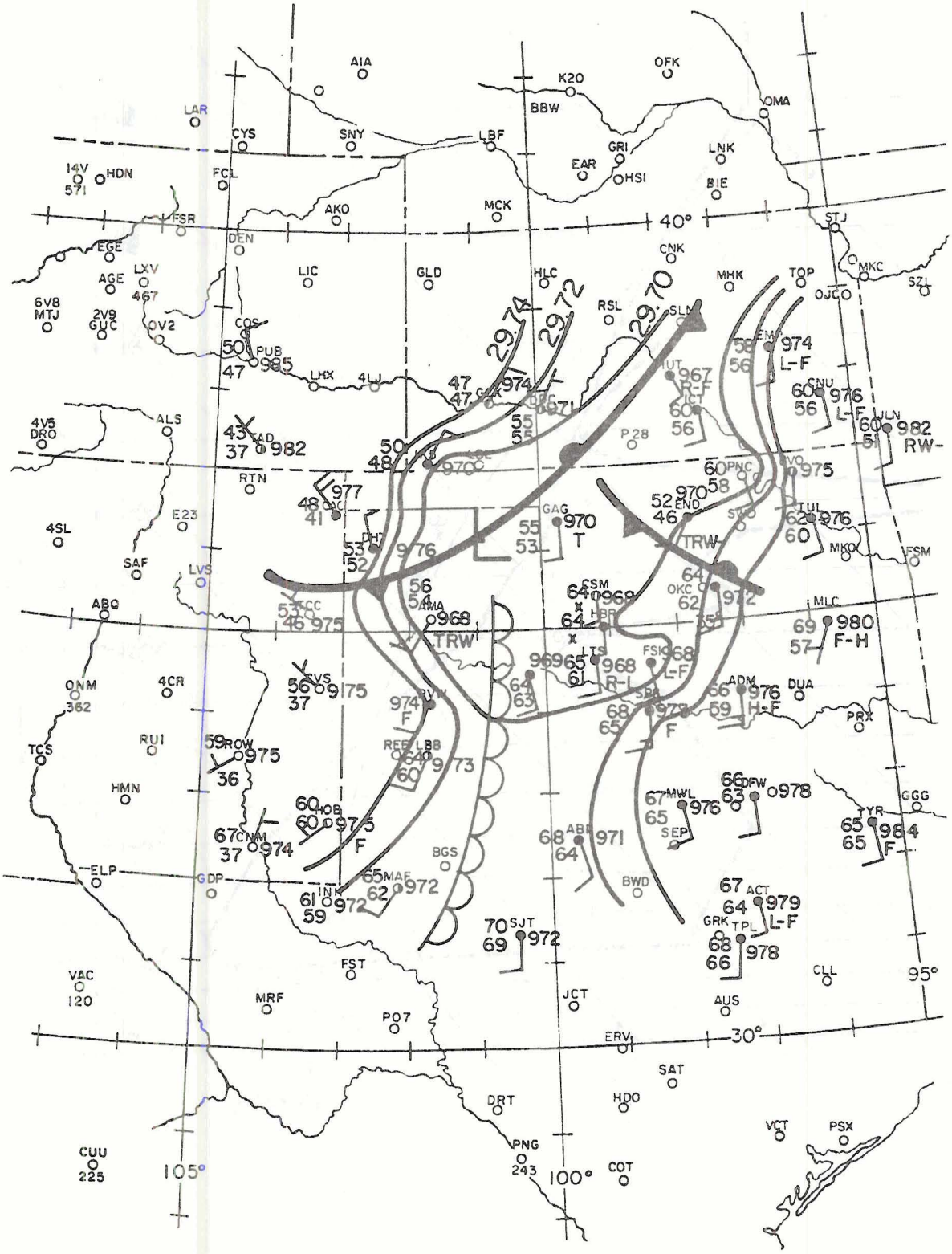

Figure 4.1-1. May 2, 1979 1200Z surface map. Pressure is in altimeter settings.

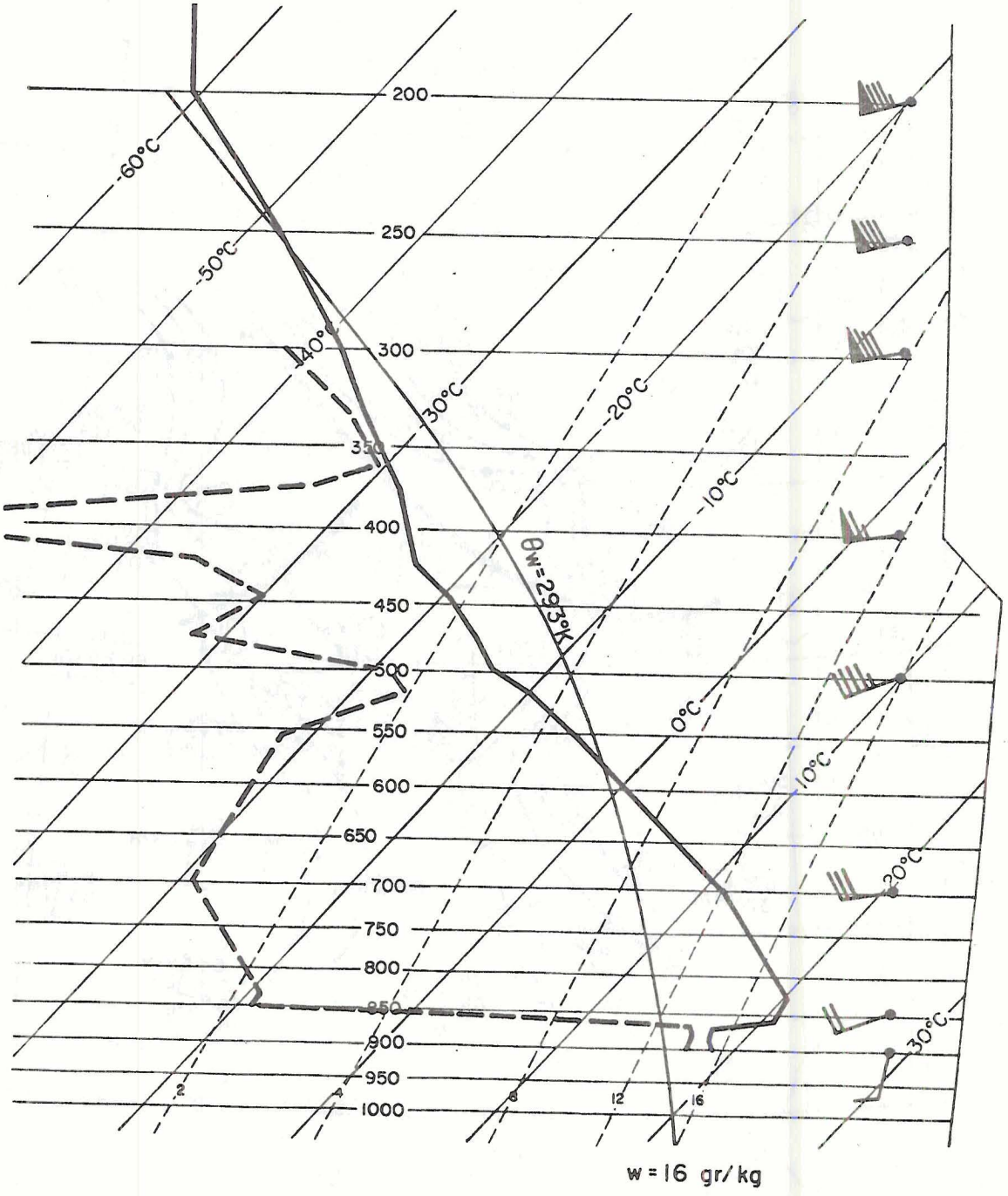

Figure 4.1-2. Midland Texas (MAF) sounding for 1200Z, May 2, 1979.

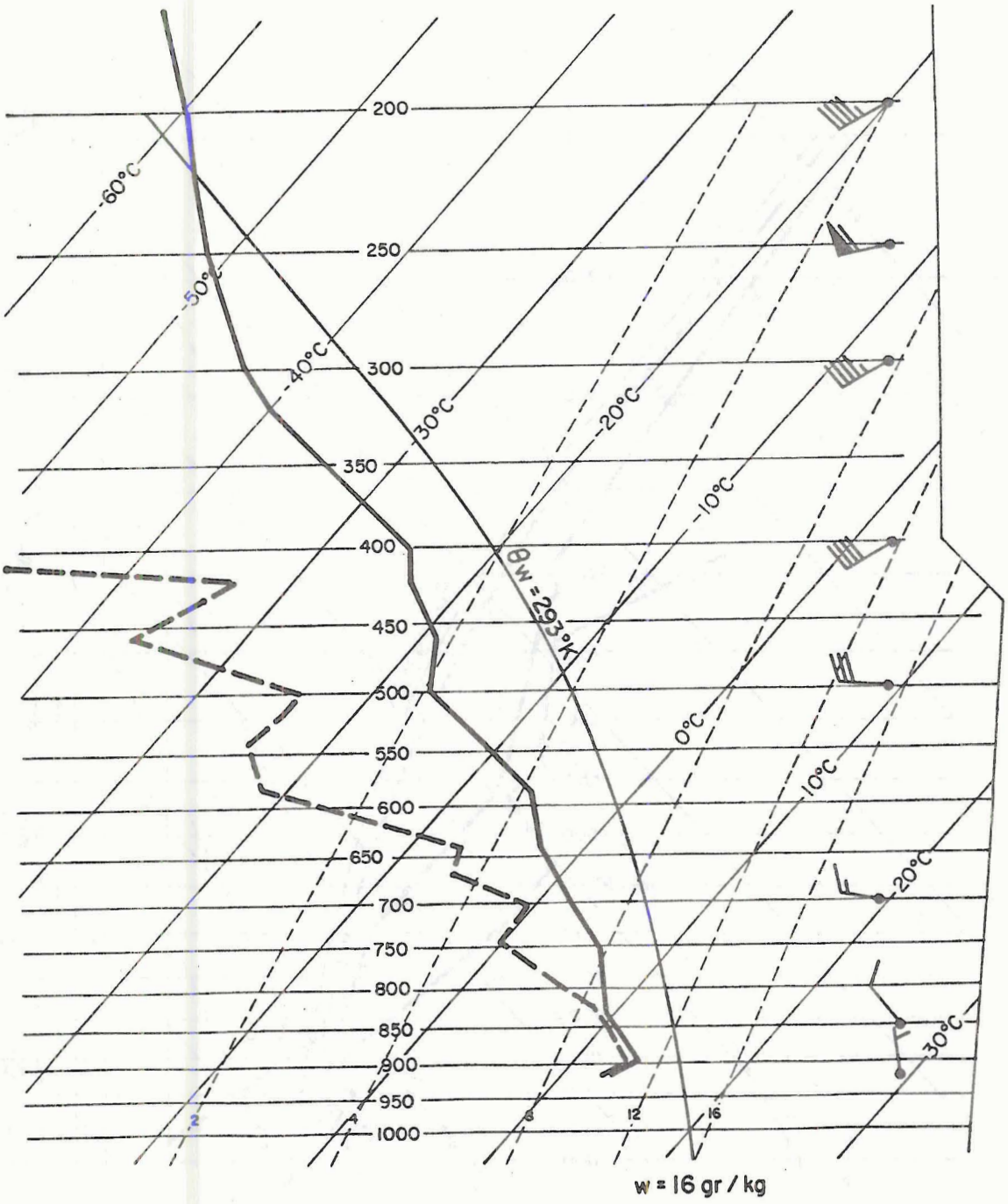

Figure 4.1-3. Dodge City Kansas (DDC) sounding for 1200Z, May 2, 1979.

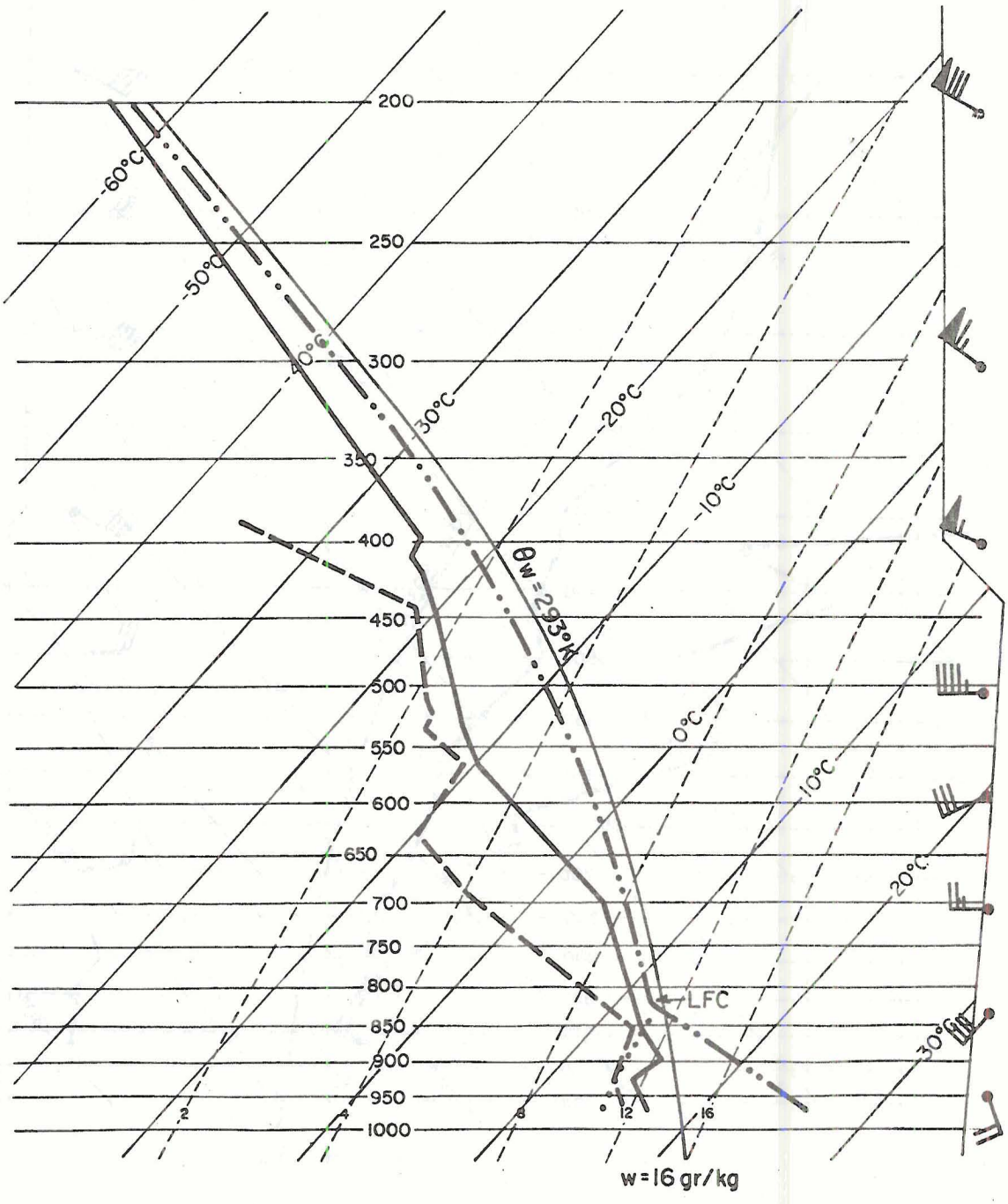

Figure 4.1-4. Oklahoma City, Oklahoma sounding for 1200Z. Parcel lapse rate is for a surface temperature of 80°F.

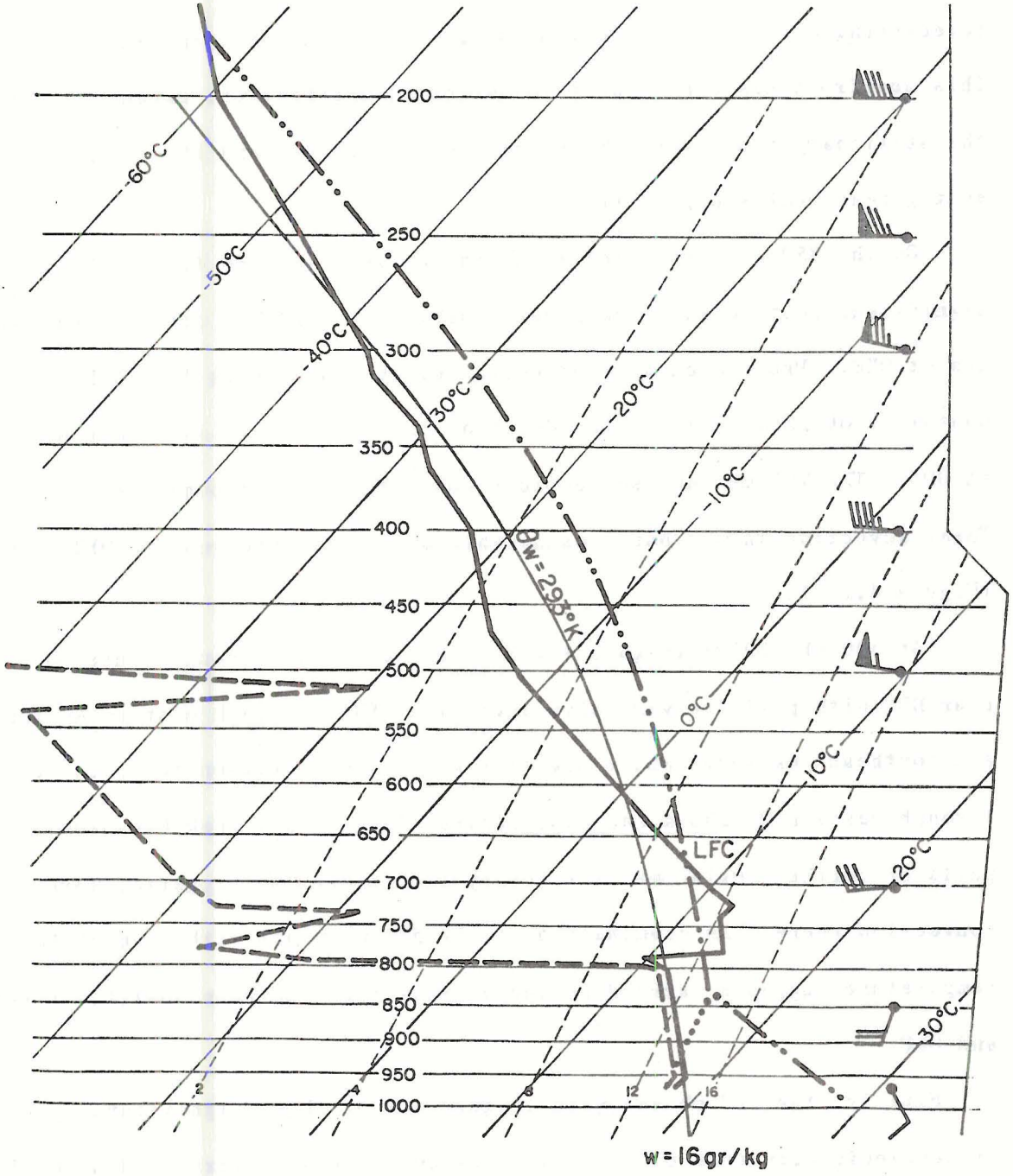

Figure 4.1-5. Stephenville Texas (SEP) sounding for 1200Z. Parcel lapse rate for surface temperature of 80°F.

to this being a distinct air mass despite no rawinsonde data taken within it and despite the fact that the National Weather Service central forecasting office in Washington, D.C. did not analyze a front for it. This mesofront has a northwest to southeast orientation, extending from the stationary front through the region between OKC and END before ending near McAlester, OK (MCK).

On the 850 mb streamline-isotherm analyses (Figure 4.1-6) the most significant feature is a low level southerly jet with a core of over 40 kts at OKC. Pronounced warm advection exists on an axis from MAF to southwest Oklahoma while cold advection is occurring in southwest Kansas at DDC. The 700 mb analyses depicts westerly winds through western Texas advecting warmer but considerably drier air into western Oklahoma (Figure 4.1-7).

At 500 mb, 1200Z (Figure 4.1-8) there is a weak trough centered near DDC with positive vorticity advection (PVA) through eastern Kansas and northeast Oklahoma while negative vorticity advection (NVA) exists through western Oklahoma and west central Texas. The weak PVA over parts of northern Oklahoma is probably the mechanism triggering morning convection there. An examination of the 500 mb winds with respect to temperature suggests warm advection at this level between Amarillo (AMA) and OKC.

Finally, the 300 mb analysis (Figure 4.1-9) shows significant anticyclonic curvature of the wind flow over northern Texas and most of Oklahoma with the isotach maximum lying to the west of the Red River region. Figure 4.1-9 also shows the position of the 850 mb low-level jet with respect to the 300 mb flow features.

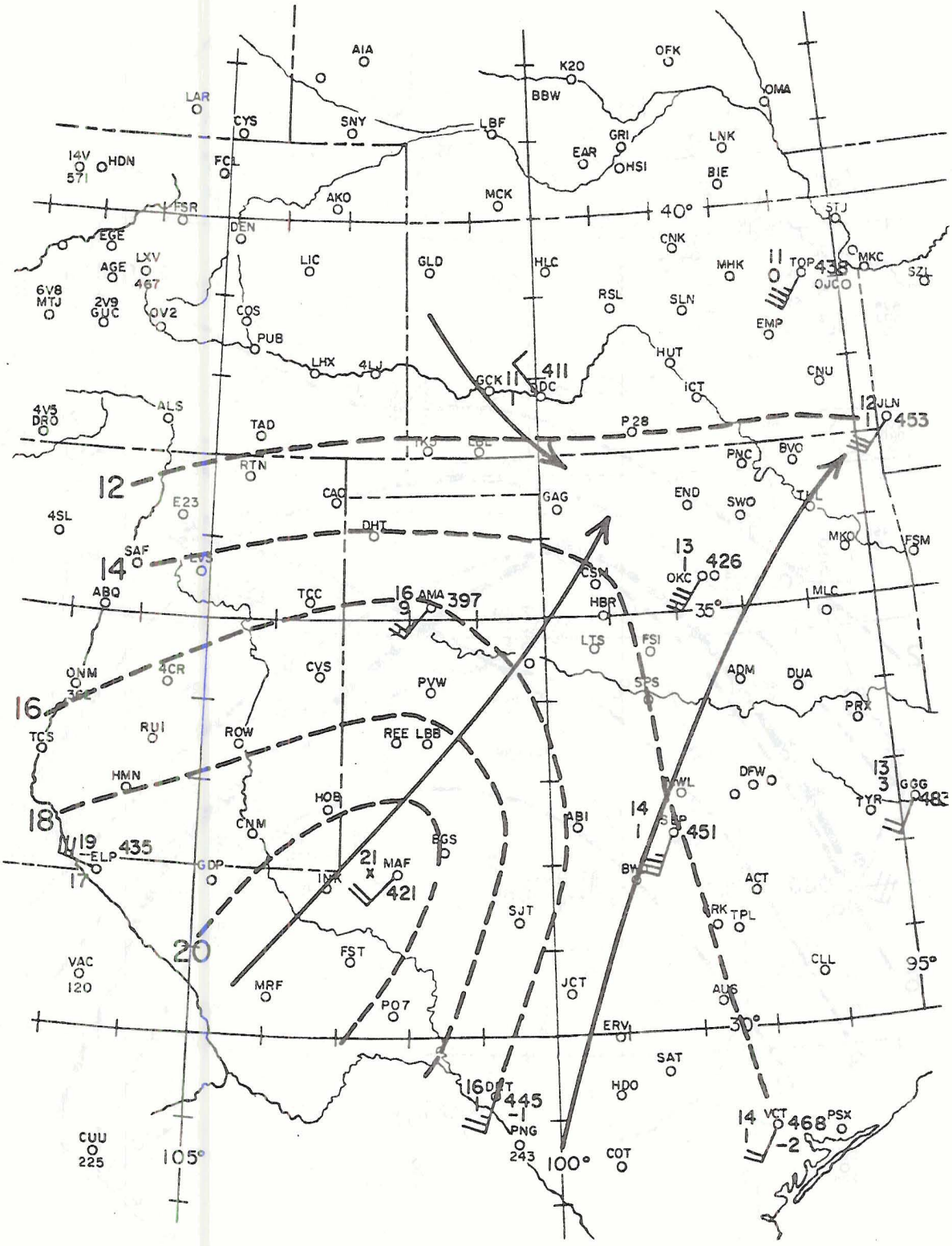

Figure 4.1-6. 1200Z 850 mb analyses. Dashed lines are isotherms for temperature in degrees C.

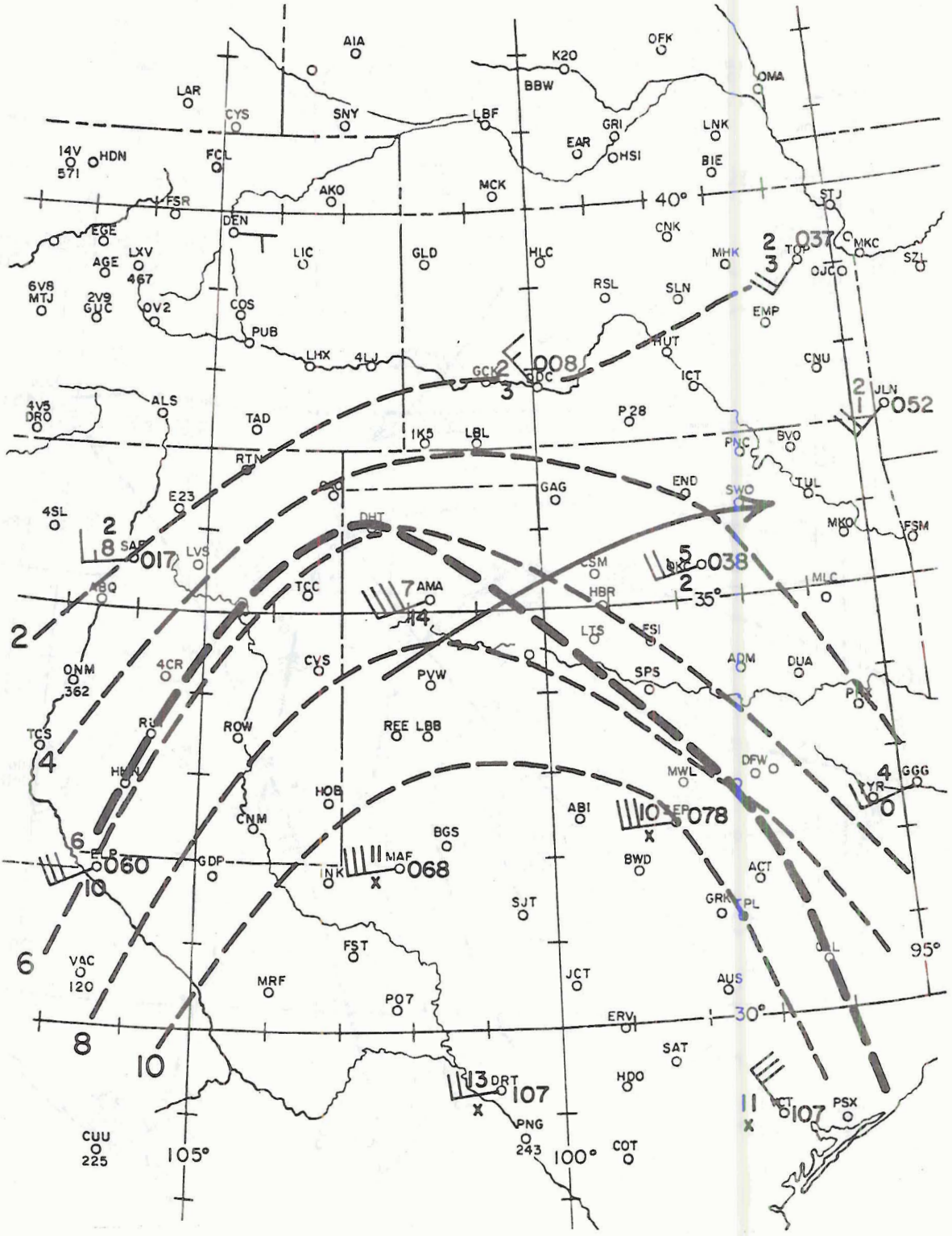

Figure 4.1-7. 1200Z 700 mb analyses. Heavy dashed line delineates regions where dewpoint depressions are greater than 10°C.

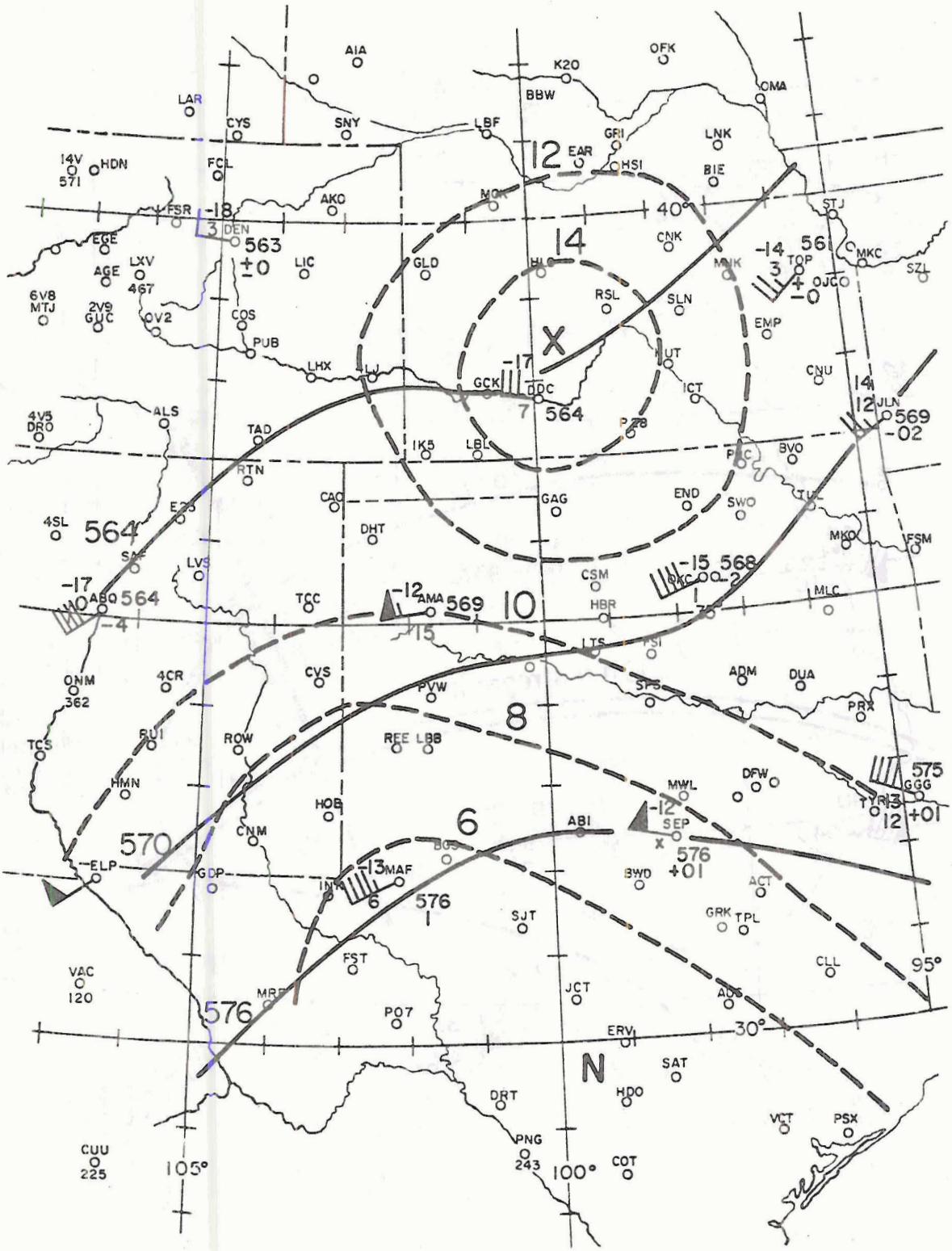

Figure 4.1-8. 1200Z 500 mb analyses. Dashed lines are absolute vorticity contours. Solid lines represent constant heights.

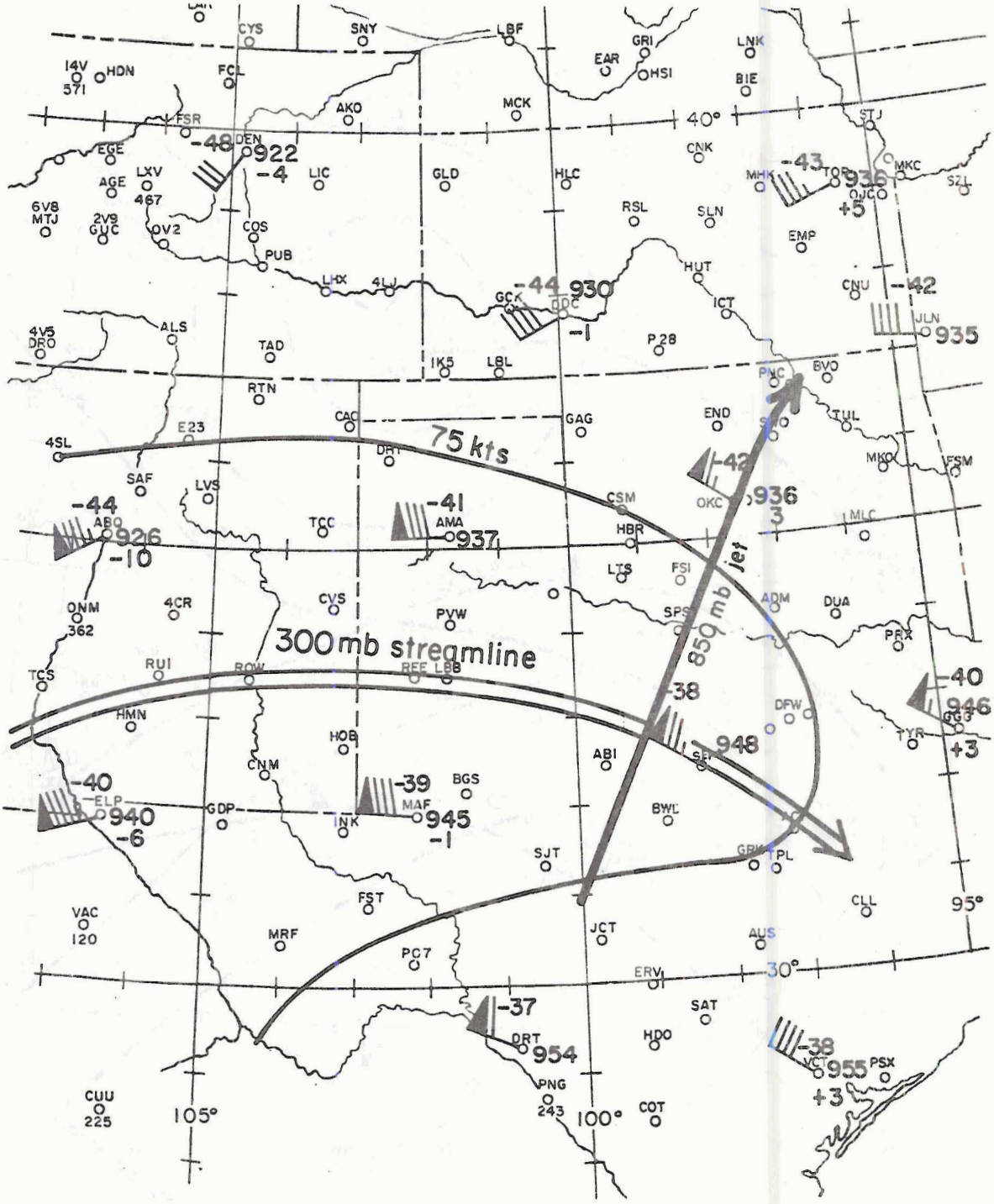

Figure 4.1-9. 1200Z 300 mb analyses showing relative position of the low level jet to the isotach maximum.

4.1.2 Thermodynamic Characteristics of the Pre-Storm Environment

What makes this particular time and place difficult for a forecaster is that while there may be thermodynamic potential instability in some areas, there is an absence of conventionally favorable dynamic or mechanical trigger mechanisms.

For example, to determine the severe weather potential for the area, the Total Totals and Severe Weather Threat (SWEAT) indexes are used (Miller, 1972) where:

$$\text{Total Totals} = 2T_{850} - 2Td_{850} - 2T_{500} \qquad (4.1.1)$$

$$\text{SWEAT} = 12T_{850} + 20(\text{TotalTotals} - 49) + 2F_8 + F_5 + 125(S + .02) \qquad (4.1.2)$$

T_{850} and T_{500} are the 850 and 500 mb temperatures, respectively (in degrees centegrade), Td is the 850 mb dewpoint depression, F_8 and F_5 are the respective 850 and 500 mb wind speeds in knots and S is the sine of the directional angle between these winds.

The Total Totals is an indicator of low-level air parcel buoyancy (and thus thunderstorm updraft strength) and considers the excess temperature of a parcel lifted from 850 through 500 mb due to both low level warmth and latent heat release. A Total Totals value of over 50 is usually a sign that the airmass is potentially unstable enough to support severe thunderstorms.

The SWEAT index not only takes into account parcel buoyancy, but low to mid level vertical wind shear which is an important ingredient

for tornadic storms (Newton, 1963). A 400 SWEAT index is considered the threshold for tornadoes.

An analyses of the 1200 Z northern Texas, Kansas, and Oklahoma soundings indicate that the MT air mass is potentially unstable enough to allow deep convection. The OKC and SEP soundings (Figures 4.1-4,5) represent this air mass with a moist layer from the surface through 850 mb and a significant directional shear between 850 and 500 mb. The Total Totals are 55 and 52 while the SWEAT index values are 517 and 496 respectively. Figures 4.1-4 and 4.1-5 also depict parcel lapse rates when they have been lifted above the level of free convection (LCL) assuming surface temperatures of 80°F. Parcel temperatures are projected to be over 6°C warmer than the surrounding environment at 500 mb indicating potentially vigorous updrafts.

The DDC sounding also indicates the air mass in that sector was potentially unstable enough to support deep convection with a Total Totals of 55. The remaining stations did not indicate nearly as much instability as the one's mentioned above (Table 4.1).

Table 4.1

Stability Indices for Selected Stations at 1200Z, May 2, 1979

	Total Totals	SWEAT
Dodge City (DDC)	55	288
Topeka (TOP)	49	230
Amarillo (AMA)	47	226
Longview (GGG)	48	356
Midland (MAF)	38	128
Stephenville (SEP)	52	496
Oklahoma City (OKC)	55	517

Other thermodynamic factors favorable for severe weather include characteristics of the 850 mb wind. The warm moist flow of the low-level jet would tend to further destabilize the regions near its axis. Also, the maximum temperatures lie west of the areas of highest dewpoints, another element associated with a favorable severe storm environment (Miller, 1972; Moller, 1979).

At 700 mb, the dryness of the atmosphere would allow relatively large amounts of evaporative cooling causing any air intruding into an updraft to become negatively buoyant and sink as a cool downdraft. A second factor is the wind veers with height through this level. Such a vertical shear not only implies warm advection, but it means the downdraft motion will be toward the storm's rear flank allowing it to converge more air into the updraft or generate new updrafts along its gust front with relatively little entrainment (Baxter, 1971). Recent numerical modelling experiments also show that anticyclonic turning of the wind with height favors the evolution of cyclonically rotating

storms, provided updraft strength is intense enough (Klemp and Rotunno, 1982).

4.1.3 An Investigation of Convective Trigger Mechanisms for This Day

As favorable as these wind, temperature, and moisture factors may be, they cannot initiate convection, only support it or enhance it once it has begun. What is needed is a mechanism to lift the potentially unstable air to its level of free convection, especially in lieu of the inversion layers in the MT air mass.

Large scale lifting is almost always associated with 500 mb PVA because as stated, this indicates upper tropospheric divergence and compensating vertical motion. In fact, Miller, in his Technical Report 200 (Miller, 1972) considers it the most important severe weather forecasting parameter. But upon examination of Figures 4.1-8 and 4.1-10 one sees there is negative vorticity advection over the potentially unstable air mass during the morning hours with neutral vorticity advection twelve hours later. Furthermore, Figure 4.1-9 shows the low-level jet entering the forward quadrant of the 300 mb jet. For such a jet stream profile, the forward left quadrant corresponds to upper tropospheric convergence (and therefore subsidence) while the front right quadrant has generally weak, ill-defined divergence (Beebe and Bates, 1955). Studies by Beebe and Bates (1955) and McNulty (1978) show severe weather development is favorable where the low-level jet enters the right rear quadrant of an upper jet axis with anticyclonic curvature, where divergence and upward vertical motion is at a maximum.

There is no evidence of a short wave trough approaching the MT air mass. Winds actually veer with height betwen 600 and 300 mb indicating

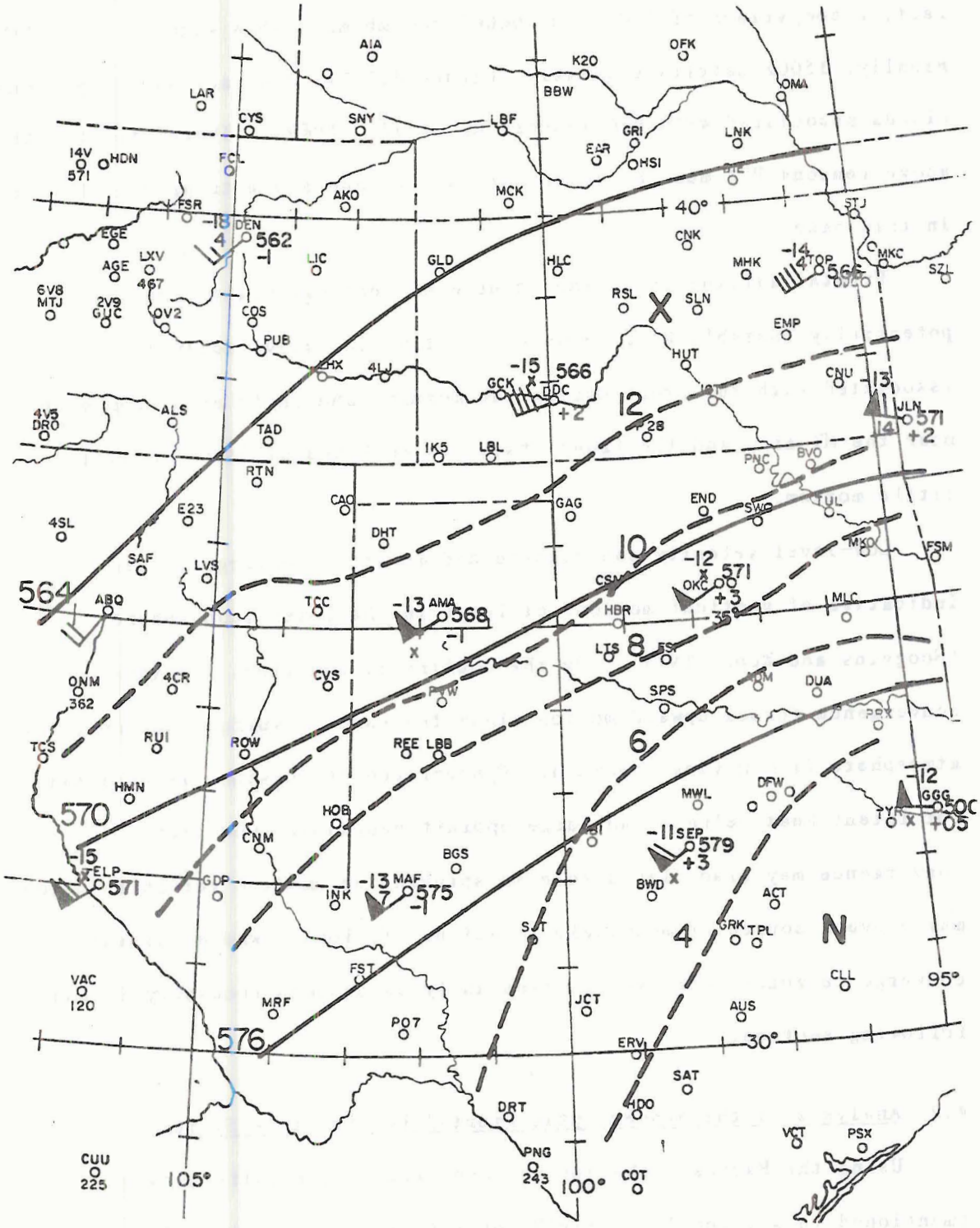

Figure 4.1-10. 0000Z, May 3, 500 mb analyses. Dashed lines are absolute vorticity contours.

warm advection instead of cooling normally associated with a trough. In fact, a comparison of 1200Z and 0000Z 500 mb maps show warming over OKC. Finally, 1500Z satellite imagery (Figure 4.1-11) does not show any comma clouds associated with PVA (Anderson, et al., 1969). Therefore, for the above reasons PVA must be ruled out as a thunderstorm trigger mechanism in this case.

Frontal lifting is another source of vertical motion for the potentially unstable air. However, little convective activity is associated with the front during the morning and early afternoon hours near the MT air, and the front itself is weak and diffuse, showing little motion.

Low-level velocity convergence and moisture convergence are indicative of vertical motion, at least in the lower troposphere (Scoggins and Wood, 1971). By the continuity equation, low level convergence forces upward motion since the earth's surface prevents the atmosphere from moving downward. Convergence of moisture is necessary for latent heat release and large updraft buoyancy. Low level convergence may also play a role in spinning up ambient vorticity which may prove a source of mesoscale rotation. To locate where and why convergence zones form, the surface analyses becomes necessary in the following section.

4.2 Analysis of the Sub-Synoptic Frontal Low Pressure System

Using the Barnes technique and centered finite differencing (mentioned in section 3.3), fields of relative vorticity, velocity, convergence, moisture convergence, vorticity production, and temperature advection were analyzed, then plotted. In Figure 4.2-1 and 4.2-2 1200Z maximum convergence and moisture convergence are located along the

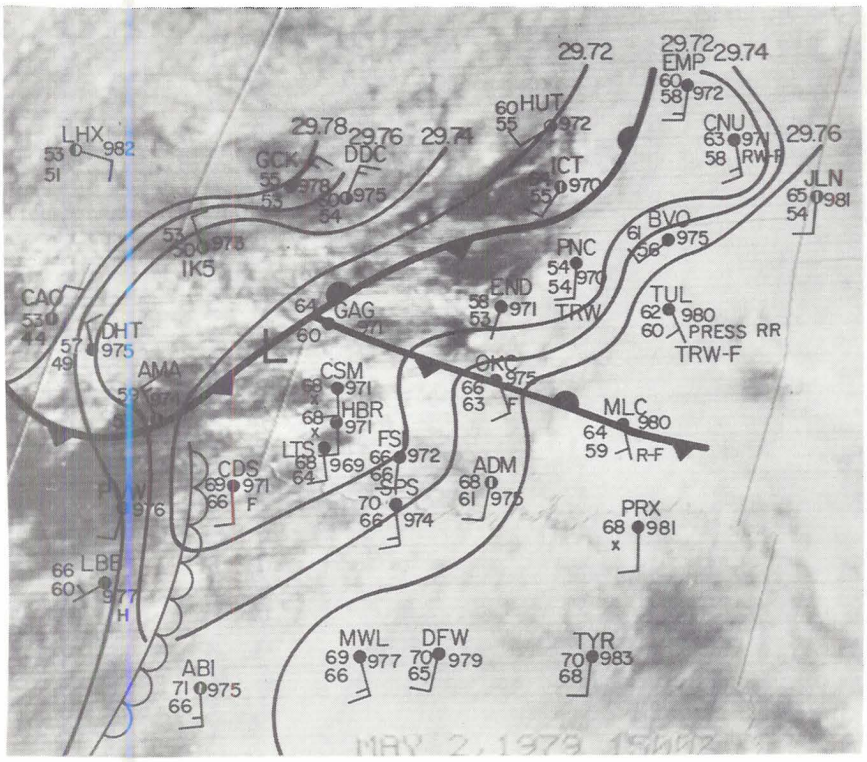

Figure 4.1-11. 1500Z satellite and surface composite analyses.

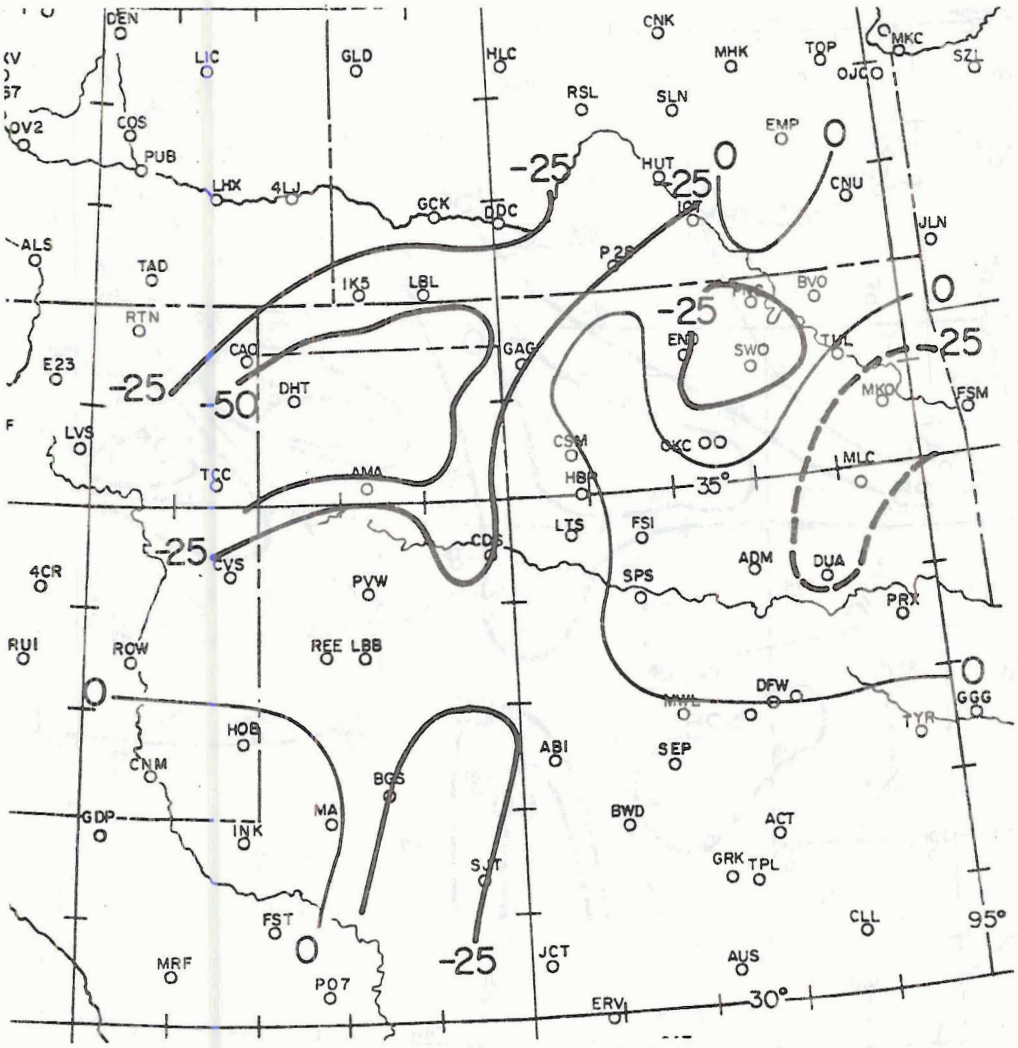

Figure 4.2-1. 1200Z surface velocity divergence (sec^{-1} X 10^{-6}).

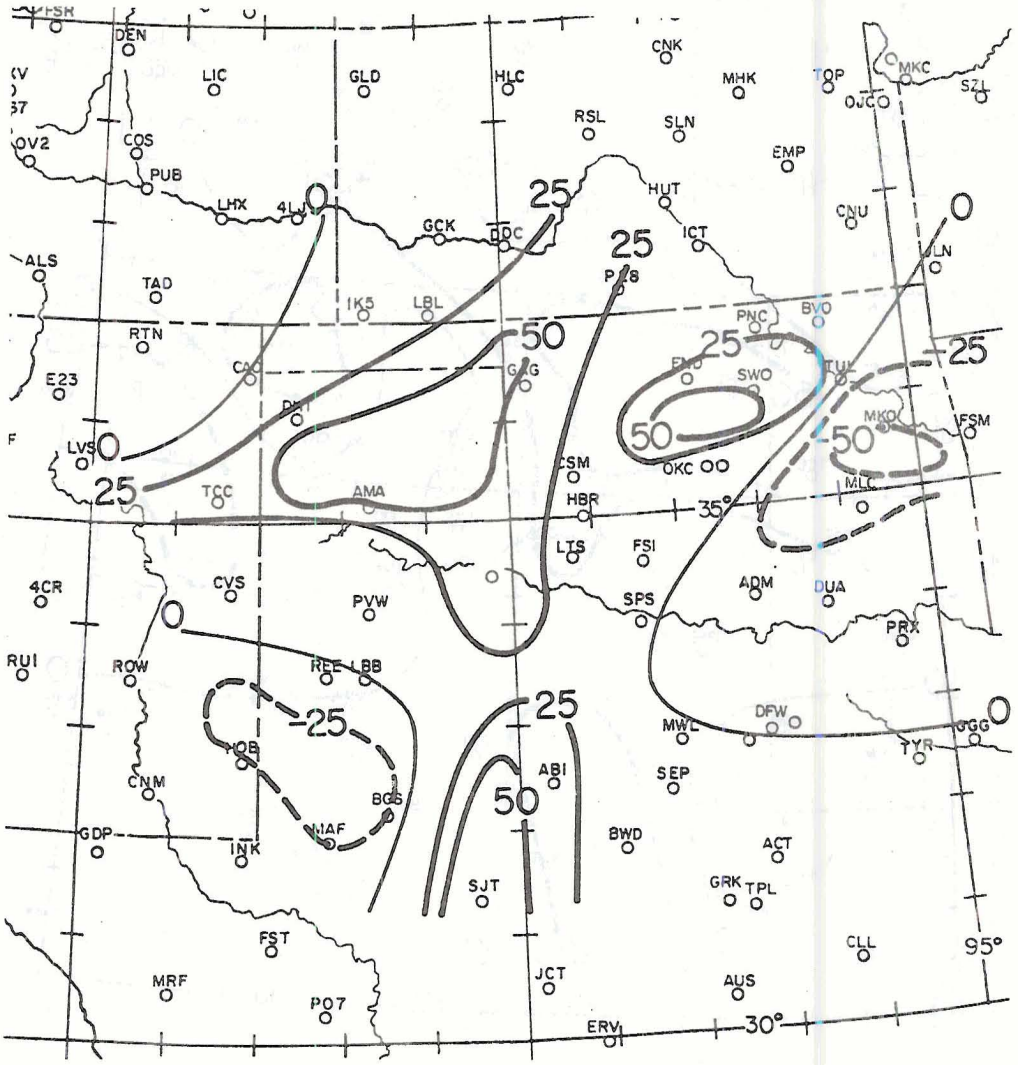

Figure 4.2-2. 1200Z surface moisture convergence (sec^{-1} X 10^{-6} gr kg^{-1}).

surface front through the Texas panhandle near the center of the frontal low pressure wave. In Figure 4.2-3, largest values of vorticity are similarly located near the low center. Temperature advection is also relatively strong here (Figure 4.2-4) although it has maximum values to the east near OKC where warm humid MT air is meeting the outflow boundary or mesofront. For the most part, then, the position of the frontal low coincides with significant zones of advection, convergence and vorticity so that any severe storm outbreak is highly dependent on its existence.

First, if the low is to deepen or even maintain itself, it must be as a result of diabatic heating and/or warm advection. No trace of this low is evident above 850 mb indicating it is warm cored, and it has already been shown that there is no PVA at mid levels. Likewise, for the vorticity of this system to increase or remain at a maximum, it must be due to localized zones of diabatic heating and warm advection. Adiabatic heating through subsidence is a factor which can cause low pressure areas the size of the SSL. Extensive areas of convection often have compensating subsidence ahead such that there is upper tropospheric warming and surface pressure falls (Hoxit, et al., 1976). But as will be seen, the area of convective activity remained very small compared to the area of the SSL during the period of largest pressures falls so it doesn't seem possible that compensating subsidence warming contributed to the deepening of this system. NVA is also associated with subsidence. However, because of the mass convergence aloft associated with NVA, there is usually surface pressure rises (Palmen and Newton, 1969). In fact, pressures generally rose in the area in question between 1200Z and 1500Z when mid level NVA was superimposed over it.

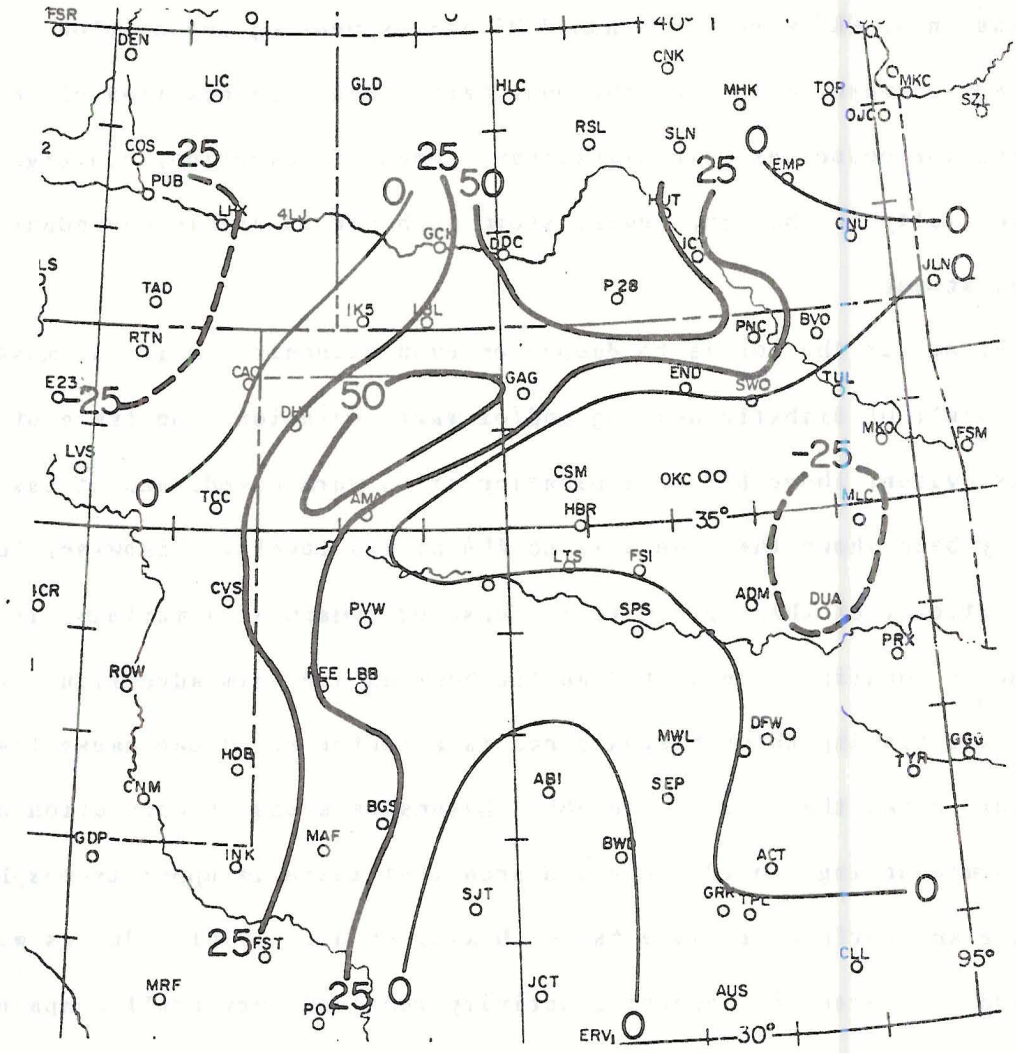

Figure 4.2-3. 1200Z surface relative vorticity (sec^{-1} X 10^{-6}).

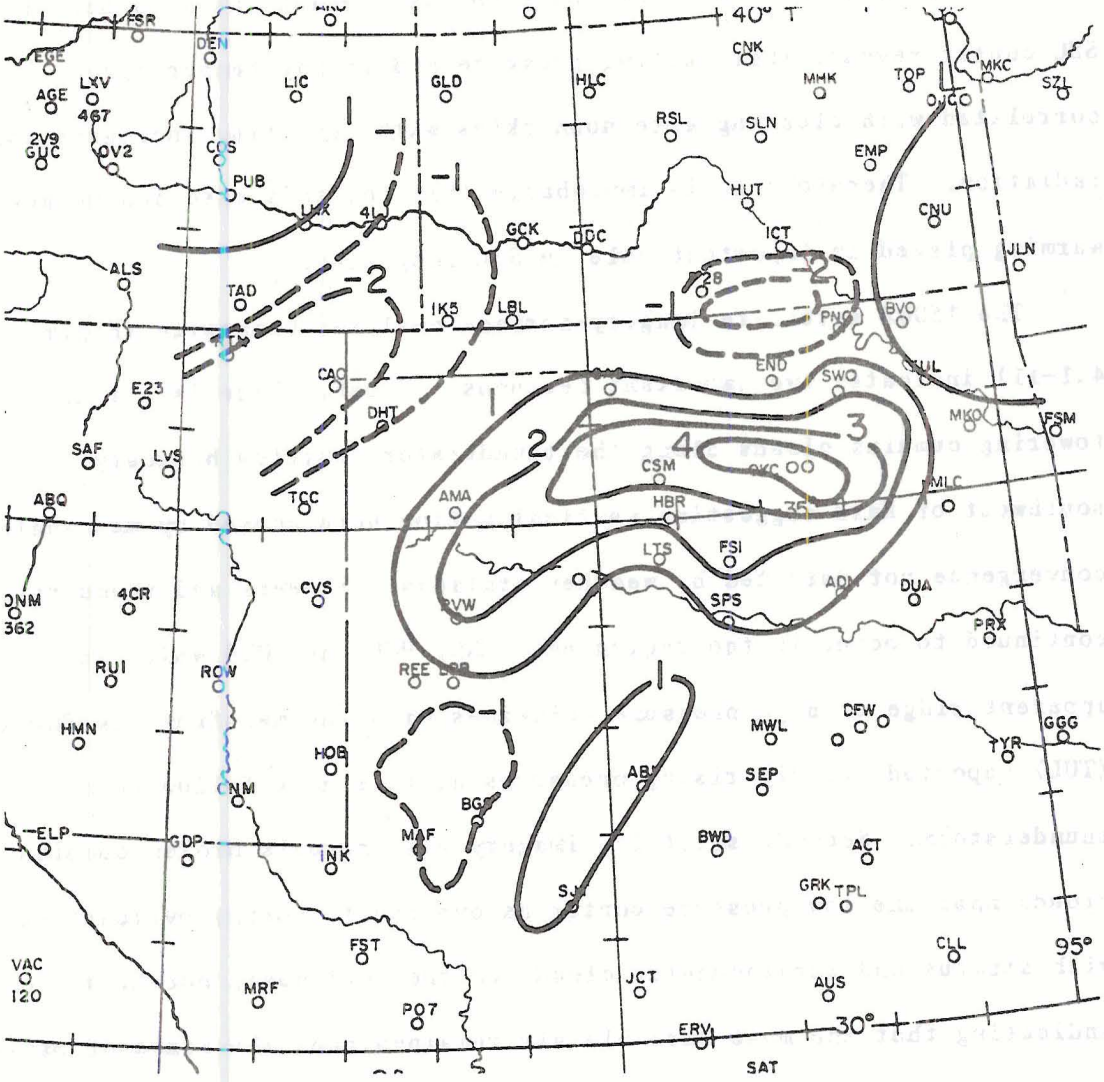

Figure 4.2-4. 1200Z surface temperature advection (sec^{-1} X 10^{-4} ^{o}F).

During this same time period there was no anomalous warming. Clinton, Oklahoma (CSM), which was near the SSL center, experienced a temperature rise of only 4°F, and a pressure rise of .04 inches. The time section for Lawton, Oklahoma (LTS) (see section 4.4), which was also near the SSL center reveals that falling pressure and rising temperatures correlated with clearing afternoon skies with resulting increased solar radiation. Therefore it is improbable that for this case subsidence warming played an important role in SSL deepening.

The 1500Z satellite imagery-surface analyses composite (Figure 4.1-11) indicates two important features. First, there is a line of towering cumulus clouds along the thunderstorm outflow boundary southwest of Enid suggesting vertical motion here caused by mesoscale convergence not detected by weather stations. Showers and thunderstorms continued to occur in the region near END, PNC, and BVO while an apparent ridge of high pressure coincides with the mesofront as Tulsa (TUL) reported rapidly rising pressures at this hour following a thunderstorm. Second, satellite imagery also reveals broken cumulus clouds near the low pressure center as opposed to mostly overcast skies with stratus and stratocumulus clouds to the northwest, north, and east indicating that the most unstable air remained near the zones of maximum convergence.

By 1800Z certain events were occurring which favored intensification of this low pressure system through localized warming. Satellite-surface composite analyses (Figure 4.2-5) shows the low center coinciding with a region of relatively clear skies between Gage (GAG) and Childress (CDS). Stratiform cloud cover also is breaking up through west Texas near Lubbock (LBB) and MAF. It is in this sector of clearing

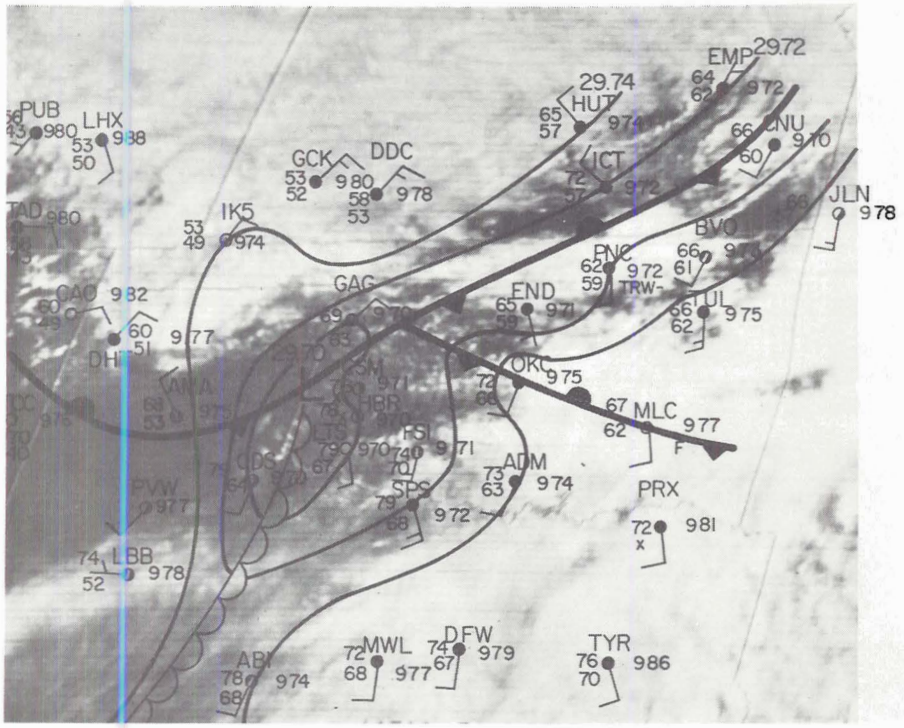

Figure 4.2-5. 1800Z satellite and surface composite analyses.

skies that solar heating should be significant. Figure 4.2-6 shows the 1800Z warm advection field having maximum values both along the dry line just outside of Abilene (ABI), and in southwest and central Oklahoma near the low center.

Of as much importance to the SSL intensification are the zones of local cooling caused by a combination of cold advection and evaporation of precipitation. Satellite imagery shows little solar heating can be expected in southwest Kansas and central Oklahoma because skies are generally overcast. Rain was falling during the morning at Dodge City and Garden City (GCK) which would suggest evaporative cooling. Meanwhile northerly winds continued to advect colder air into the Texas panhandle as the cold front moved south of AMA at about 1500Z. Finally, one should remember that cold advection was occurring at 850 mb in southwest Kansas as well.

A comparison of the isotherm-streamline surface analysis between 1200Z and 1800Z (Figures 4.2-7 and 4.2-8) shows the result of these horizontal variations in differential warming. Note that the warm sector is more localized at 1800Z between Wichita Falls (SPS) and LBB as compared to six hours earlier. Streamlines also reveal southerly winds from Fort Sill (FSI) through PNC. This flow results in the warm moist MT air overriding the rain cooled air behind the mesofront, triggering continuous shower activity. Thus the mesofront is almost self sustaining and helps confine the regions of significant diabatic warming to western Oklahoma and most of the Texas panhandle.

The satellite surface composite at 2100Z (Figure 4.2-9) when deep convection was beginning shows this warming pattern remains. Rain and thundershower activity continued to occur behind the outflow boundary

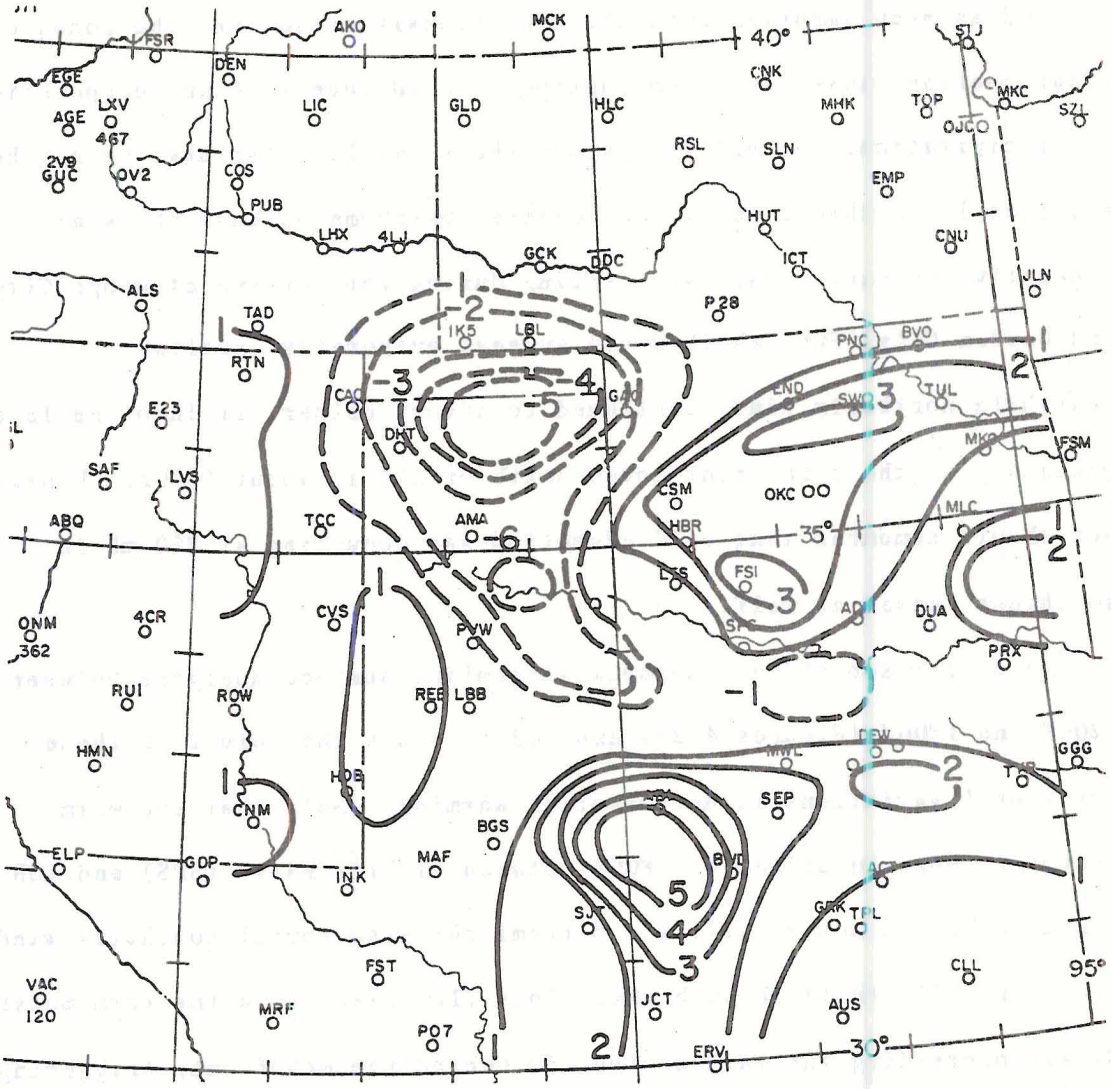

Figure 4.2-6. 1800Z surface temperature advection (sec^{-1} X 10^{-4} ^{o}F).

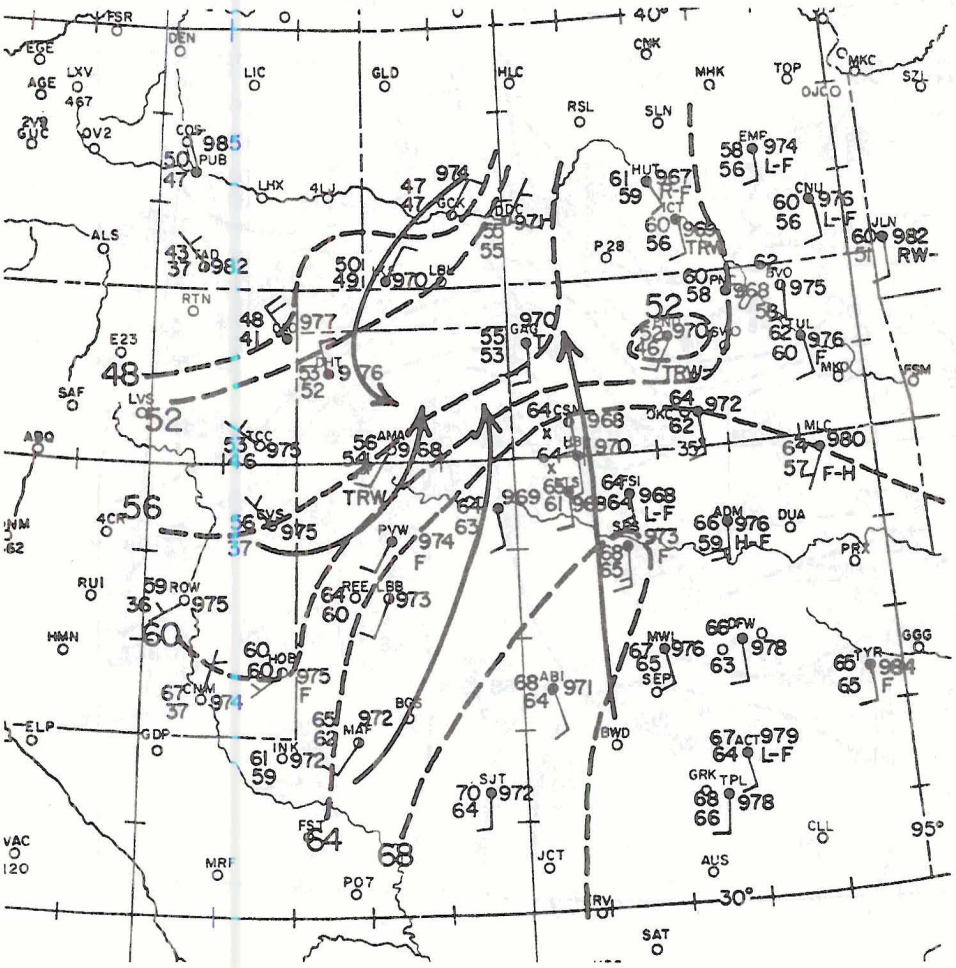

Figure 4.2-7. 1200Z surface streamline-isotherm analyses.

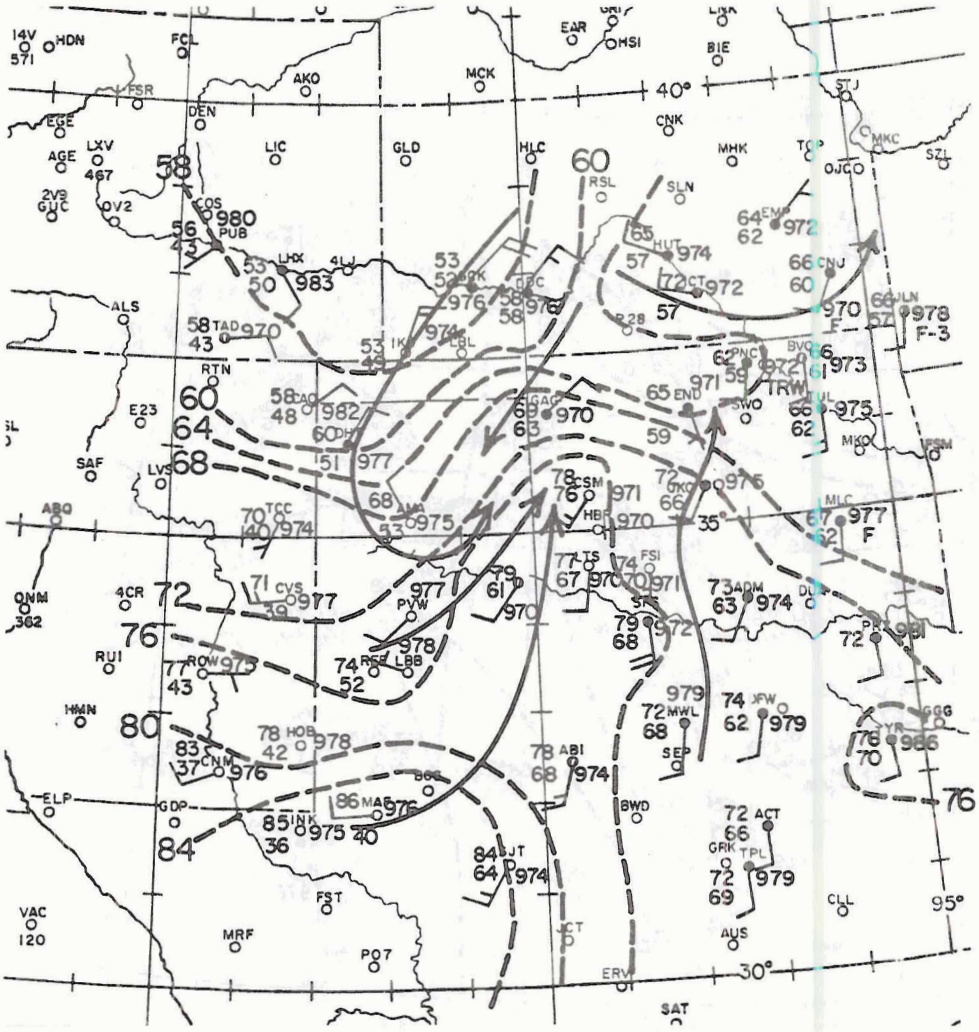

Figure 4.2-8. 1800Z surface streamline-isotherm analyses.

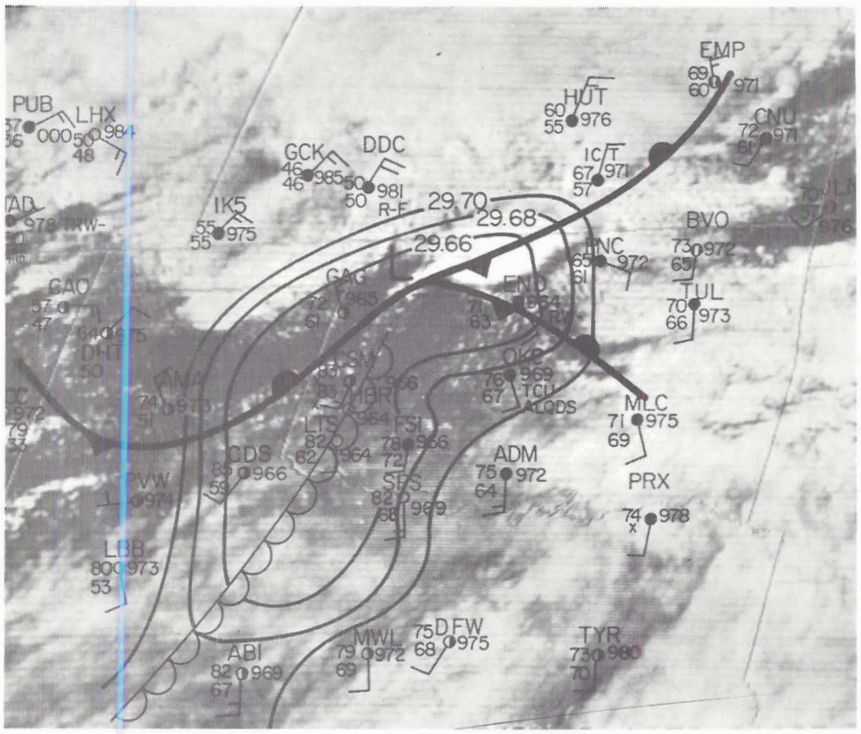

Figure 4.2-9. 2100Z satellite and surface composite analyses.

near END. The stationary front showed little movement. The satellite picture again reveals overcast skies through eastern Oklahoma, most of Kansas, and in the northern portion of the Texas panhandle.

In contrast, western Oklahoma and the southern three quarters of the Texas panhandle remain relatively clear, with the exception of scattered low cumulus clouds which again indicates this region is relatively unstable. The surface streamline, temperature, and advection fields (Figures 4.2-10 and 4.2-11) continue to show strongest cold air movement through southwest Kansas into the Texas and Oklahoma panhandles while maximum warm advection occurs in southwest and central Oklahoma. Warm advection along the dry line near ABI, though still strong, had diminished from three hours earlier.

Surface temperature changes reflect these differential solar heating and advection patterns. For example, between 1200Z and 2100Z, hours normally associated with diurnal warming, DDC cooled by 5°F. Conversely during the same time period, Clinton-Sherman, Oklahoma's (CSM) temperature rose by 19°F, CDS by 21°F and SPS by 24°F. From the earlier discussion, the warm advection and diabatic heating by radiation should result in frontal low deeping. In fact, this is what happens. Notice that the pressure tendencies for 1800Z-2100Z (Figure 4.2-12) shows large falls are generally within the warm air sector within the low pressure disturbance. It is during this period that mid level NVA begins to diminish (Figure 4.1-9) while clearing skies could combine with the surface and 850 mb warm advection to produce an isallaboric maximum.

The largest pressure falls actually occurred in eastern New Mexico with the advection of warm dry CT air. Pressure falls behind the front

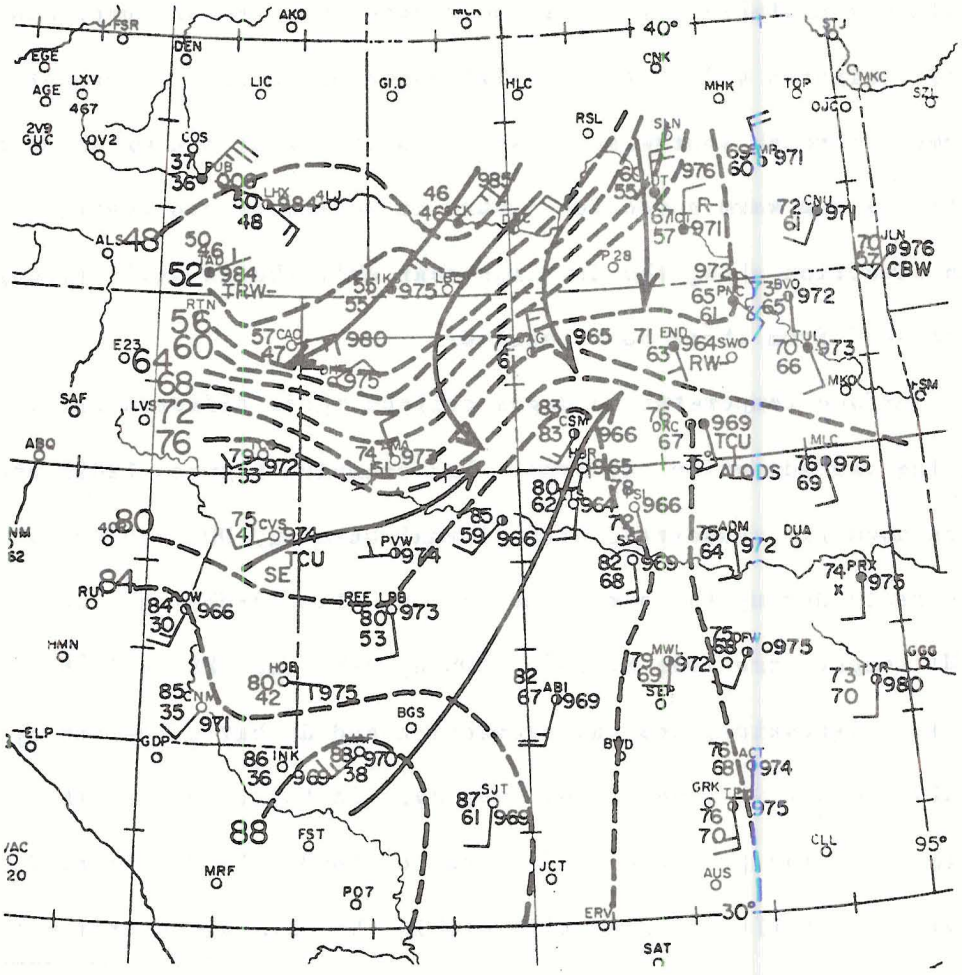

Figure 4.2-10. 2100Z surface streamline-isotherm analyses.

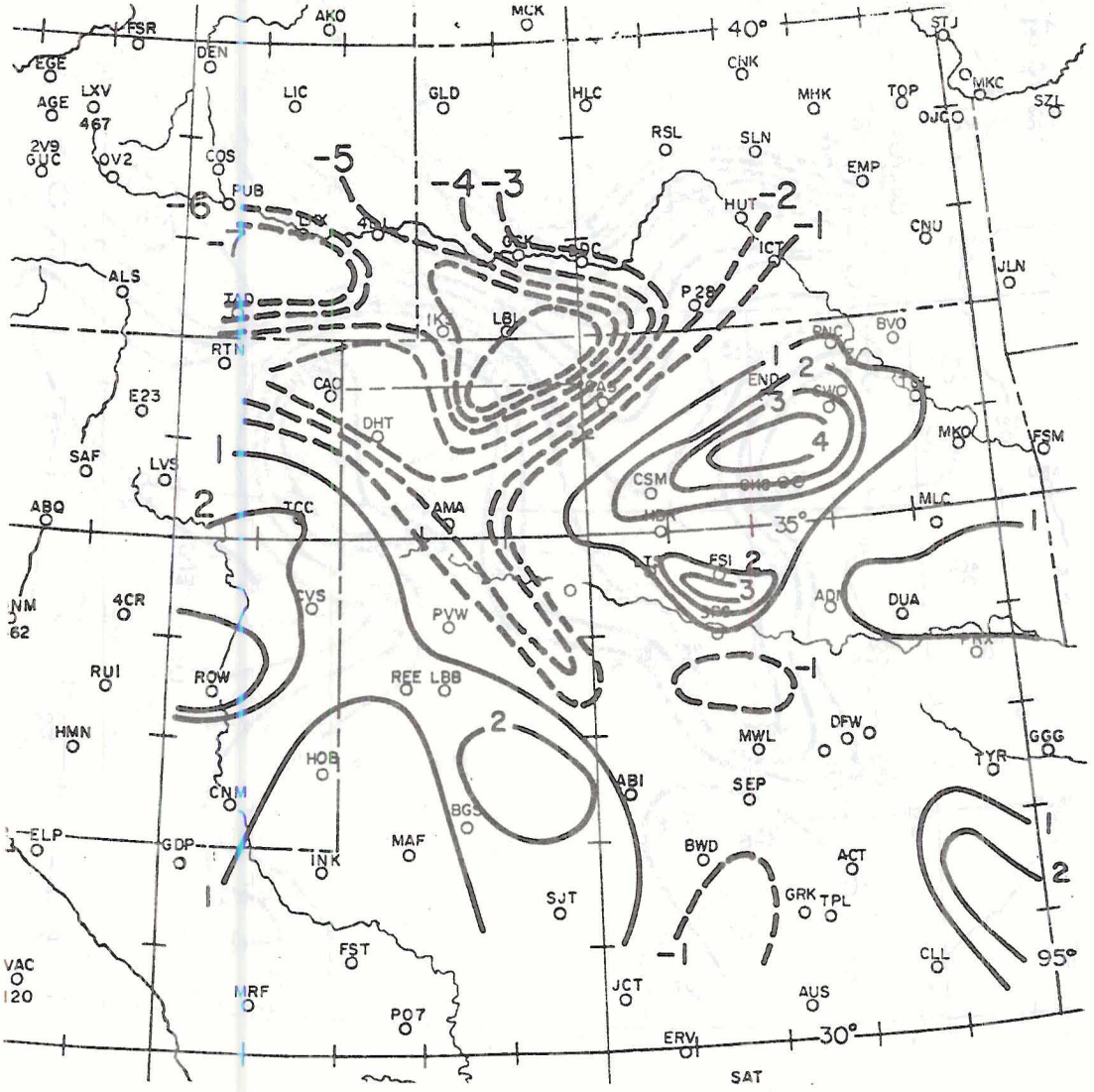

Figure 4.2-11. 2100Z surface temperature advection (sec^{-1} X 10^{-4} ^{o}F).

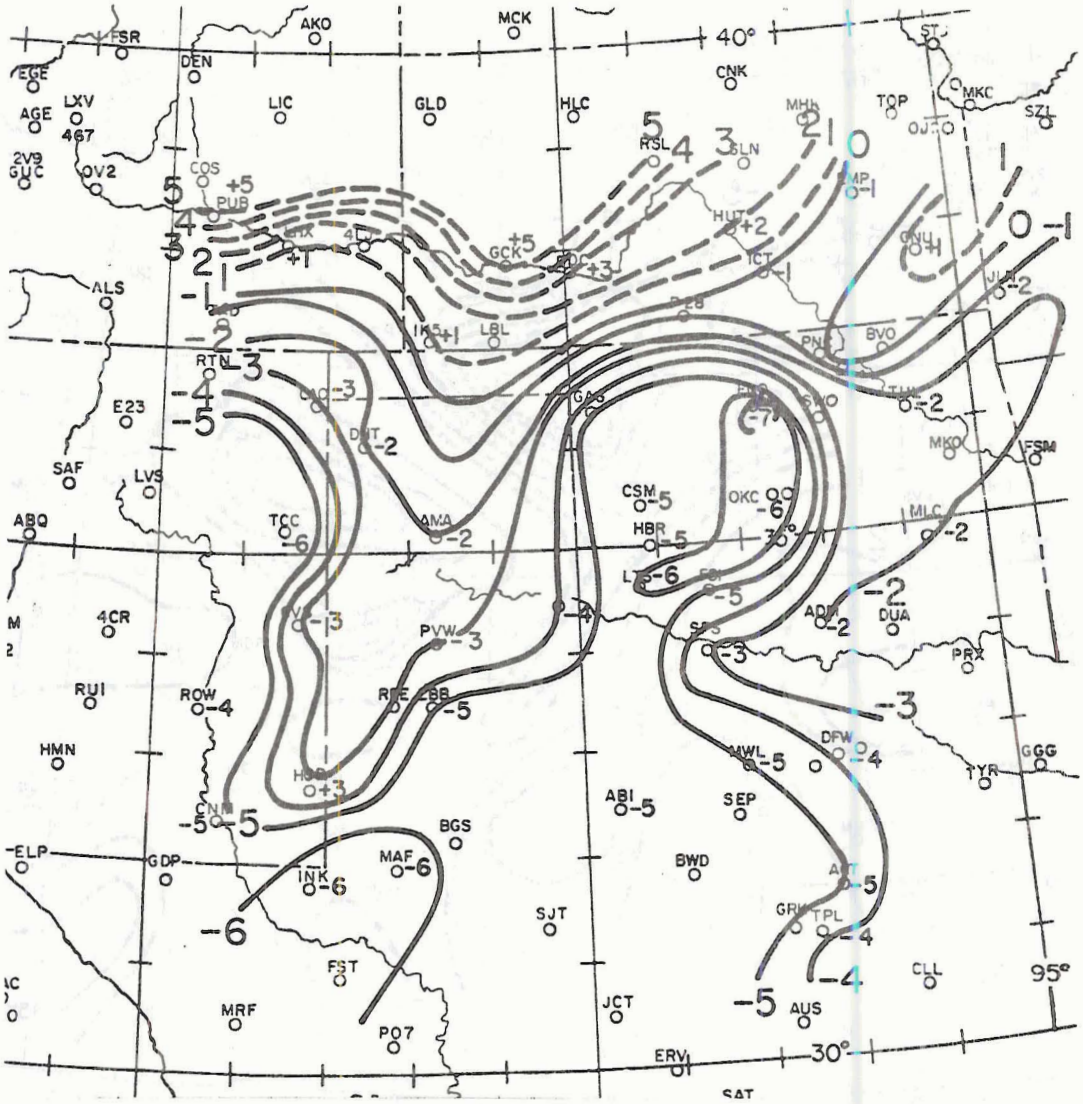

Figure 4.2-12. Surface pressure tendencies (inches X 10^{-2}) for period 1800Z to 2100Z.

at Clayton (CAO) and Dalhart (DHT) came about from convective activity triggered by upslope flow. Also during this period, pressure rises were occurring where surface and 850 mb cold advection combined with rainfall and evaporation to cause cooling.

As previously discussed, localized warming via advection and heating should be expected to increase the local vorticity. Indeed, comparison between Figure 4.2-3 and Figures 4.2-13 and 4.2.14 show a marked increase in relative vorticity associated with the low as maximum vorticity production (Figure 4.2-15 and 4.2.-16) both at 18 and 21Z occurred just south of GAG. The region of strongest vorticity production is found close to where the negative of the Laplacians of advection and heating (equation 2.2.2) would be at a maximum.

Thus, the frontal low pressure system not only maintained its existence but intensified despite morning NVA and neutral vorticity advection toward late afternoon. In the next section it will be seen how this SSL was instrumental in the development of tornadic storms.

4.3 Mesocyclongenesis Within the Sub-Synoptic Low

4.3.1 The Convective Trigger Mechanism with Respect to the Sub-Synoptic Low

Since mesocyclones consist of large updrafts, a lifting mechanism is required to initiate deep convection. The question of where and how such a mechanism exists remains an important one, especially for severe storm nowcasters. Within a low pressure system of this type, thunderstorm genesis is often favored along the dry line (Rhea, 1965), where a wave or bulge initiates mass convergence and vertical motion (Koch and McCarthy, 1977). However, for this to occur a downward

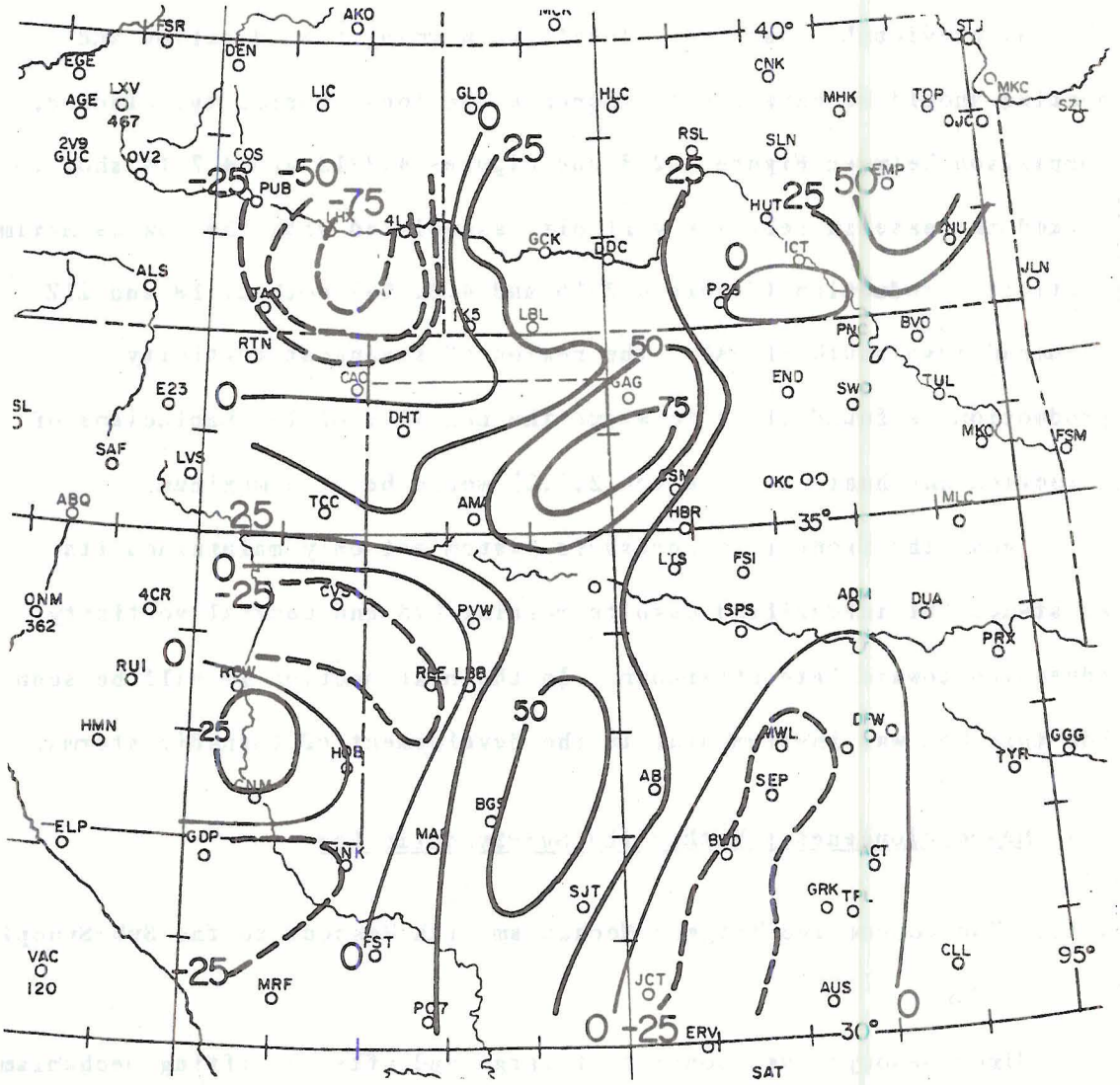

Figure 4.2-13. 1800Z surface relative vorticity (sec^{-1} X 10^{-6}).

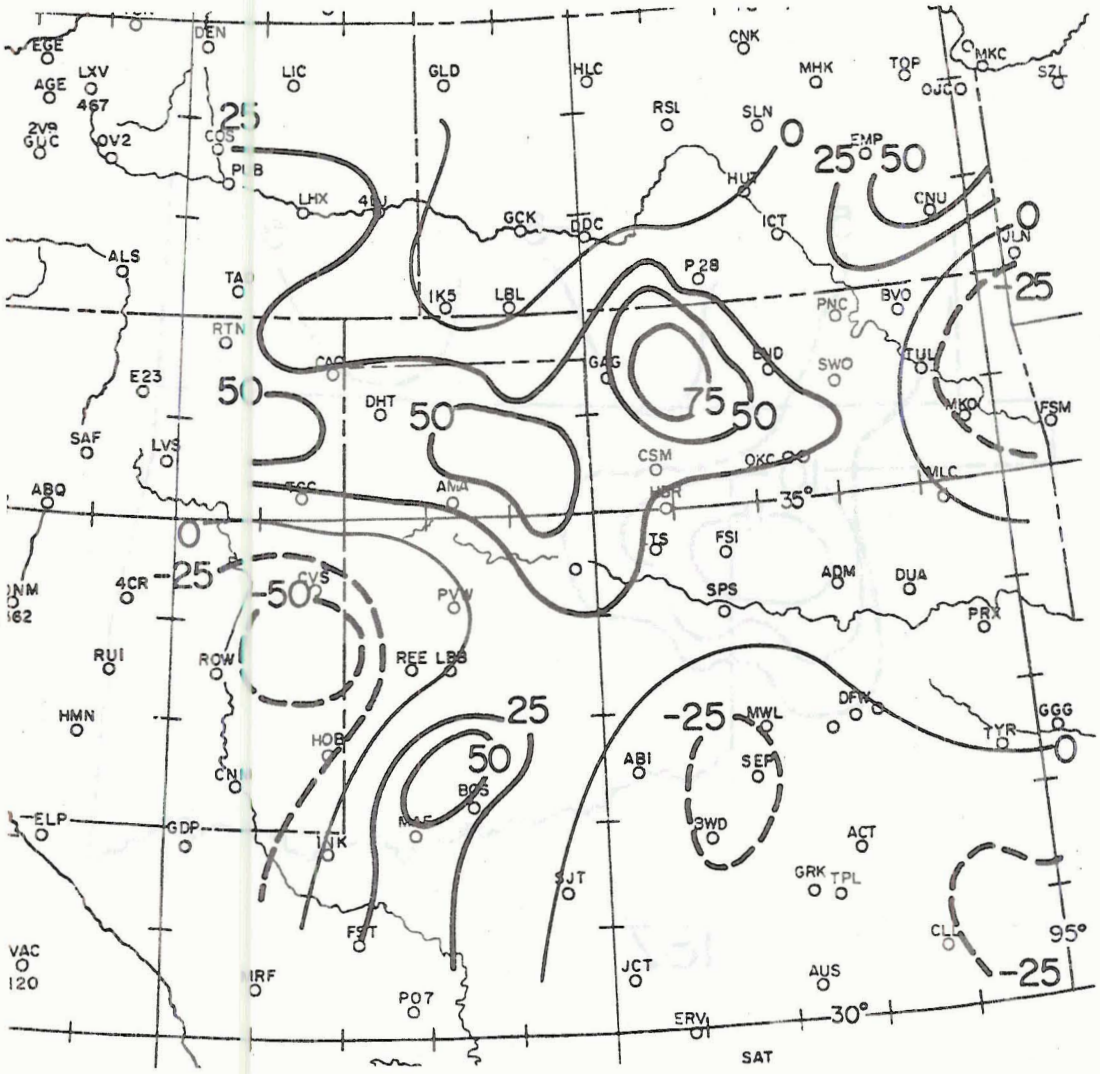

Figure 4.2-14. 2100Z surface relative vorticity (sec^{-1} X 10^{-6}).

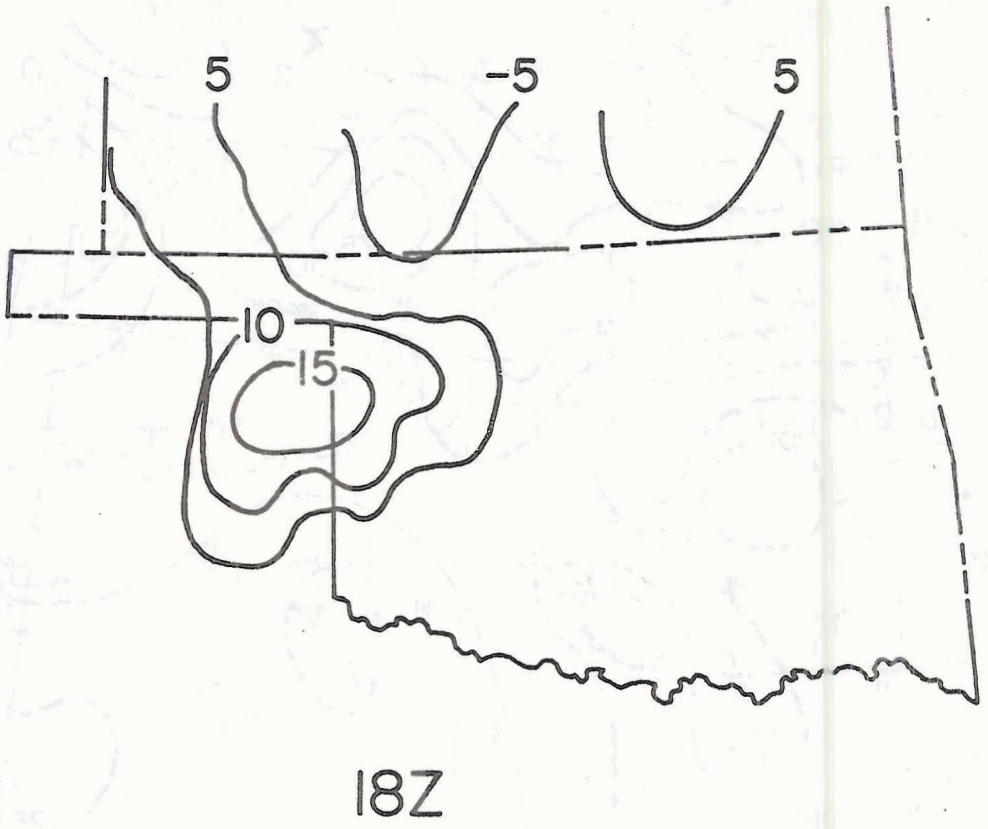

Figure 4.2-15. 1800Z surface vorticity production (sec^{-2} X 10^{-9}).

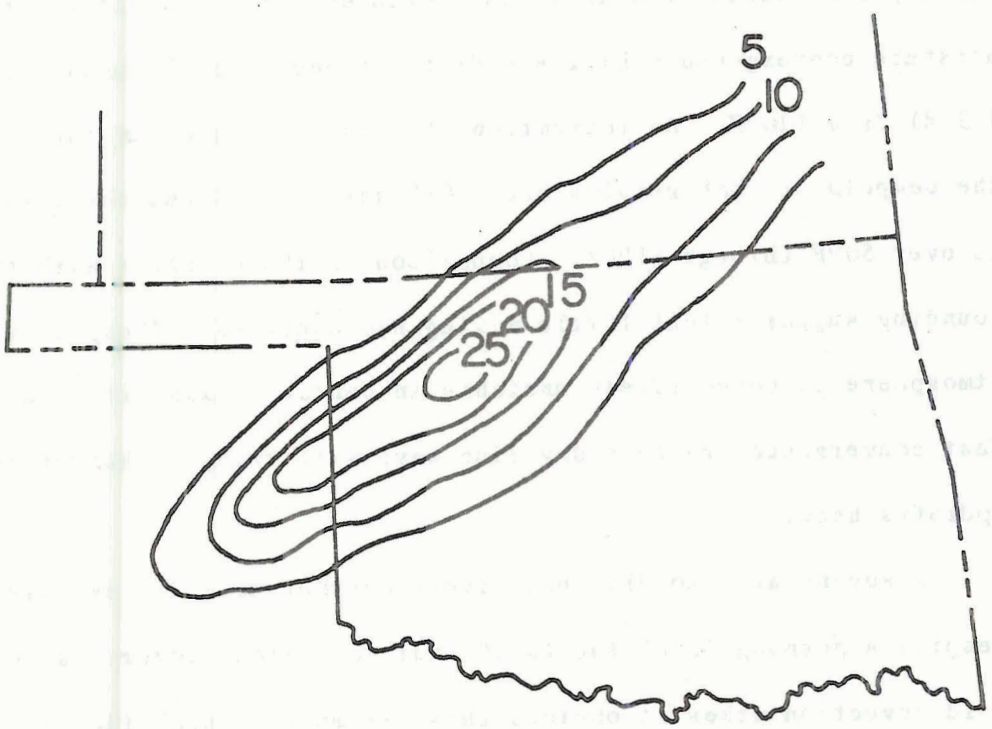

Figure 4.2-16. 2100Z surface vorticity production (sec^{-2} X 10^{-9}).

transport of momentum is usually required (McGinley and Sasaki, 1975) along with strong vertical shear and a nearly dry adiabatic lapse rate. The MAF soundings indicates that a favorable shear and lapse rate do exist, but from our earlier analysis, there is no short wave trough passing over the dry line to provide a downward momentum surge from the west. Actual analysis reveals that convergence does not increase along the dry line during the afternoon (Figures 4.3-1 and 4.3-2) while moisture convergence exhibits a distinct decrease (Figures 4.3-3 and 4.3-4) from 1200Z. An indication of a lack of momentum surge is that the dewpoint at MAF remains over 40°F until 1800Z and the value at LBB is over 50°F through 2100Z. Comparison of these values with the MAF sounding suggests that little mixing had occurred. Thus, though the atmosphere is convectively unstable in central Texas, it is unlikely that convergence due to a dry line wave will trigger thunderstorm updrafts here.

A second area to discount severe weather activity is near DDC despite a morning Total Totals of over 50. Cloud cover, rainfall, plus cold advection makes it obvious this air mass is stabilizing. The Total Totals at 0000Z supports this as it decreases to 46. Furthermore, there is no trigger mechanism in the area to lift an air parcel to its LFC.

The convective trigger mechanism for this day must be attributed to the differential heating pattern associated with the intensification of the frontal low. At 1200Z there was only a pressure difference of .03 inches between DDC and CSM, the latter station being closest to the low center. By 1800Z, pressure rises at DDC due to cooling and pressure falls at CSM due to warming causes this difference to increase to .07 inches. Three hours later it rises to.15 inches. This difference (0.3

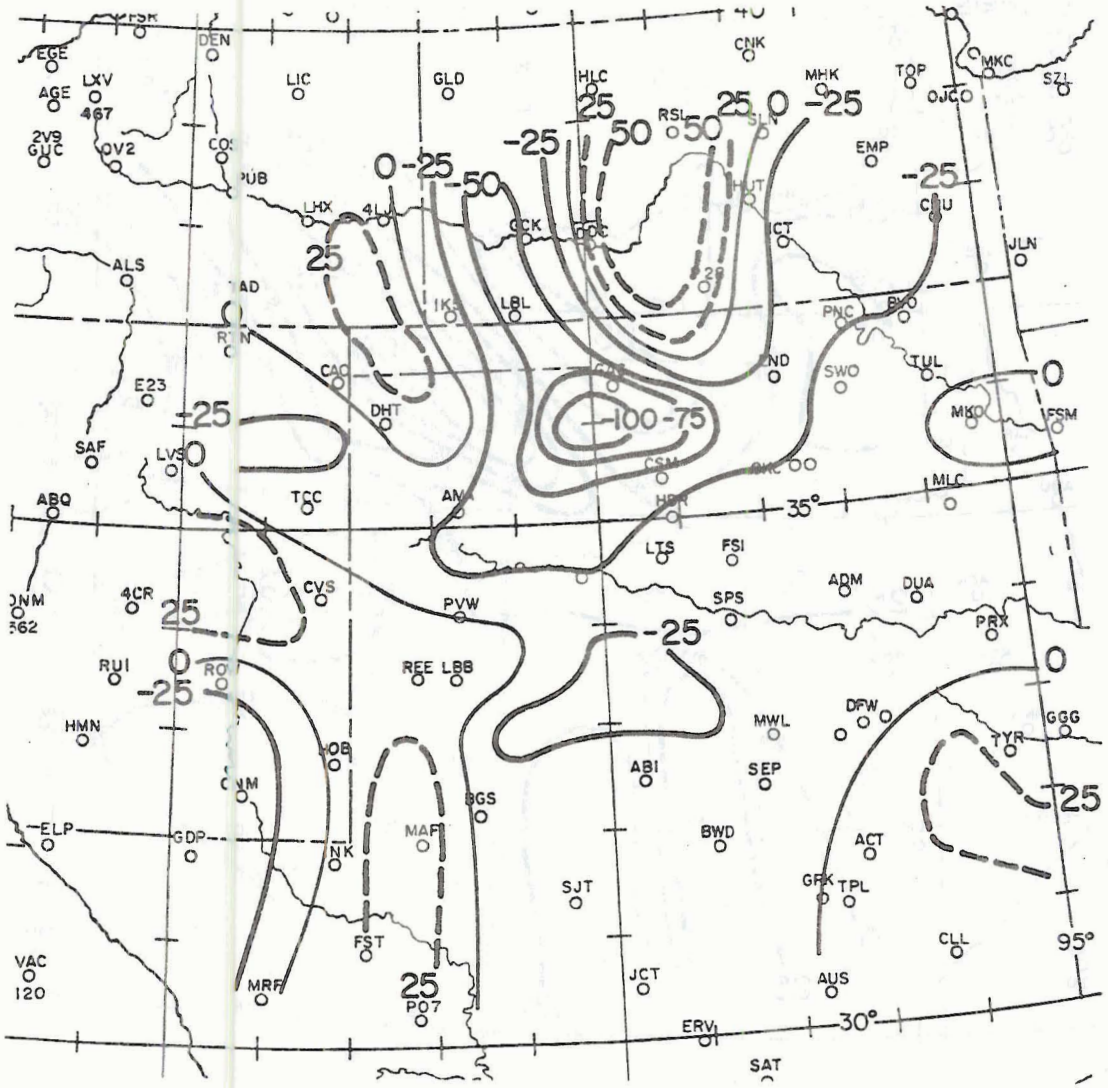

Figure 4.3-1. 1800Z surface velocity divergence (sec^{-1} X 10^{-6}).

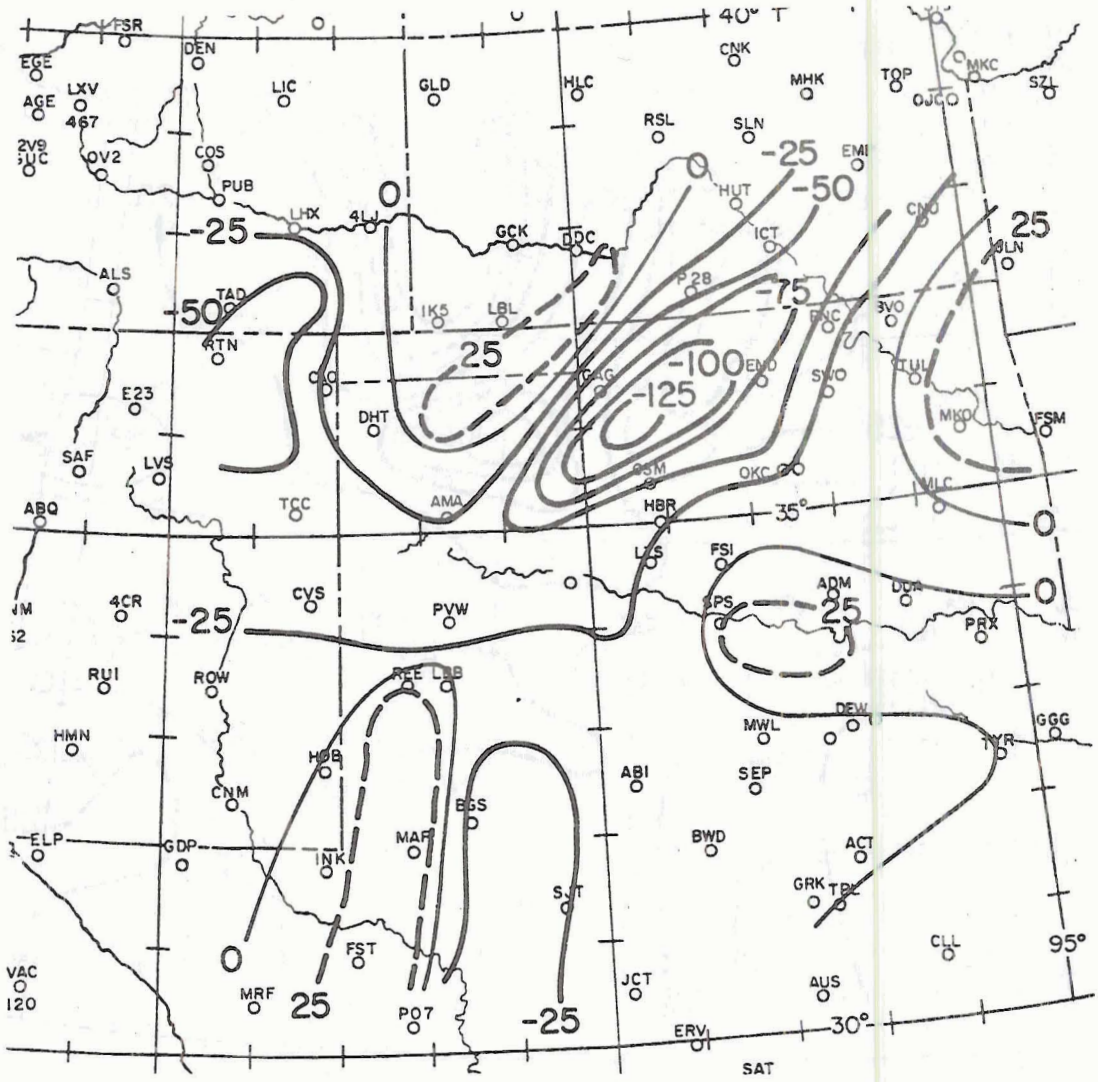

Figure 4.3-2. 2100Z surface velocity divergence (sec^{-1} X 10^{-6}).

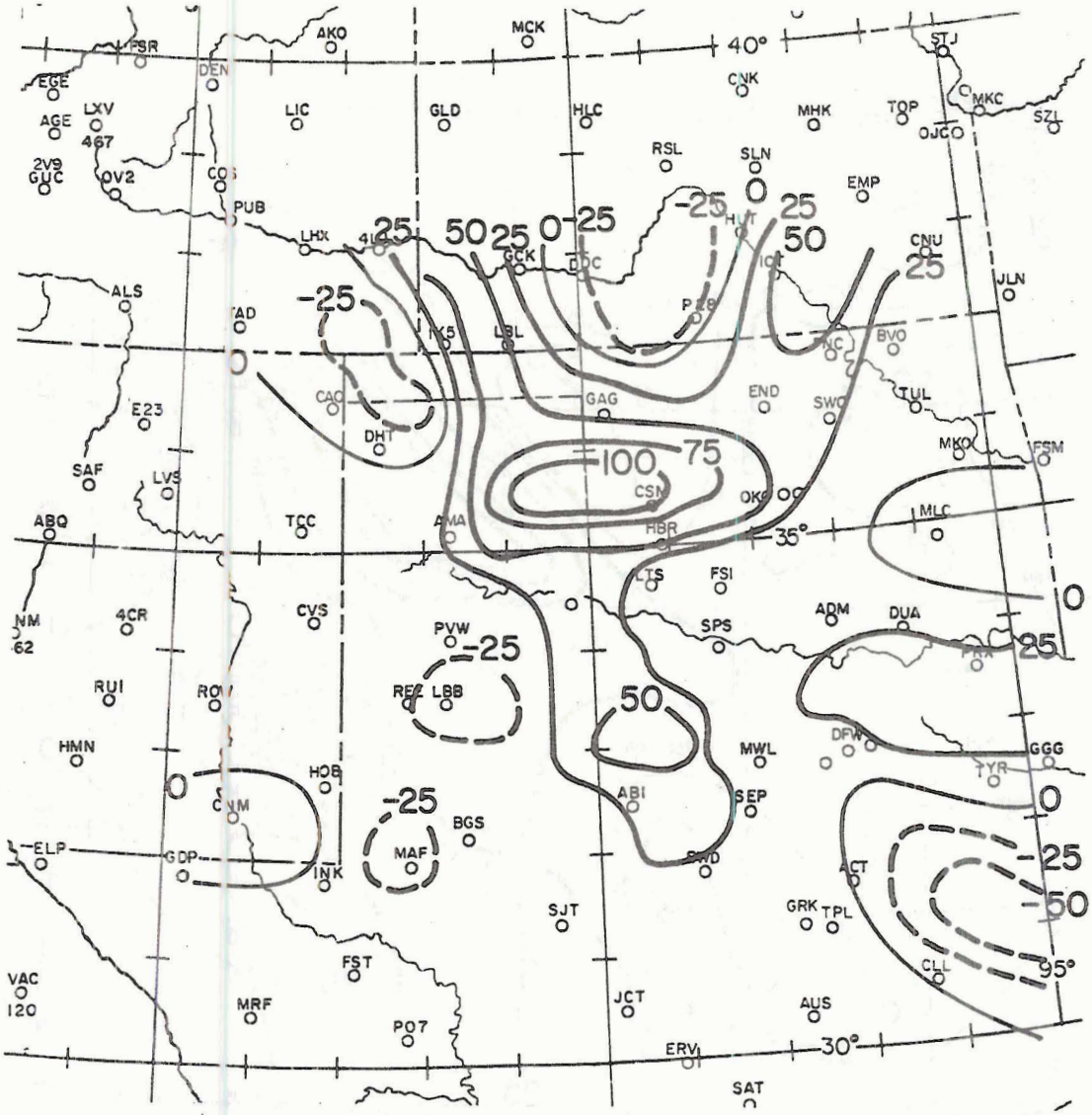

Figure 4.3-3. 1800Z surface moisture convergence (sec^{-1} gr kg^{-1} X 10^{-6}).

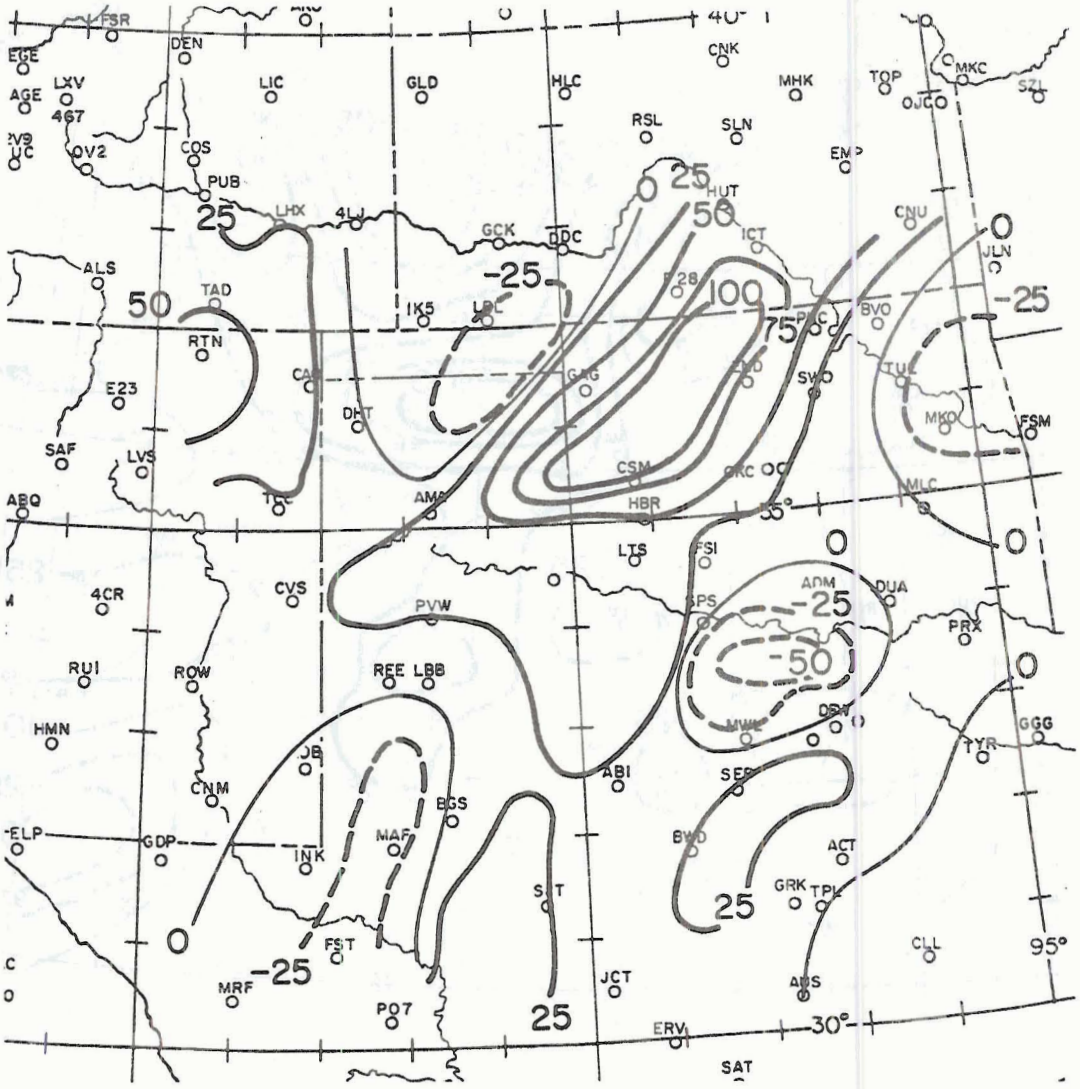

Figure 4.3-4. 2100Z surface moisture convergence (sec^{-1} gr kg^{-1} X 10^{-6}).

to .15 inches) in the pressure gradient contributes to a doubling of both velocity convergence and moisture convergence near the low center (see Table 4.2) as air flows from high to low pressure (compare Figures 4.2-1, 4.2-2 and 4.3-2, 4.3-4). Indeed it has been found that differential solar heating alone (e.g., due to cloud cover configurations) can trigger deep convection (Purdom 1973) even if marked warm advection is absent. Similarly warm advection can trigger severe storms despite an absence of mid level PVA provided the air at lower levels is convectively unstable (Maddox and Doswell, 1982).

Table 4.2

Comparison of the Pressure Difference (ΔP) in inches between Dodge City and Clinton and maximum values of velocity and moisture convergence between these stations

Time	ΔP	Velocity Convergence	Moisture Convergence
1200Z	.03	50×10^{-6} sec^{-1}	50×10^{-6} sec^{-1} gr kg^{-1}
1800Z	.07	100×10^{-6} sec^{-1}	100×10^{-6} sec^{-1} gr kg^{-1}
2100Z	.15	125×10^{-6} sec^{-1}	100×10^{-6} sec^{-1} gr kg^{-1}

Thus thunderstorm development would have to be most likely in the region bounded by GAG, END, and CSM within the low pressure center near the intersection of the dry line, stationary front, and thunderstorm outflow mesofront. This so called triple point (Purdom and Weaver, 1981) was similar to one along which the Red River tornadic storms evolved three weeks earlier. In numerous case studies, Maddox, et al., (1979) found such regions favorable for severe storms with corresponding high values of vorticity and convergence near the thermal boundary intersections. For this case the maximum values of convergence and vorticity exist here because of localized warming.

It should also be mentioned that the region near the surface low

center is subject to frontogenetical processes (Palmen and Newton, 1969). The relationship of frontogenesis and severe weather initiation is described in detail for this day by Bluestein, et al., (1980). Such a process increases baroclinicity and vertical motion, thus giving further reason to center attention between GAG CSM, and END.

4.3.2 Determining the Mesocyclogenesis Potential

A second nowcasting question to consider is after convection is initiated, will the thunderstorm become severe. As earlier mentioned, the equivalent question in many situations might be, will storms develop into supercells with mesocyclones? A method presented here will attempt to predict the answer through the vorticity equation.

The source of mesocyclone voticity in the low and mid troposphere has been attributed to both updraft convergence and tilting. Thus for a rotating thunderstorm, vorticity production can be approximated by scaling down equation 2.1.1 to the form:

$$\frac{d\xi}{dt} = -\nabla\cdot\underset{\sim}{V}(\xi + f) + \frac{\partial w}{\partial y}\frac{\partial u}{\partial z} - \frac{\partial w}{\partial x}\frac{\partial v}{\partial z}$$

Consider first the available ambient surface vorticity (ξ + f), the updraft can converge. From figure 4.2-14, ξ is 7.5 X $10.^{-5}$ sec^{-1} and f is 8.5 X $10.^{-5}$ sec^{-1} This will account for only the initial value of absolute vorticity beneath the updraft. After the updraft is initiated, it will take a finite amount of time to attain maximum strength. During this time it will continue to converge air at the boundary layer so that ξ would be well over 7.5 x 10^{-5} sec^{-1} within the storm at the time of greatest updraft intensity. Thus (ξ + f) as derived using synoptic scale data denotes a <u>lower</u> limit of ambient vorticity the updraft will converge near its core.

Actual convergence in the updraft core may be estimated by first assuming no horizontal density advection occurs (Barnes, 1970). Then by the continuity equation.

$$\frac{\partial w}{\partial z} = -\nabla_H \cdot \underset{\sim}{V} \tag{4.3.1}$$

From the equations of motion and parcel theory which assumes adiabatic ascent:

$$\frac{dw}{dt} \sim g\left(\frac{\Delta Tv}{Tv}\right) \tag{4.3.2}$$

where ΔTv is the excess virtual temperature of the parcel as compared with the ambient virtual temperature Tv. To approximate precipitation drag, a factor of gq is introduced where q is the liquid mixing ratio for cloud water, which can be estimated by the mixing ratio profile throughout a cloud assuming total saturation of the atmosphere within it. If it is assumed the updraft becomes steady state, then $\frac{\partial w}{\partial t} = w\frac{\partial w}{\partial z}$ so that we have left with the relationship:

$$w\frac{\partial w}{\partial z} = g\left(\frac{\Delta Tv}{Tv} - q\right). \tag{4.3.3}$$

This equation neglects entrainment, adverse perturbation pressures and friction from ice particles so that the vertical motion predicted by it is often too large by a factor of 1.5 (Weaver and Safford, 1979). Thus a more realistic equation for the updraft profile will be of the form

$$\frac{1}{2}\frac{\partial w^2}{\partial z} = .67g\left(\frac{\Delta Tv}{Tv} - q\right). \tag{4.3.4}$$

This equation is now regularly applied to severe storm forecasting procedures in the PROFS project at Boulder, Colorado (David Reynolds, personal communication).

For this case study, the OKC 0000Z for May 3 (Figure 4.3-5) sounding is used since it is most representative of the unstable airmass within the region of high thunderstorm probability prior to convection. The surface temperature of the sounding, however, will be assumed the value of 80°F which is about what the temperatures were at 2100Z in the MT air mass in the high convergence zone. If we lift a parcel of these characteristics to the LFC and apply Equation 4.3.4 the resultant vertical velocity profile is predicted as in Figure 4.3-6 (as determined by a computer program used by PROFS). This profile does not consider elements favorable for updraft intensification such as downdraft convergence, wind shear induced dynamic effects, and subcloud hydrostatically induced pressure deficits. Therefore, the profile could very likely underestimate updraft strength.

Notice that the updraft is very intense up to 200 mb with values of 60m sec^{-1}. Since the 200 mb level is about 12060 m above the ground, the amount of vorticity produced near the surface through updraft convergence is: $\frac{\Delta\xi}{\Delta t} \simeq -\nabla_H \cdot \underset{\sim}{V}(\xi + f) = \frac{\Delta w}{\Delta z}(\xi + f)$ which is calculated to be about 8×10^{-7} sec^{-2}.

In summary, it is found that if an updraft is triggered in the convectively unstable air mass within the SSL, it will be intense enough to produce significant amounts of vorticity near its core by converging the absolute vorticity already existing in the larger scale environment.

To predict potential vorticity production from tilting in the mid-troposphere several assumptions must be made. First, it is assumed the

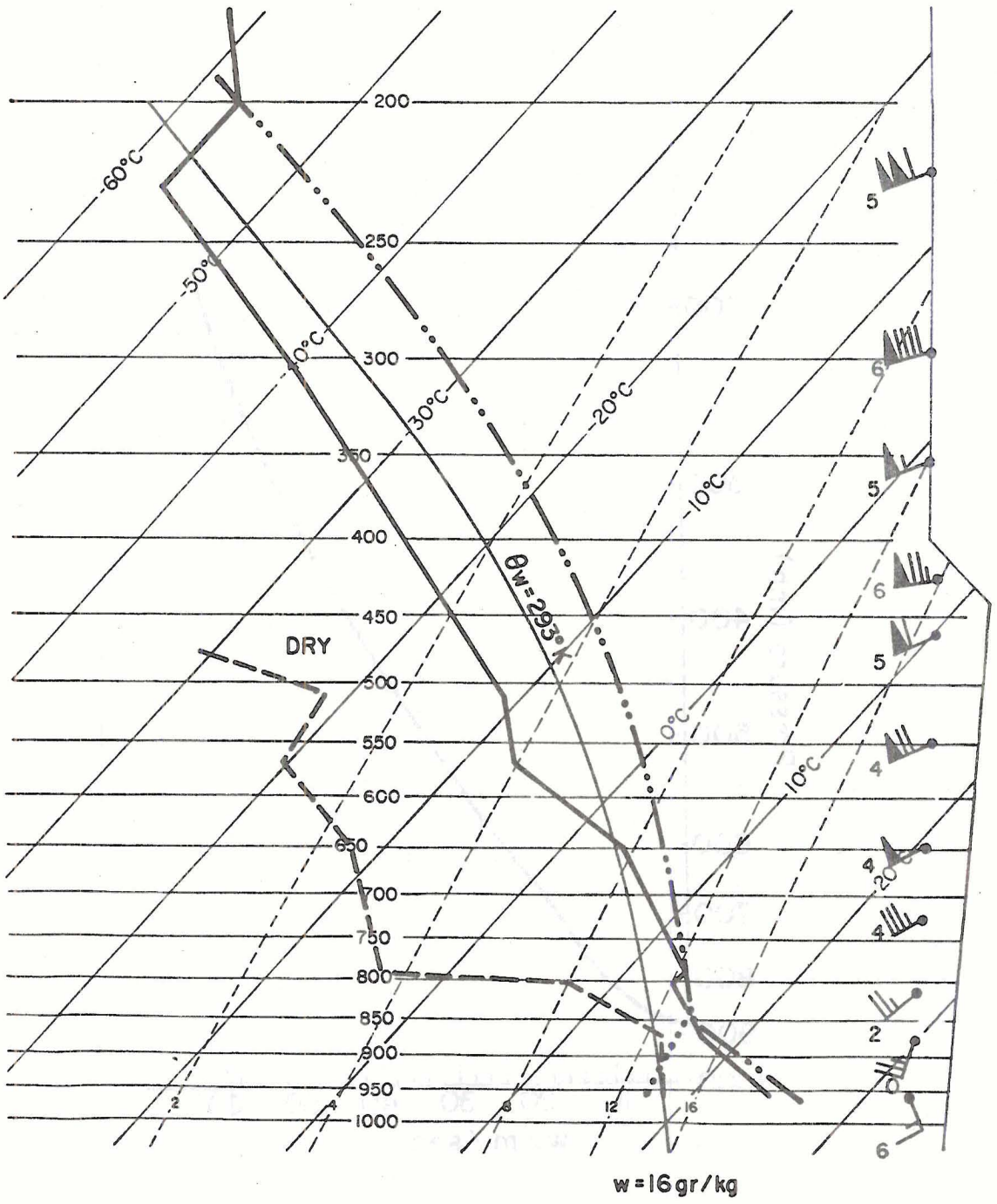

Figure 4.3-5. 0000Z May 3, 1979 OKC sounding showing parcel lapse rate for a surface temperature of 80°F.

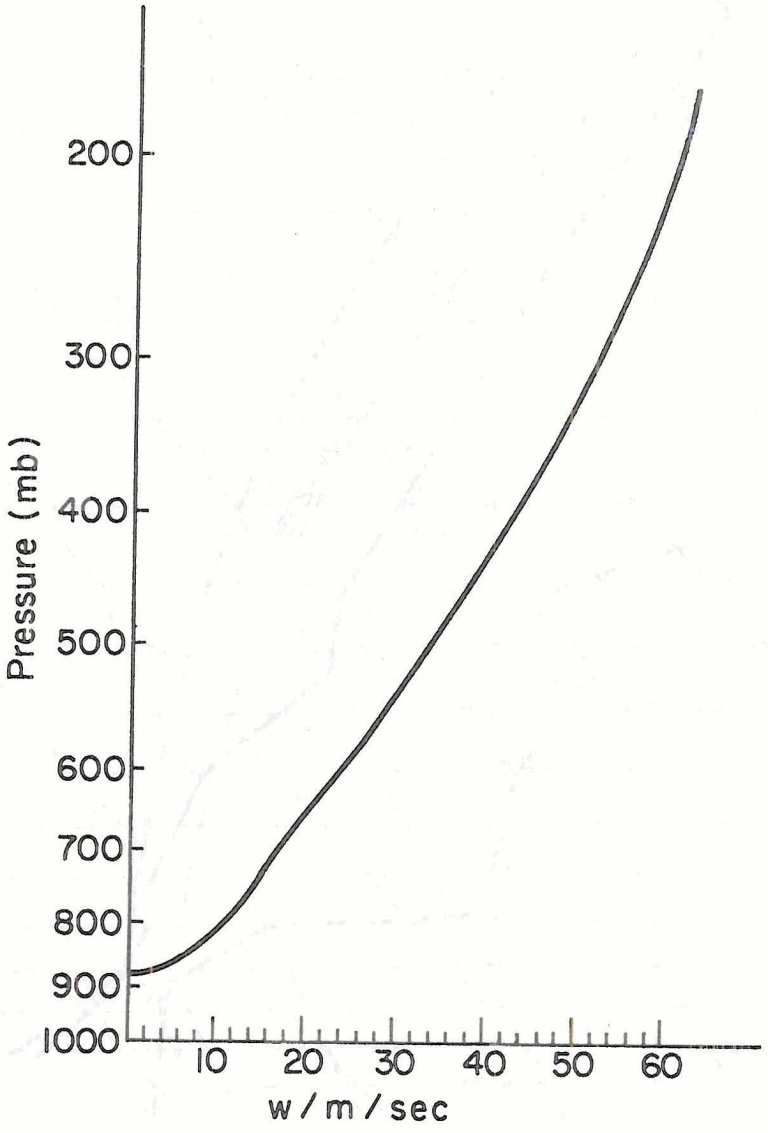

Figure 4.3-6. Predicted velocity profile of an updraft in western Oklahoma based on 0000Z OKC sounding.

updraft perimeter is circular with a diameter of 6 km (Brandes 1978, Heymsfield, 1978). Second, the updraft is assumed to have an undiluted core with entrainment effects not extending anywhere near the center (Newton, 1963). Finally, it is assumed that the air feeding into the updraft originates from the subcloud layer (Marwitz, 1972). Thus, initial tilting of horizontal vorticity by the updraft effects air inflowing into the thunderstorm between the surface and cloud base which ascends through the mid troposphere.

Subcloud vertical wind shear can be approximated in real time by combining surface wind data and satellite cloud tracked wind vectors of low level cumulus bases. The tracking of the cloud bases prevents contamination of the wind vector data by vertical wind sheer within the cloud. Figure 4.3-7 illustrates low level cumulus wind vectors computed between the times 2114Z-2122Z during the early stages of the severe storm complex's lifetime. Cloud bases are estimated at 1.5 km above the ground based on OKC rawinsonde data and stereographic image techniques (Hassler, 1981). All cloud vectors exhibit a southwesterly flow with a direction between 185 and 225 degrees at speeds ranging from 9-15 m sec^{-1}.The 2100Z OKC surface wind is measured at 6 m sec^{-1} from 160 degrees which means the wind continues to veer with height in association with warm advection and Ekman veering (Holton, 1979). Such vertical sheer is favorable for increasing vorticity through the tilting term at mid levels where:

$$\frac{\Delta w}{\Delta y}\frac{\Delta u}{\Delta z} > 0 \text{ and } \frac{\Delta w}{\Delta x}\frac{\Delta v}{\Delta z} < 0.$$

Using the mean cloud tracked wind velocity as 210^{o}, 12 m sec^{-1} and assuming an average maximum updraft speed of 20 m sec^{-1} (based on Figure 4.3-5) with a total updraft diameter of 6 km, we have:

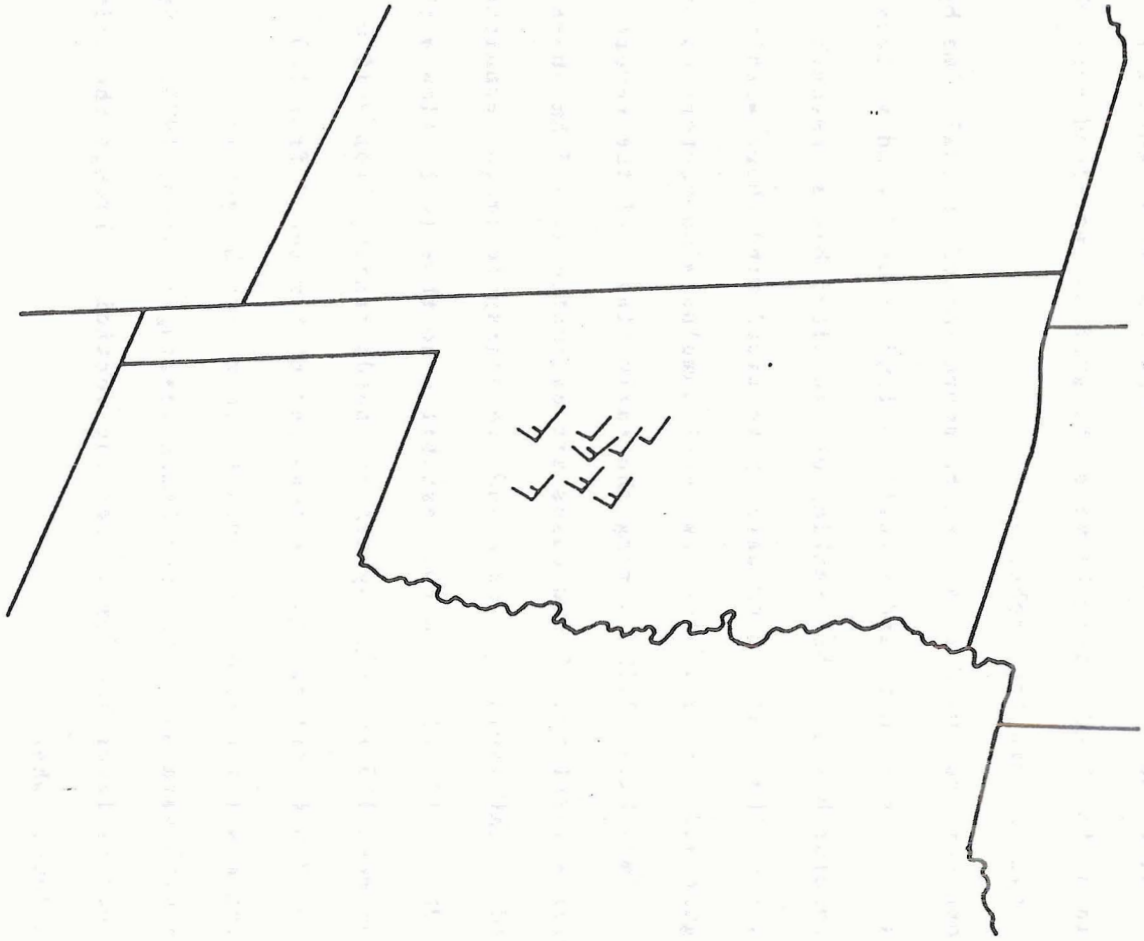

Figure 4.3-7. Selected wind vectors of low level cumulus tracked in central Oklahoma between 2114Z and 2122Z.

$$\frac{\Delta\xi}{\Delta t(\text{tilting})} = \frac{\Delta w}{\Delta y}\frac{(u_{1.6km} - u_{sfc})}{1.5km} - \frac{\Delta w}{\Delta x}\frac{(v_{1.6km} - v_{sfc})}{1.5km} \simeq 4 \times 10^{-5}\,sec^{-2}$$

The calculation for vorticity generation through tilting is similar to that for convergence in that it represents a lower limit based on the environment during the earliest stages of convection. It is an attempt to identify features in the subsynoptic scale environment favorable for mesocyclogenesis. As the storm intensifies flanking downdrafts and dynamic and hydrostatic pressure perturbations will act to increase the subcloud vertical sheer and the vertical velocity gradient and thus tilting generation in the mesocyclone can become much greater especially in the mid troposphere (Heymsfield, 1978). It should be mentioned that the vertical sheer is non linear through the lower 1 km due to boundary layer effects (Holton, 1979). This factor should not change the magnitude of the tilting term however.

The vorticity production rates evaluated here have been found sufficient to account for the circulations observed in mesocylones (Barnes, 1970, Negri, 1976, Weaver and Safford, 1979, Maddox, et. al., 1979). Since the low level ambient vorticity is of the order of 10^{-4}, the amount of time it would take an updraft to spin up to a vorticity of 10^{-2} (which is the value associated with tornado cyclones) would be under an hour assming steady state conditions. In actuality, tornadoes touched down within the first mesocyclone about 90 minutes after convection began. Thus it becomes apparent that the environment within the warm sector of the SSL was conducive to mesocyclogenesis because:

1. there are large values of convergence so to trigger an updraft;

2. the air is extremely convectively unstable meaning the updrafts will be intense
3. there is a large amount of ambient vorticity;
4. there is low level veering with height associated with warm advection and Ekman veering in this region.

4.4 Remote Sensing and Surface Observations of the Mesocylones

The 2000Z surface-radar composite analyses from the OKC radar (Figure 4.4-1) shows a light rainshower north of OKC was continuing to maintain the mesofront there. It was between 2000Z and 2100Z (see Figure 4.4-2) that explosive convective growth occurred between END and GAG, in the zone of high convergence near the triple point. On the satellite picture (Figure 4.4-3) shadows from the overshooting top almost coincide with the 2100Z thermal boundary intersection. Fifteen minutes later, baseball size hail was falling at Waynoka indicating a supercell storm with an extremely vigorous updraft. Infrared (IR) temperatures (Hasler, 1981) at this time were as low as -65°F in the anvil tower which is 5°F colder than the tropopause temperature based on the 0000Z OKC sounding. Thus, there is evidence that mesocyclogenesis and attendent severe weather is underway (Wexler, 1977 and Reynolds, 1980). Henceforth this first cell will be referred to as the Lahoma storm.

The 2130Z OKC radar (Figure 4.4-4) depicts another cell evolving to the west which will be designated the Orienta storm. Like the Lahoma storm, this cell was experiencing spectacular growth, in fact producing golf ball size hail at Moorland, OK. Curiously, radar reflectivity values were only 30 dBz at this time while satellite pictures did not exhibit an overshooting top for this storm.

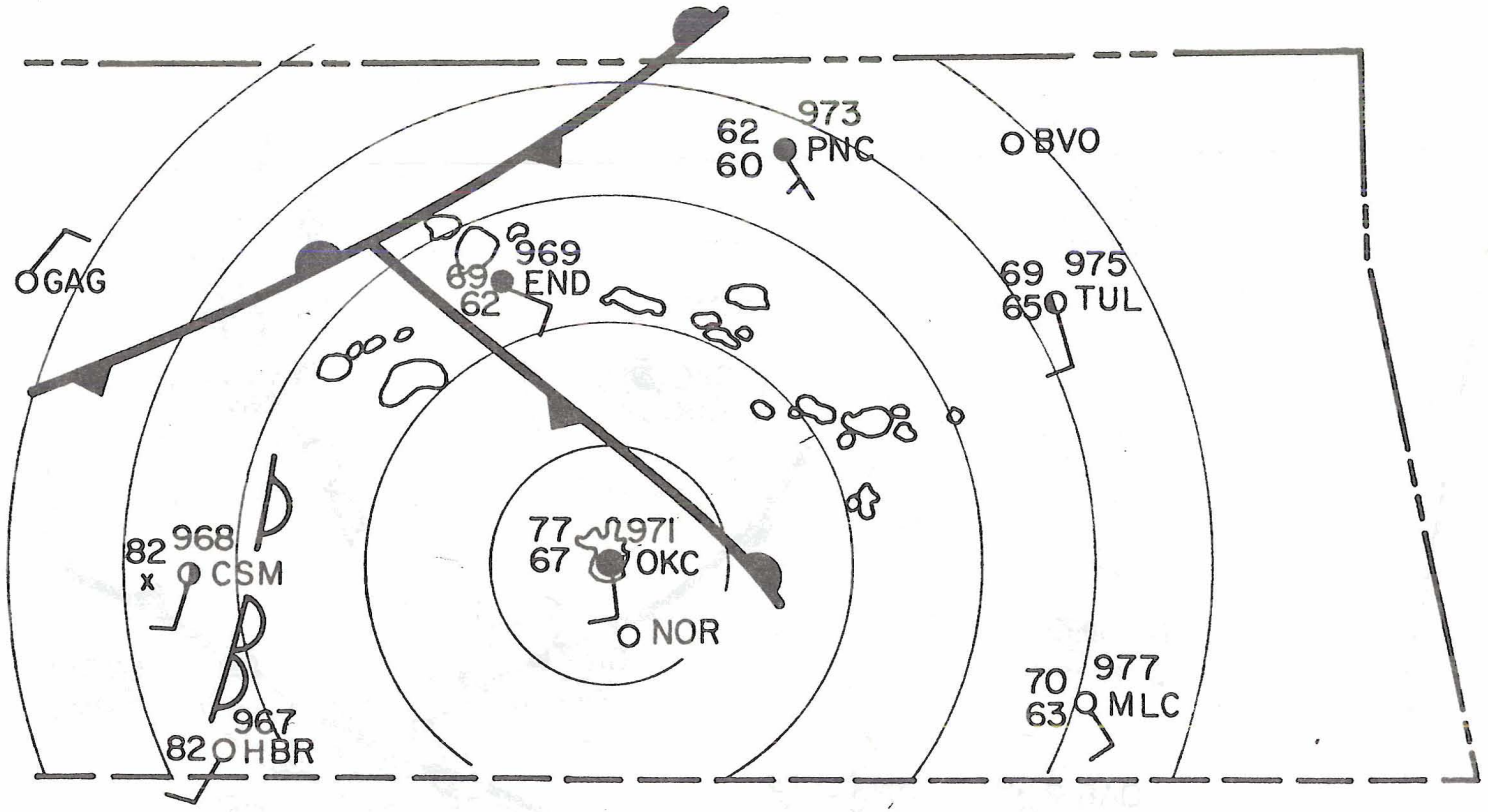

Figure 4.4-1. 2000Z surface WSR-57 OKC radar composite analyses. Reflectivity contours are at 10dB intervals. Concentric circles are plotted at 25 mile intervals from OKC.

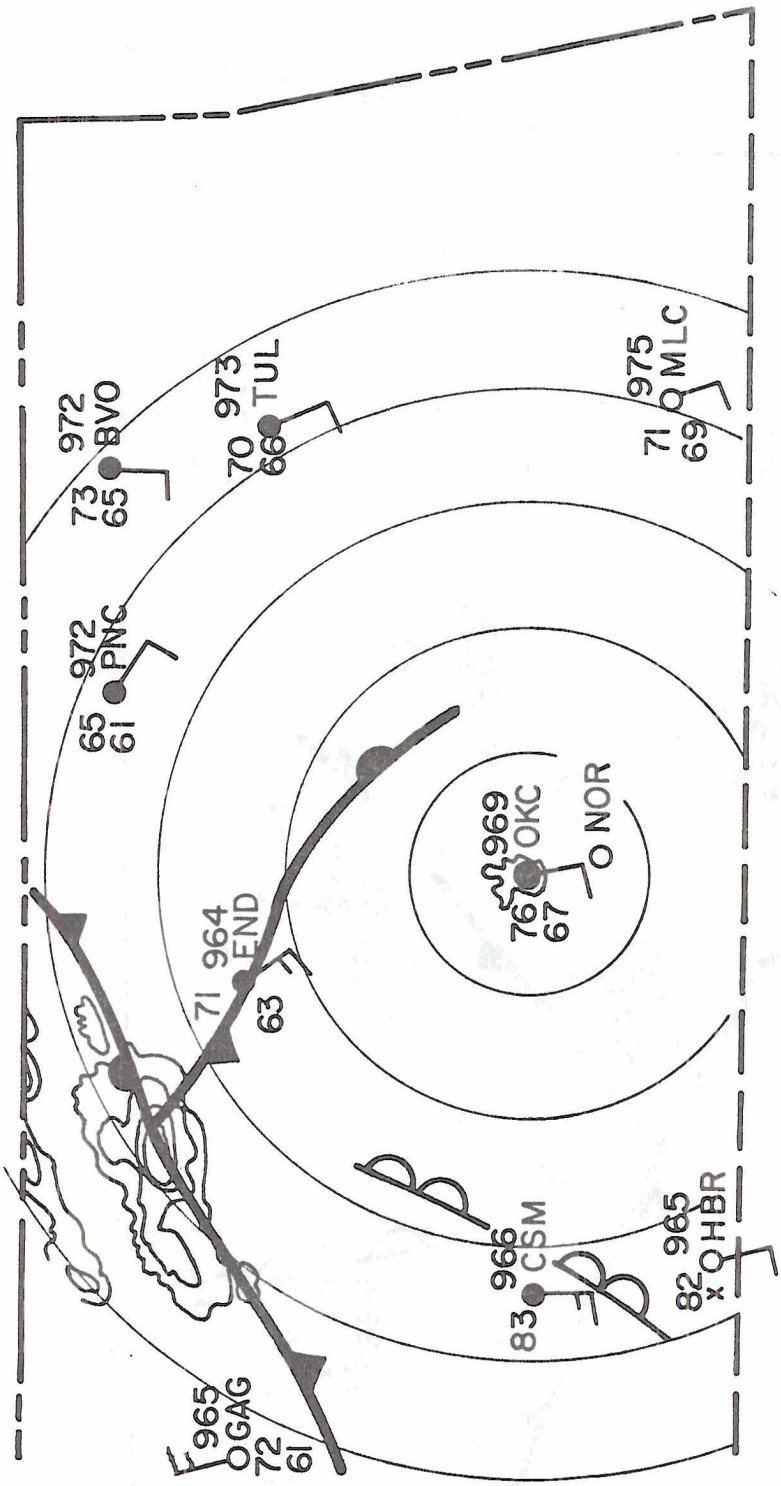

Figure 4.4-2. 2100Z surface - WSR 57 OKC radar composite analyses.

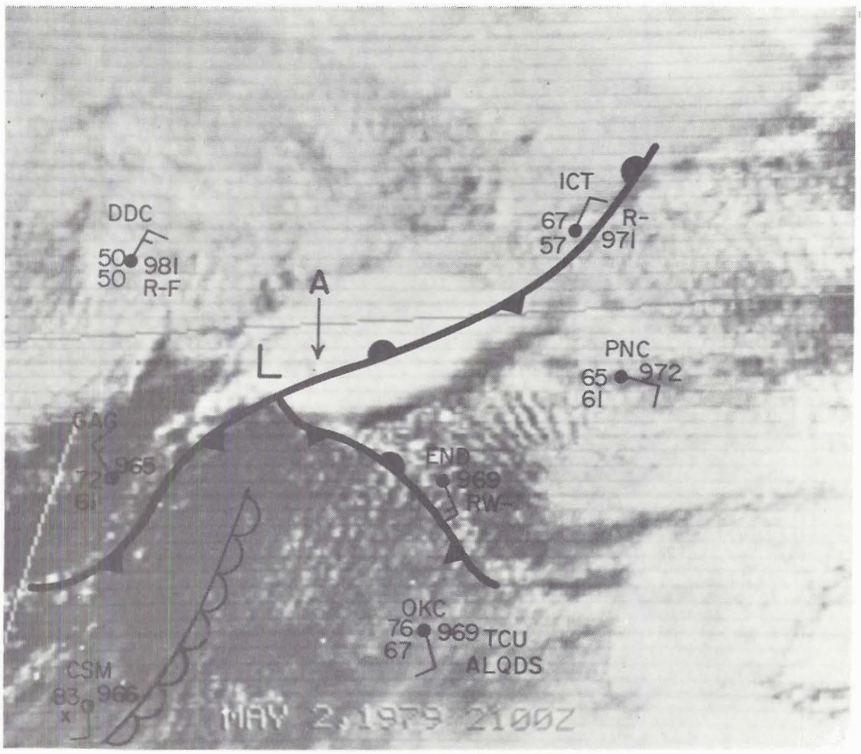

Figure 4.4-3. 2100Z satellite-surface mesoscale analyses. A designates tower of Lahoma storm

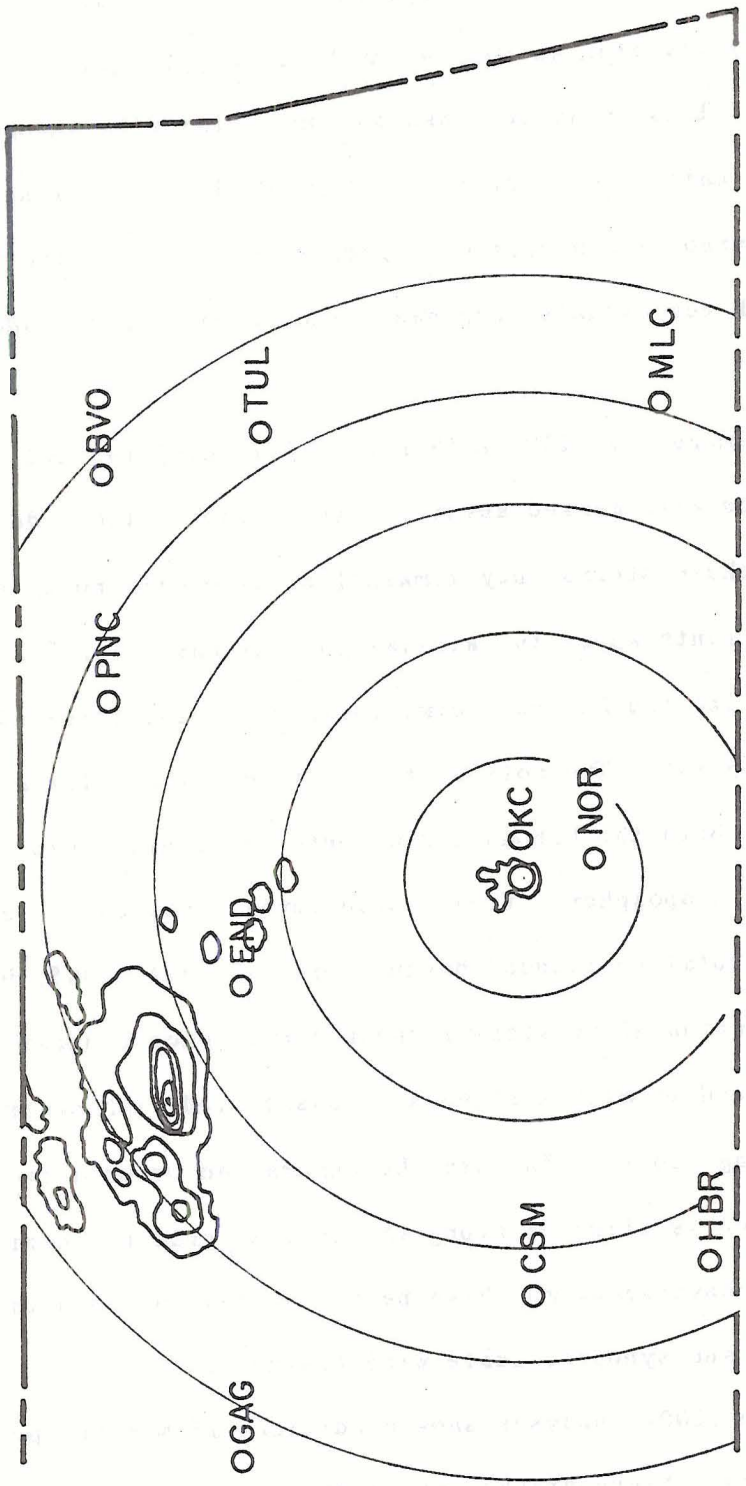

Figure 4.4-4. 2130 WSR 57 OKC radar reflectivities.

But by 2200Z (Figure 4.4-5), OKC radar echoes depict both storms at over 50 dBZ with heights measured by the radar to be at 60000 ft. (Storm heights attributed by radar are generally higher than that detected by satellite data. See Reynolds, 1980). Figure 4.4-6 depicts 2212Z cell refelctivities as seen by NCAR CP3 Doppler radar located at Roman Nose, OK. This radar unit was not only closer to these storms than the WSR-57 unit at OKC but had a shorter (3 cm) wavelength. Thus it was able to resolve 2 hooklike or pedant echoes which the OKC unit could not. Such echoes have long been associated with tornadocyclones (Fujita, 1965).

Satellite imagery at 2200 Z (Figure 4.4-7) displays two overshooting tops with marked anvil growth. Despite the sudden development of these storms they remain localized with no disturbances anywhere to the south where the air was just as unstable. In fact the Orienta storm, like the Lahoma storm, appears to experience rapid growth near the triple point. The motion of the storms also gives a clue to their severity. Both the Lahoma and Oriento cells are moving to the right of the mid tropospheric flow. Such deviate motion has been attributed to a rotation induced Magnus force (Fujita, 1965, Heymsfield, 1978) and propagation along storm induced convergence boundaries (Weaver, 1979), and in most instances is associated with severe supercell rotating storms. In both the Lahoma and Orienta storms it appears the motion is directed along the thermal gradient near the mesofront where convergence may have been enhanced due to both thunderstorm and sub-synoptic scale wind features.

Finally, the 2200Z analyses show conditions 15 minutes prior to tornado touchdowns. Stereographic analyses indicate tower growth

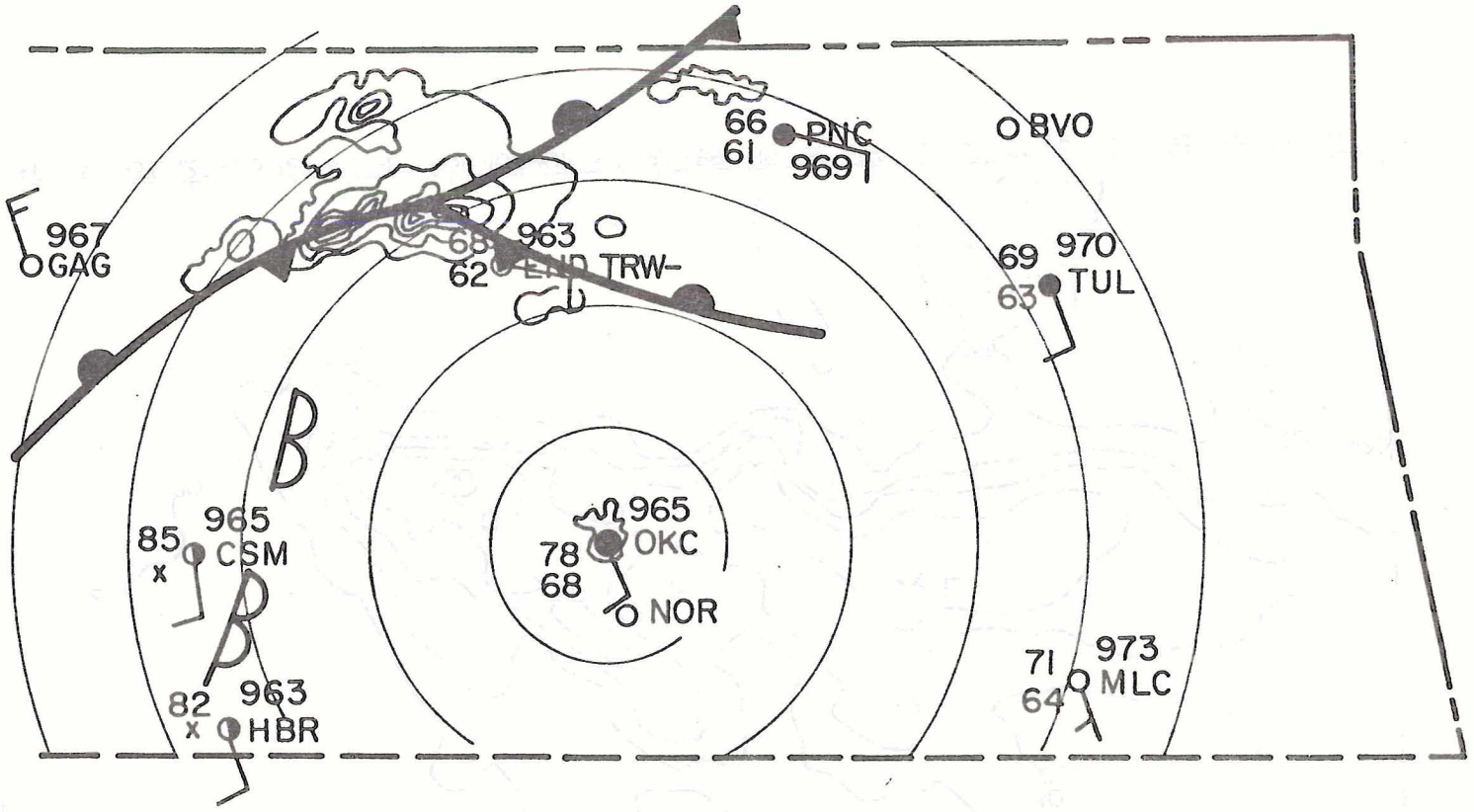

Figure 4.4-5. 2200 surface - OKC radar composite analyses.

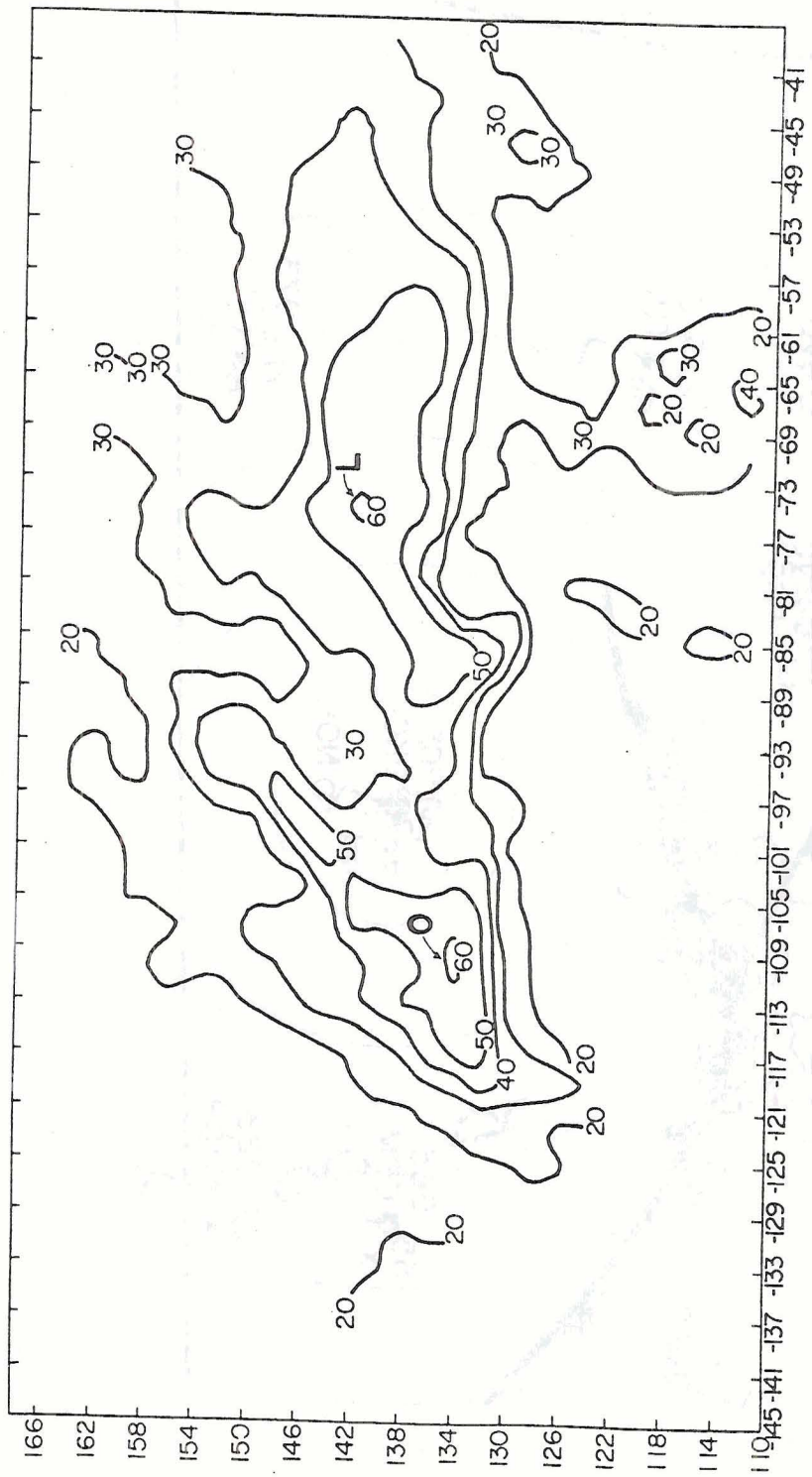

Figure 4.4-6. 2212Z reflectivities as measures of NCAR CP3 Doppler radar located at Roman Nose. Position coordinates are with respect to Norman, Oklahoma. L, O represent echo centroids of Lahoma and Orienta storms respectively.

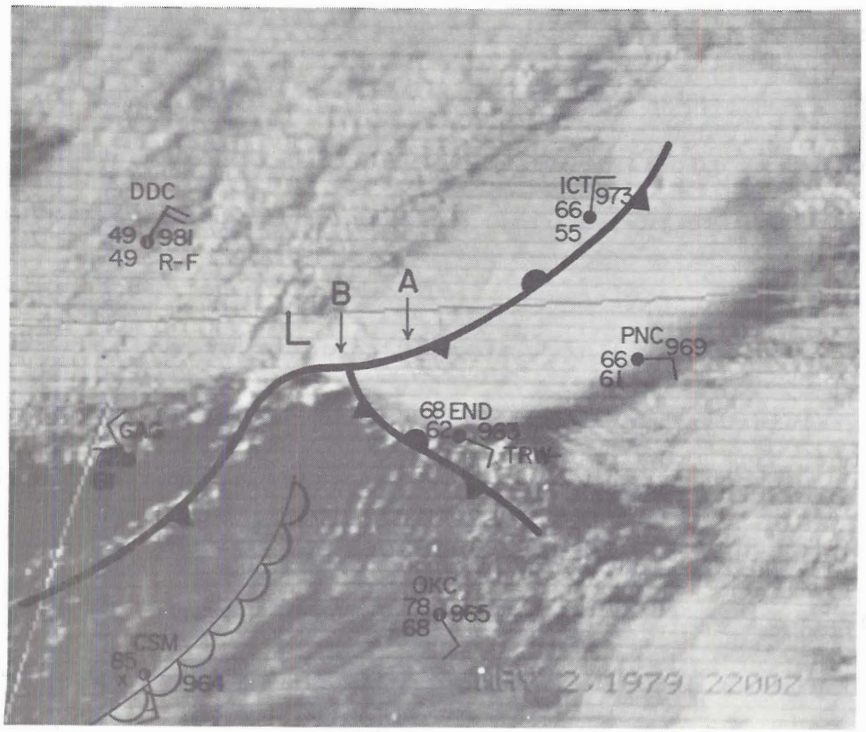

Figure 4.4-7. 2200Z satellite-surface mesoanalyses. B designates tower of Orienta storm.

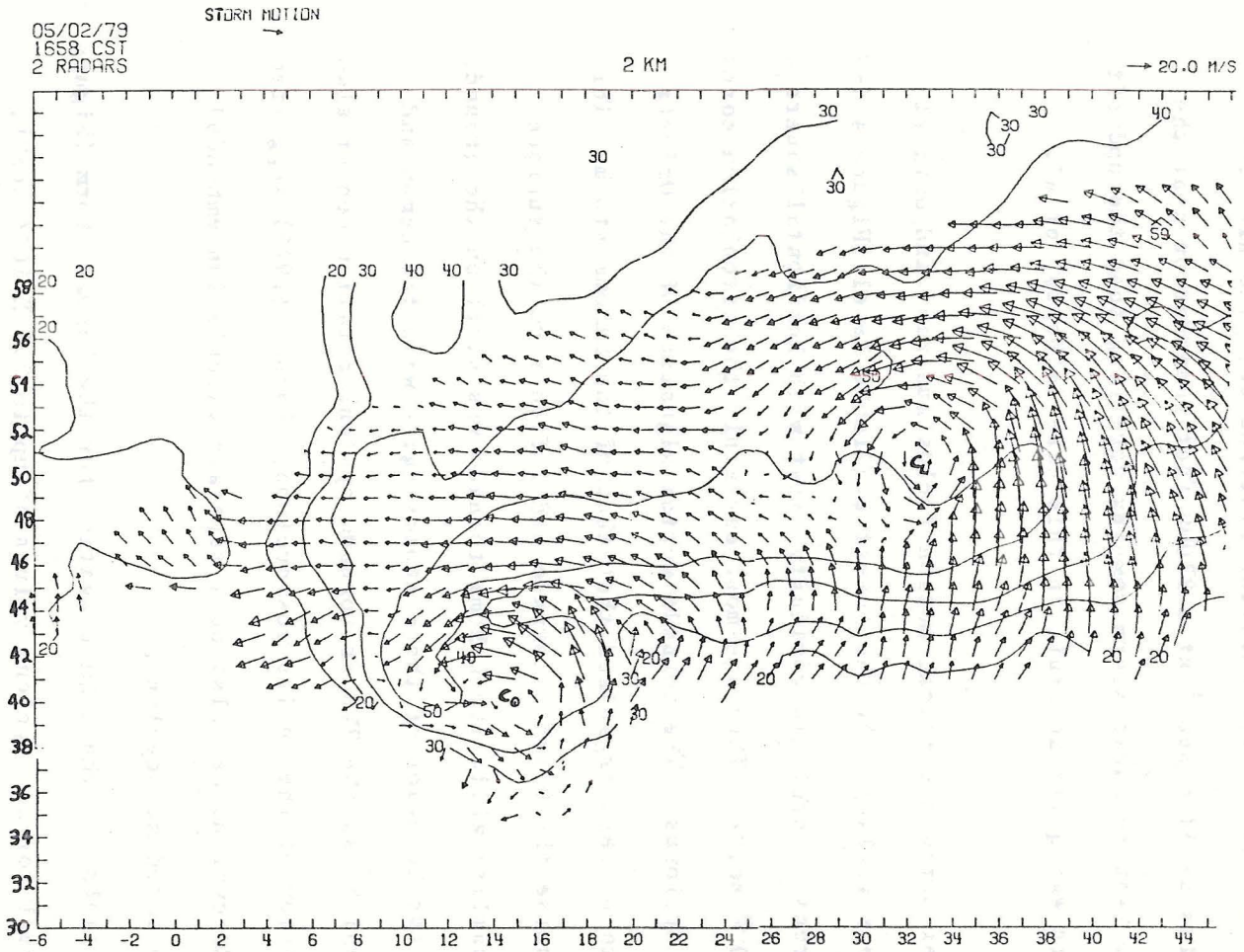

Figure 4.4-8. 2258 dual Doppler storm relative wind fields for 2 km elevation. Position coordinates are with respect to Roman Nose. C_L and C_O designate circulation centers of Lahoma and Orienta mesocyclones respectively. (Courtsey of N.S.S.L.) Vector length of one km corresponds to wind speed of 10 m sec^{-1}. Storm velocity vector given at top of figure. Reflectivity contours also given.

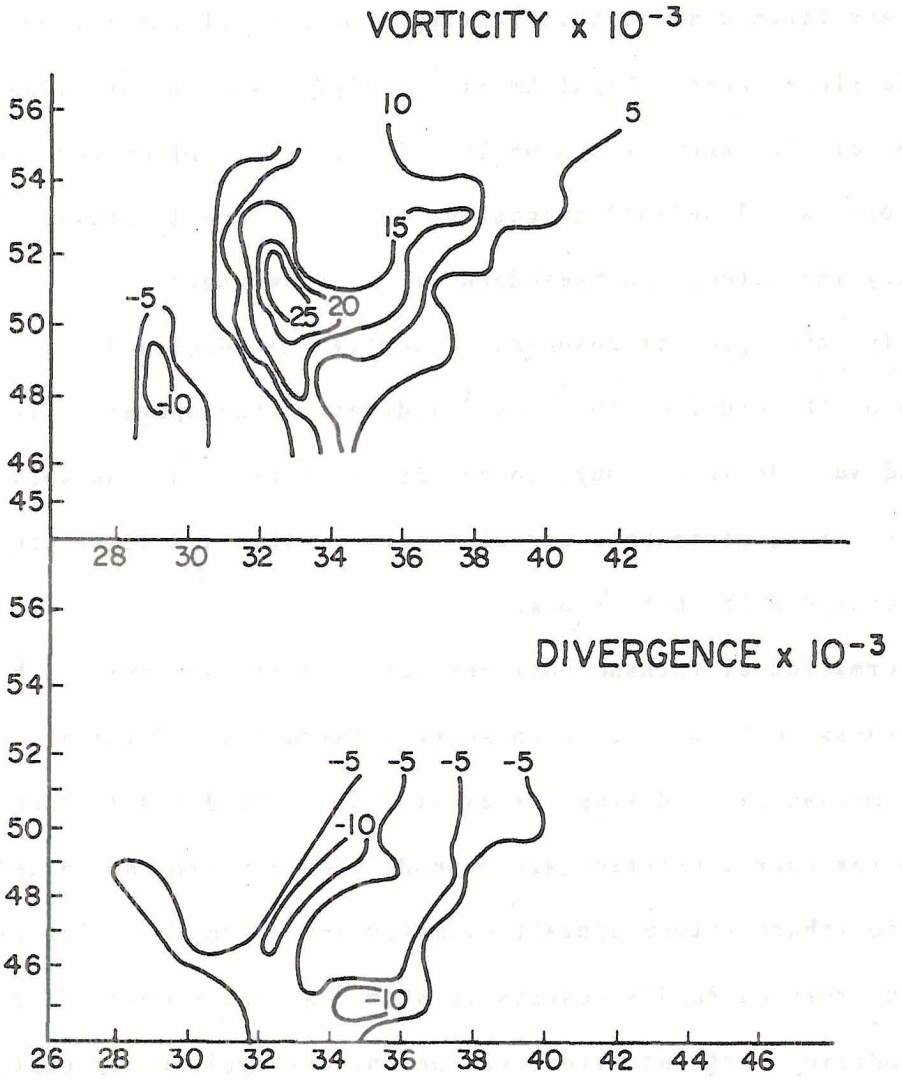

Figure 4.4-9. Vorticity and divergence fields for the Lahoma tornado cyclone based on the 2258Z 2 km wind fields. Units are sec^{-1}.

4.4-10). This agrees with observations that during the tornado phase, the mesocyclone is no longer just a warm updraft but a two-cell cyclonically rotating structure. Notice also there is anticyclonic flow near the rear flank downdraft indicating some sort of outflow boundary may have developed here. Eight km winds (Figure 4.4-11) still show a marked TVS for the Lahoma storm while cylconic circulation for the Onienta storm is ill defined suggesting that the tornado dissipation may be initially indicated by a breakdown of the flow aloft.

Finally, the upper tropospheric flow (14 km) (Figure 4.4-12) shows divergence of the order of 10^{-3} sec^{-1} indicating the updraft core is intense and well defined enough to act as an obstacle to the ambient wind. This strong divergence may also play a role in surface pressure falls associated with these storms.

The formation of tornado vortices within a mesocyclone has been found by others to be dependent on several variables. Using a laboratory mechanically driven vortex simulator, Ward (1972) found that certain vortex characteristics are dependent on a parameter called aspect ratio (thunderstorm updraft diameter/inflow depth). Davies Jones (1973) reinterpreted Ward's results to show that the growth of turbulent tornado producing vortices within the parent mesocyclone circulation was dependent on the swirl ratio S where $S=\frac{V_\theta'}{\bar{w}}$. $V\theta'$ is the tangential wind speed of the air in the inflow layer at the updraft perimeter and $\bar{w}$ is the mean updraft speed.

Barnes (1978b) using surface mesonet data only, found that the swirl ratio for a tornadocyclone was at least .2. Brandes (1978) obtained a minimum value of .5 using multiple Doppler derived wind

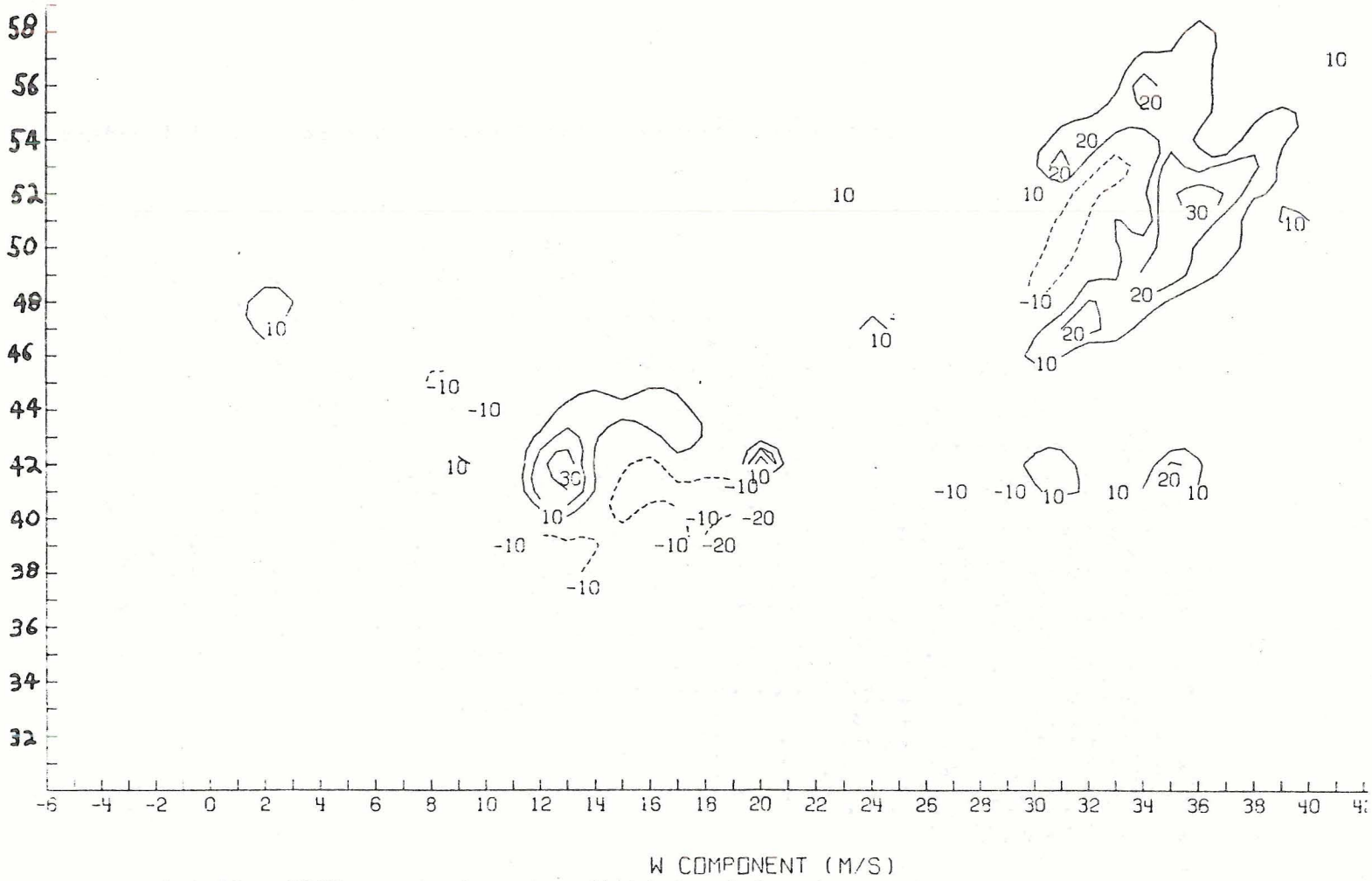

Figure 4.4-10. 2258 vertical motion field for 2 km elevation based on dual Doppler radar winds. (Courtsey of N.S.S.L.)

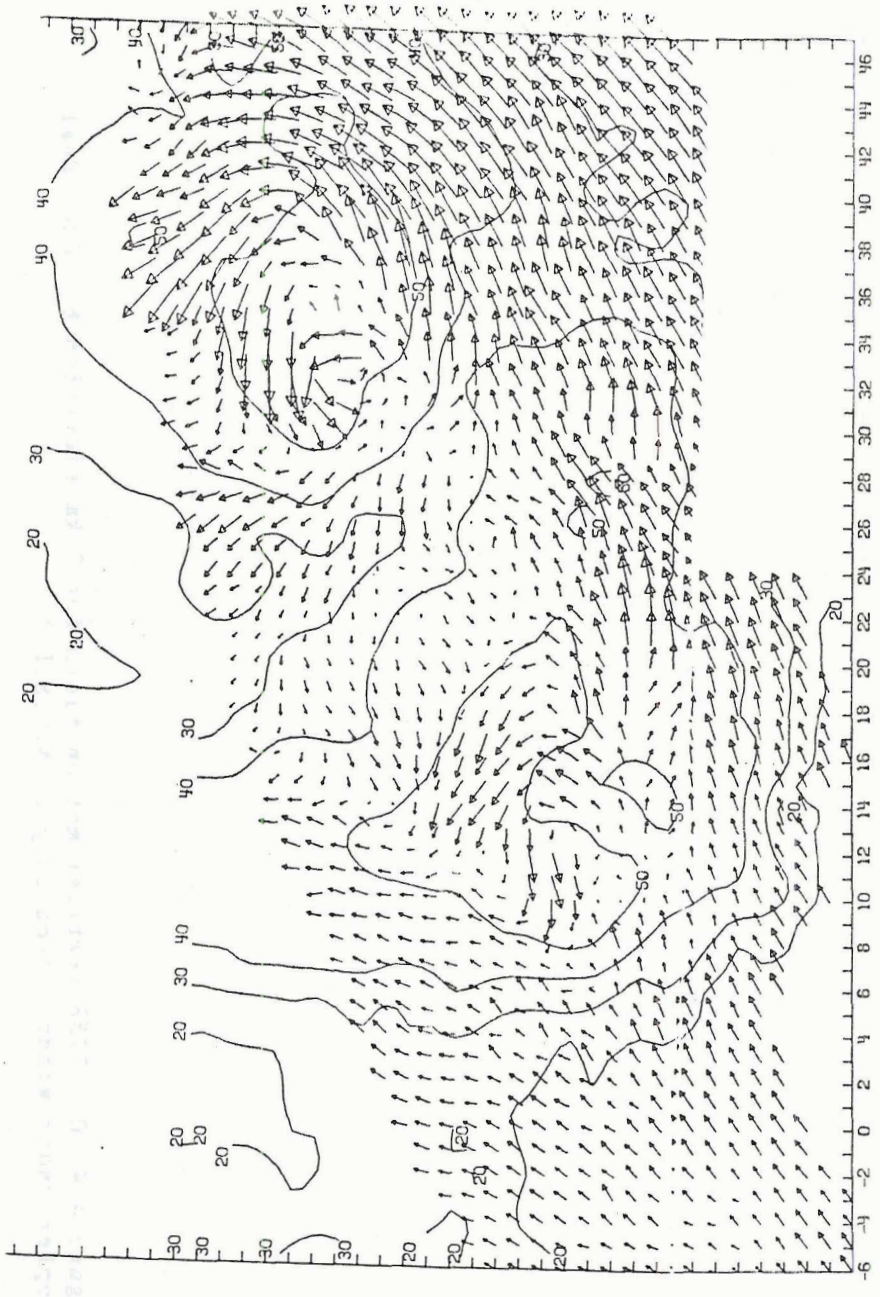

Figure 4.4-11. 2258Z 8 km wind field. (Courtsey of N.S.S.L.)

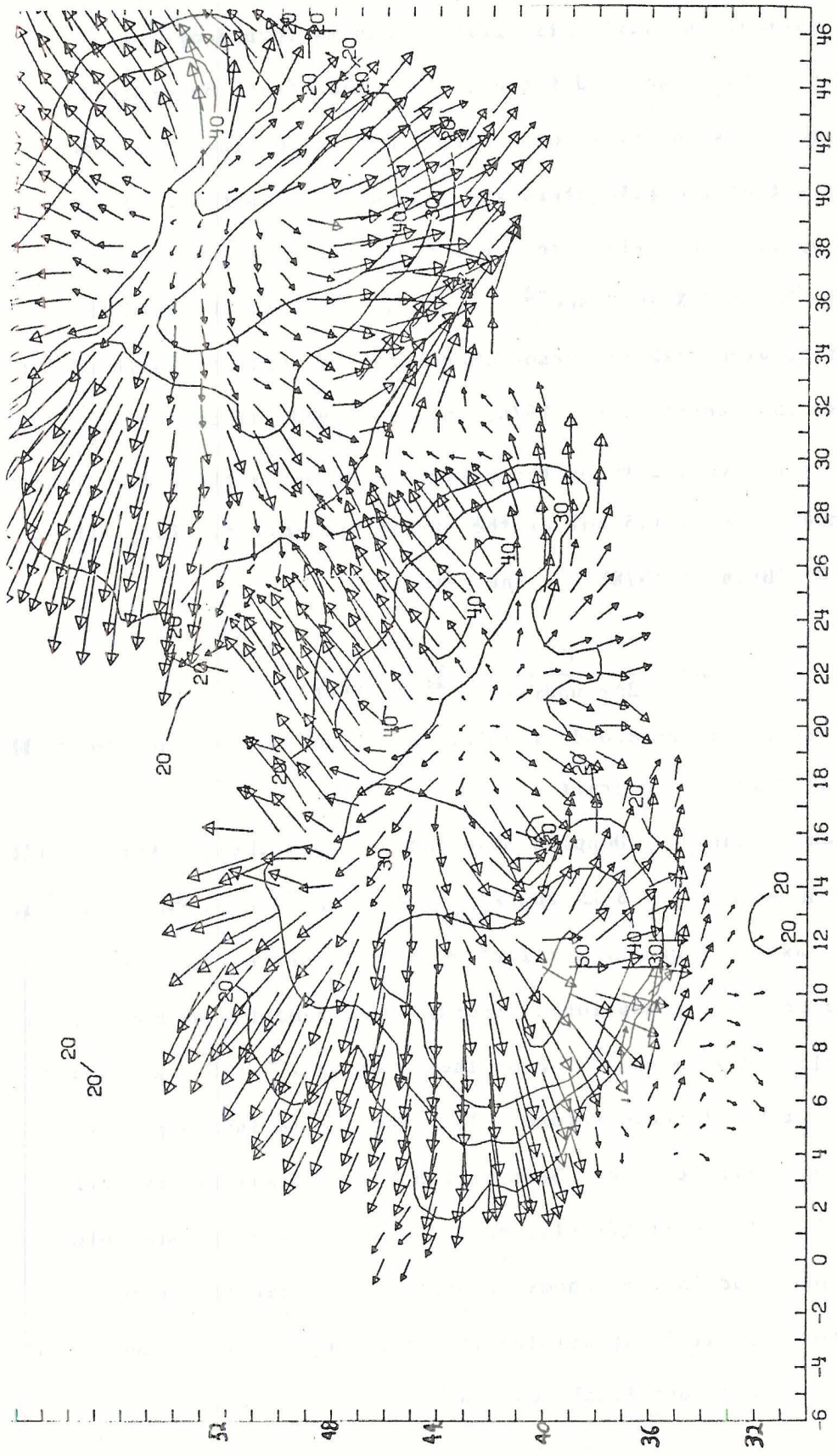

Figure 4.4-12. 2258Z 14 km wind field. (Courtsey of N.S.S.L.)

fields. From the Doppler radar available for this project it is possible to estimate a swirl ratio for the Lahoma tornadocyclone.

Using the 2258Z 2 km wind fields, it is seen that the central updraft perimeter, since it is oval shaped may be considered to have a radius no less that two kilometers and no greater than four. At the mesocyclone updraft perimeter, in the circulation core ξ was measured previously to be at 2×10^{-2} sec^{-2}. Since it has been observed that vorticity associated with the mesocyclone core is about the same at 2 km as it is near the surface (Ray, 1976, Brandes, 1978) we can let $\xi_{2\ km} = \xi_o$ where ξ_o is the vorticity of the inflow layer below cloud base (which was determined to be at 1.5 km) at the updraft perimeter. This allows us to find $V\theta'$ (Barnes, 1978b) by the relation

$$V\theta' = \frac{C_o}{2\pi r_{\ updraft}} = \frac{1}{2}\xi_o r_{\ updraft}$$

where C_o refers to the subcloud circulation. From this we have $V\theta' = 20 - 40$ m/sec for 2 km $< r_{\ updraft} <$ 4 km.

If we next examine w, Doppler observations show that in the updraft core, $w_{max} = 50$ m sec^{-1} at 8 km and $w_{max} = 30$ m sec^{-1} at 2 km and 14 km. Taking into consideration the vertical velocity profile from Figure 4.3-5 and the previously mentioned aircraft measurements, we may assume $\bar{w}$ is between 15 and 20 m sec^{-1}. From these values $1.0 < S < 2.7$ which is associated with a tornadocyclone. The increase in the tangential wind along the updraft core has been attributed to flanking downdrafts (Brandes, 1978). Since it has also been shown that the maximum values of vorticity occurred in the Lahoma tornadocyclone near the updraft-downdraft interface, it is speculated that tornadogenesis was dependent on the descent of the rear flank downdraft for this storm.

Echo position is also an important factor in supercell life cycles. Storms which move nearly parallel to the low level heat and moisture tongue can destructively interact as the southernmost cell absorbs the unstable air flow at the expense of those to its north (Haglund, 1969). However, in this case the first two cells could mature into tornado cyclones because they formed and moved perpendicular to the low level air flow. But it does appear the Orienta system's close proximity to the Lahoma storm may have partly played a role in an occlusion of its mesocirculation. An examination of the 2 km winds and vertical velocity fields reveal downdrafts existed along the southern and eastern flanks of the Orienta updraft. CP3 radar reflectivity data for 0km (Figure 4.4-13) at 2229Z reveals the pedant associated with the Lahoma storm was about 40 km from the refelctivity core of the Orienta storm. Pedants or hooks have been ifentified with the leading edges of gust fronts (Hagland, 1969), behind which may be cool mesoanticyclones. In fact, in Figure 4.4-8 one sees there is anticyclonic flow corresponding to the Lahoma storm's rear flank downdraft. Thus, it may be inferred the orientation of the Oreinta and Lahoma storm downdrafts cut off the warm moist unstable air feeding into the former cell's updraft. In fact, thunderstorm chase teams on this day noticed that outflow from the Lahoma storm moved into the vicinity of the Onienta cell's updraft (Bluestein, Weaver, personal communication).

The interaction between these storms continued to influence surface weather events into the next hour. The Magnus force has been attributed to causing a rotating storm to decrease in speed as well as move to the right (Heymsfield, 1978, Fujita, 1965). Conversely as storms weaken and their rotation breaks down they should accelerate. Though dual Doppler

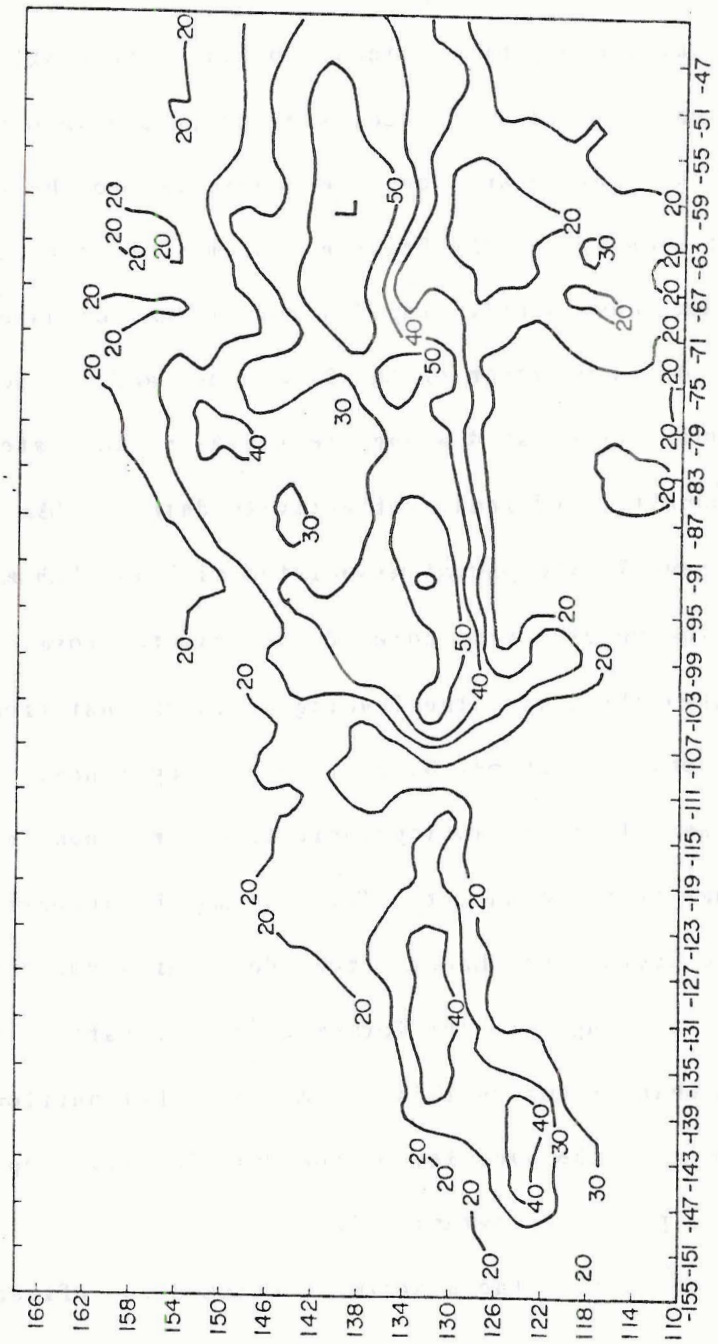

Figure 4.4-13. 2229Z NCAR CP3 radar reflectivities for 0 km elevation.

data is not available for both storms before 2247Z, echo centroids for these cells could be tracked for the period between 2212Z and 2229Z when both storms were tornadic (The Lahoma and Orienta tornadoes touched down at 2215Z and 2217Z respectively). In this time period both storms had velocities of about 15 m sec^{-1} moving from 285°. After 2247Z, it was possible to track these storms through the motion of their circulation centers derived from dual Doppler radar. An examination of the low level wind field (Figures 4.4-14 and 4.4-15) shows the circulation of the Orienta mesocyclone was definitely breaking down while that of the Lahoma storm remained intact even though its tornado had lifted by 2247Z. Correspondingly, we see in Figure 4.4-16 that the Onienta storm first accellerated and generally moved faster than the Lahoma storm between 2247Z and 2314Z.

Storm motion and accelleration has also been attributed to gust front forcing (Barnes, 1978b). On this particulr day, a strong gust front developed near the pedant of the Onienta storm. F1 and F2 force westerly straight lined winds destroyed a trailer home north of Ames while trees, power lines, and roof damage occurred between Vance AFB and Waukomis. Thus by 2330Z, the rapidly moving Orienta storm merged with the Lahoma cell with it's gust front moving to the southern flank of the Lahoma's cell mesocyclone core (Figure 4.4-17).

Gust front interaction between storms has been shown to increase covergence and cyclonic wind shear (Weaver and Nelson, 1982). Perhaps this is what happened during the Onienta-Lahoma storm mergers because by 2347Z, a third tornado of F2 intensity evolved within this system west of Marshal. Storm merger here could have been responsible for the

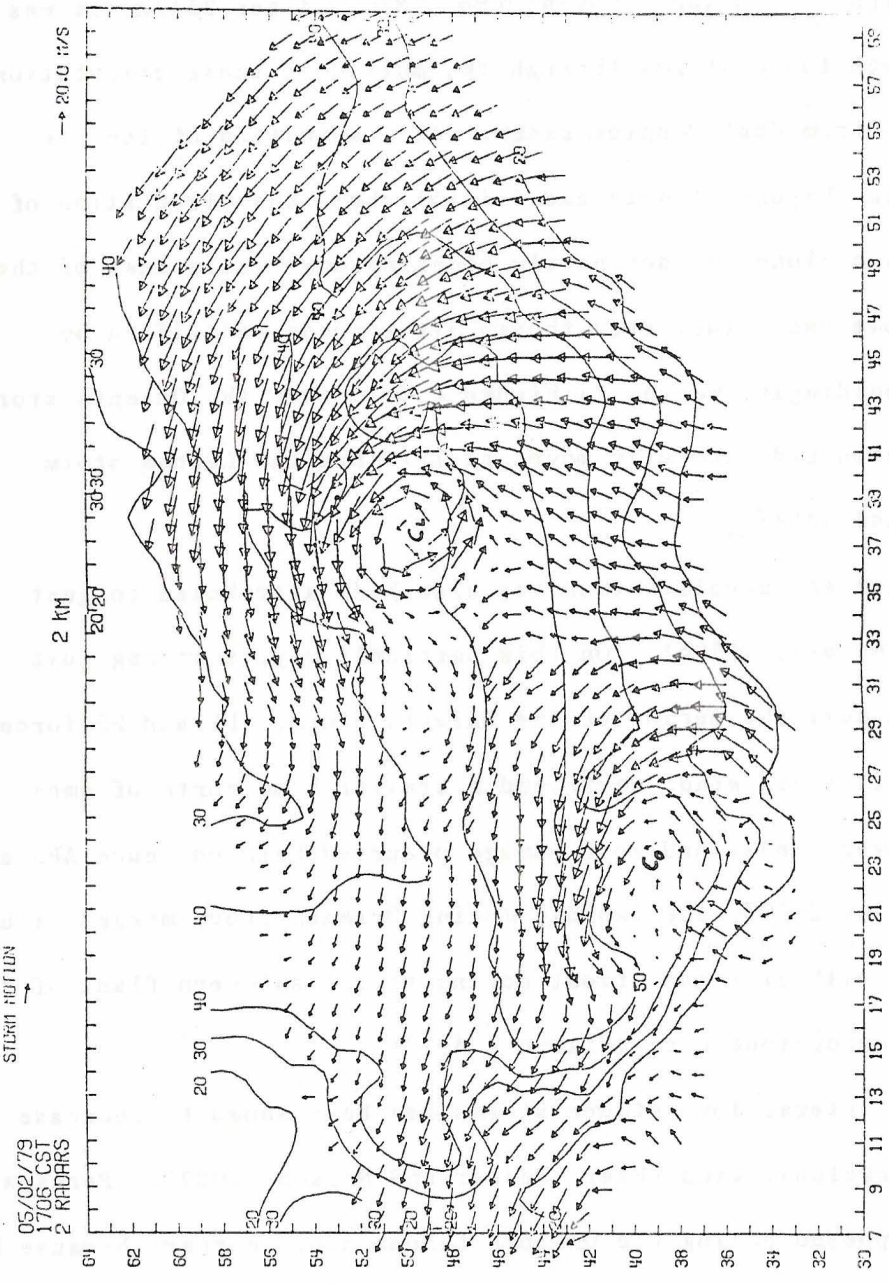

Figure 4.4-14. 2306Z 2 km Doppler derived wind fields. (Courtsey of N.S.S.L.)

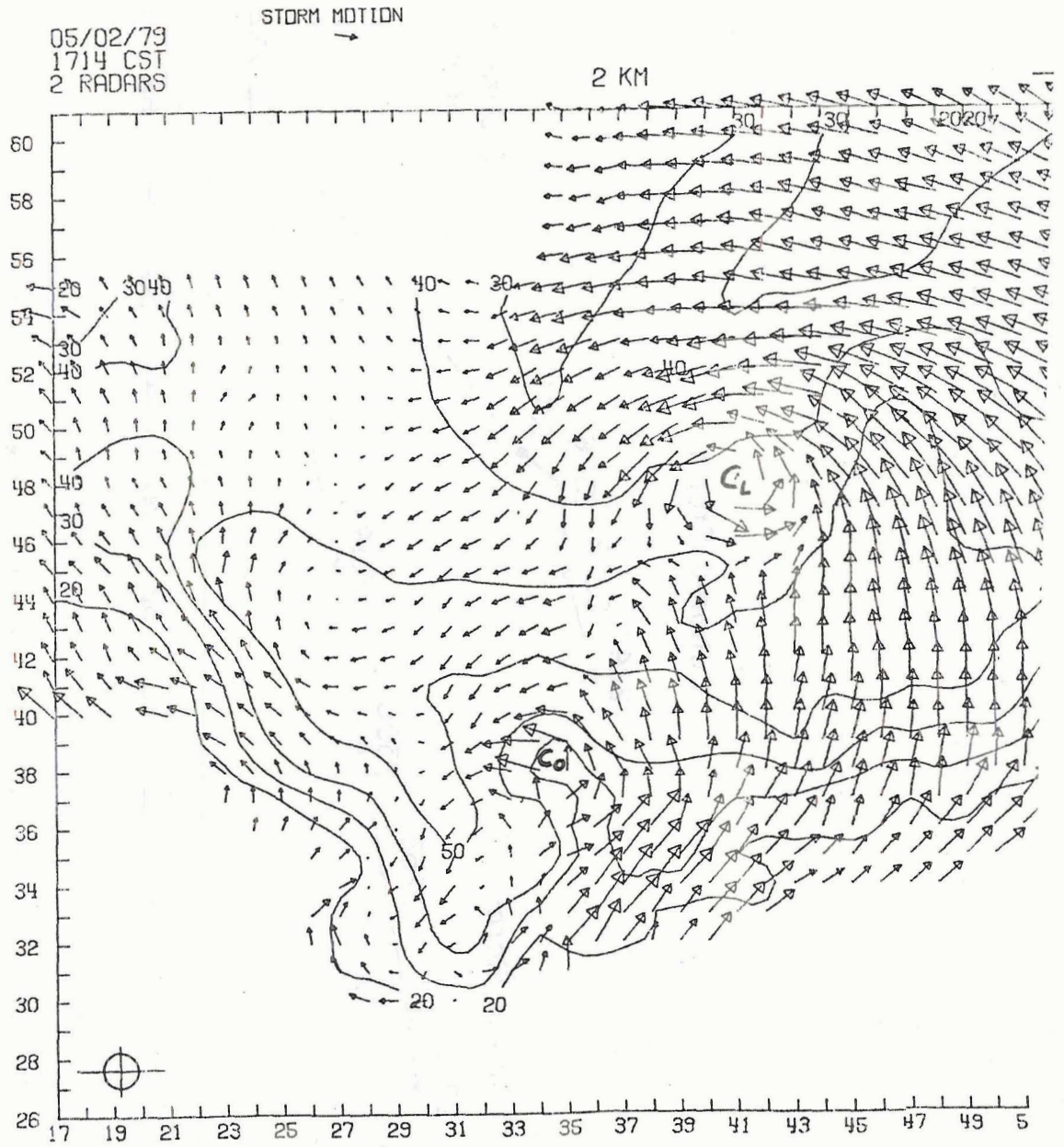

Figure 4.4-15. 2314Z 2 km Doppler wind fields. (Courtsey of N.S.S.L.)

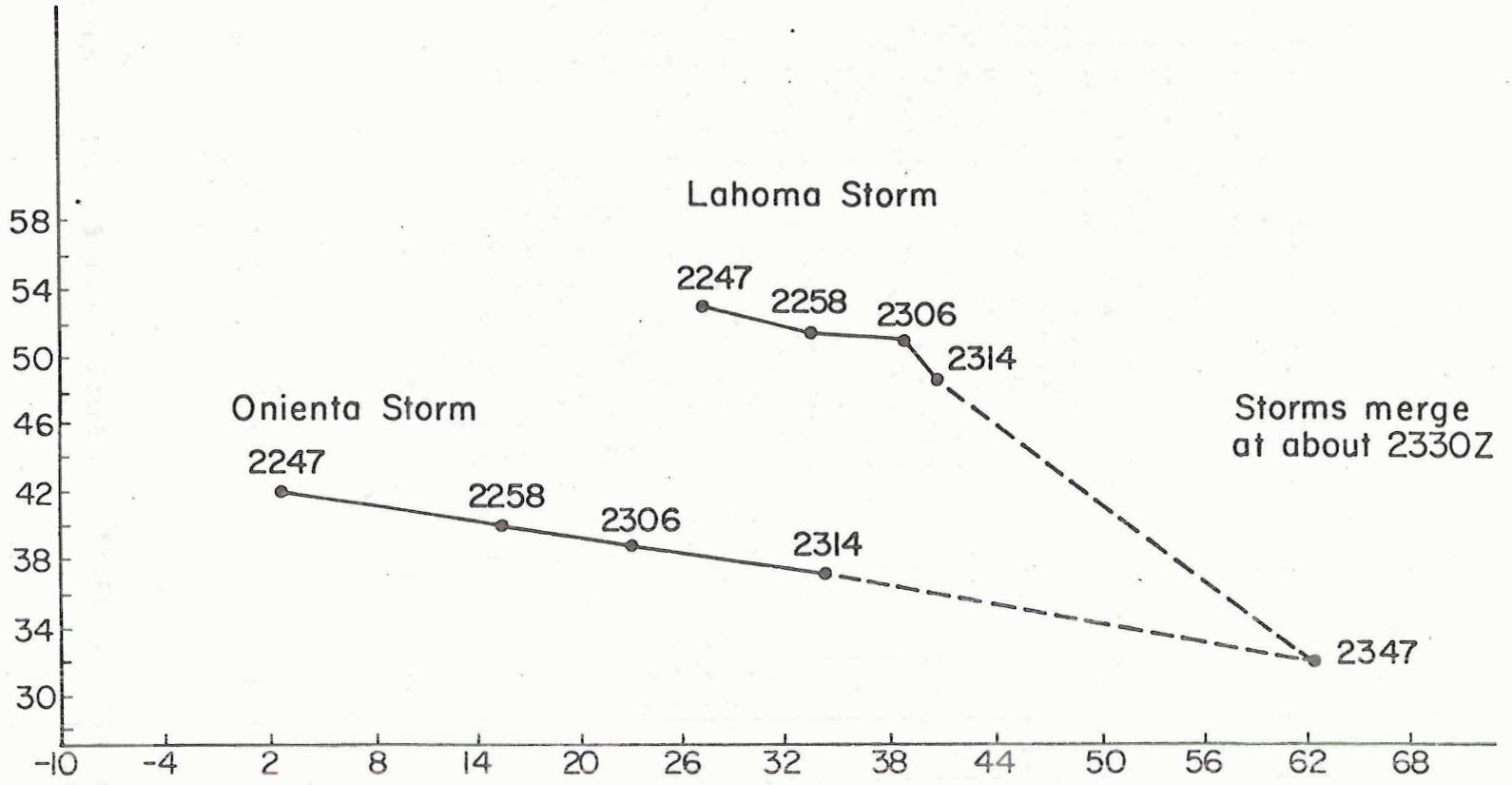

Figure 4.4-16. Positions of Orienta and Lahoma mesocyclones with respect to Roman Nose.

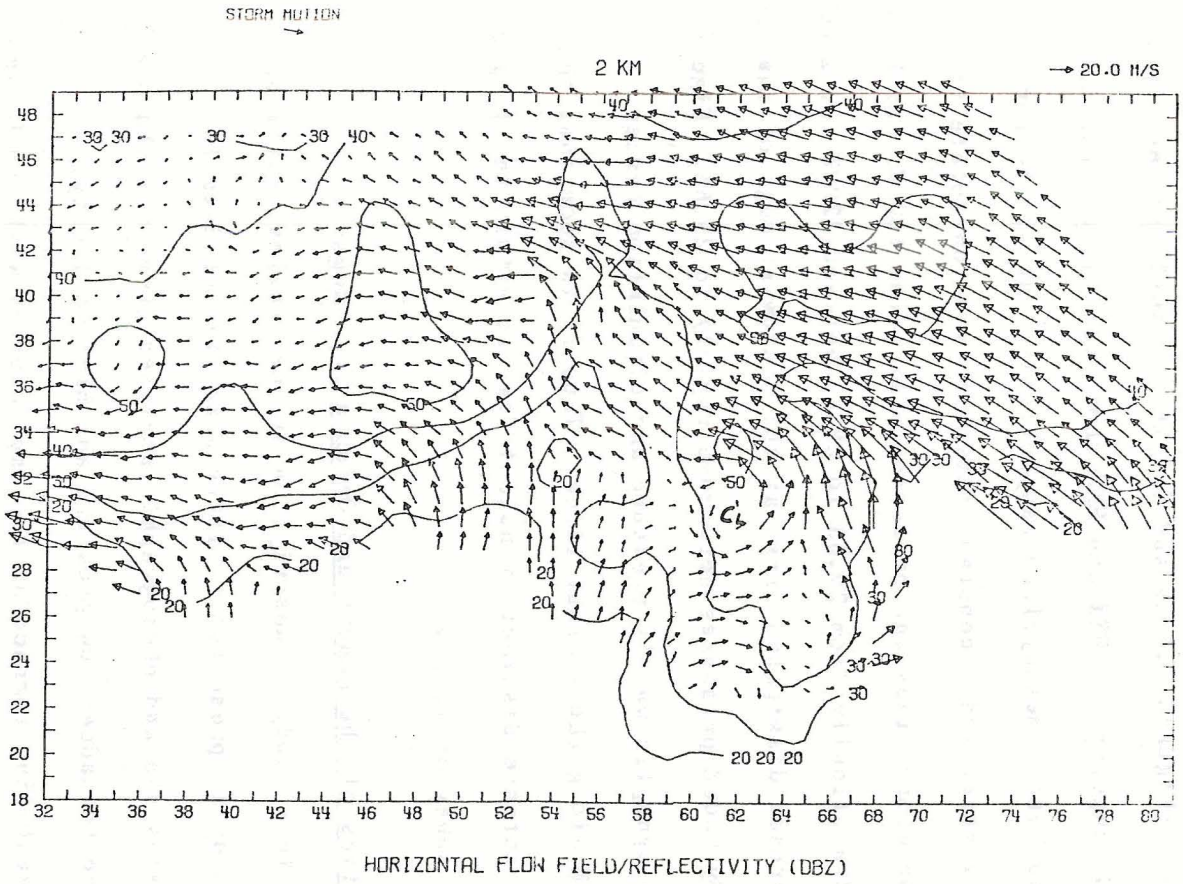

Figure 4.4-17. 2347Z 2km Doppler wind fields. (Courtsey of N.S.S.L.)

reintensification of the Lahoma mesocyclone due to the flanking gust front of the Onienta storm.

Not analyzed in this study is the presence of a third supercell which also formed at the triple point at about 2300Z (Figure 4.4-18). This produced softball sized hail and two small tornadoes.

Time sections (Figures 4.4-19 and 4.4-20) of surface pressures, temperatures and dewpoints at FSI and END show stations closest to the SSL's cyclone and Lahoma mesocyclone respectively. At the former station, clearing skies and a constant southerly wind correlate to significant temperature rises and pressure falls after 1800Z. At Enid, pressures fell dramatically from 29.63 to 29.47 between 2200Z and 2300Z as the Lahoma tornado dissipated first at the southwest edge of the town (Figure 1-1). By 0000Z pressures here rose rapidly to 29.65. Figure 4.4-21 shows the synoptic wave's pressure and circulation center remained near CSM along the thermal ridge. Thus it is seen that the mesocylones were intense distinct transient feature within the larger scale system, the subsynoptic low.

4.5 Characteristics of the Lahoma and Onienta Tornadoes

To complete this study, a description of the smallest scale of cyclone, the tornado is presented. Little quantitative data is available but rawinsonde and photographic analyses give some clues as to the origins of the tornadoes low pressure and high vorticity.

The most devastating tornado of the day occurred with the Lahoma storm, so called because the associated tornado heavily damaged the town of Lahoma, OK. Damage reached F4 levels as farm buildings, a community building, grain elevators, and some mobile homes were among the structures destroyed (Alberty, et al., 1979). Total casualities from

this tornado were: one dead, and 25 injured with millions of dollars worth of damage (NOAA, 1979).

From Equation 3.4.1 the tangential wind velocity is dependent on the pressure gradient of the tornado. Put in another way, the wind intensity is proportional to the gradient of the perturbation pressure the disturbance imposes on the environment.

For a rotating updraft (which is essentially what the vortex core is), if we consider it's entire column, we can neglect dynamic pressure effects due to its upward accelerations. This allows us to attribute the surface pressure deficit at the base of the updraft solely to hydrostatic effects due to the updraft core being warmer than the undisturbed surrounding environment.

The pressure perturbation at the surface may be expressed by the relation:

$$\left[\frac{-p}{pe}\right]_o^H = \frac{g\,H\,\hat{\bar{T}}ve}{R\,\bar{T}ve^2} \qquad (4.5.1)$$

where pe is the ambient pressure before the updraft exists, p the pressure change within the updraft column, H is the height of the updraft, $\bar{T}ve$ the mean virtual temperature of the air surrounding the updraft column, and $\hat{\bar{T}}ve$ is the mean deviation of virtual temperature of the tornado updraft compared to the environment (Davies Jones and Kessler, 1974). Using the approximate parcel equilibrium level on the 0000Z OKC sounding gives (Figure 4.3-5) H = 12060 m, $\bar{T}ve = T(1+.61q) = 261^{\circ}K$ and $\hat{\bar{T}}ve = 6$.

If p is assumed to be 0 at the equilibrium level H, then p at the surface is -35 mb or -1.05 inches which is an estimate of the hydrostatic pressure deficit in the tornado core. A combination of

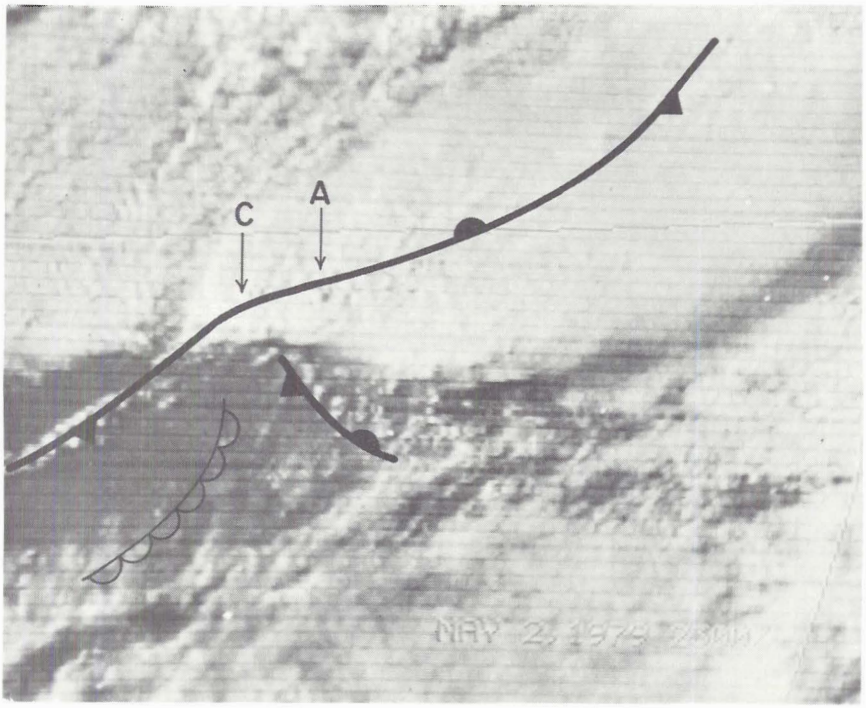

Figure 4.4-18. 2300Z visible satellite image. C denotes tower of third supercell storm which developed on this day.

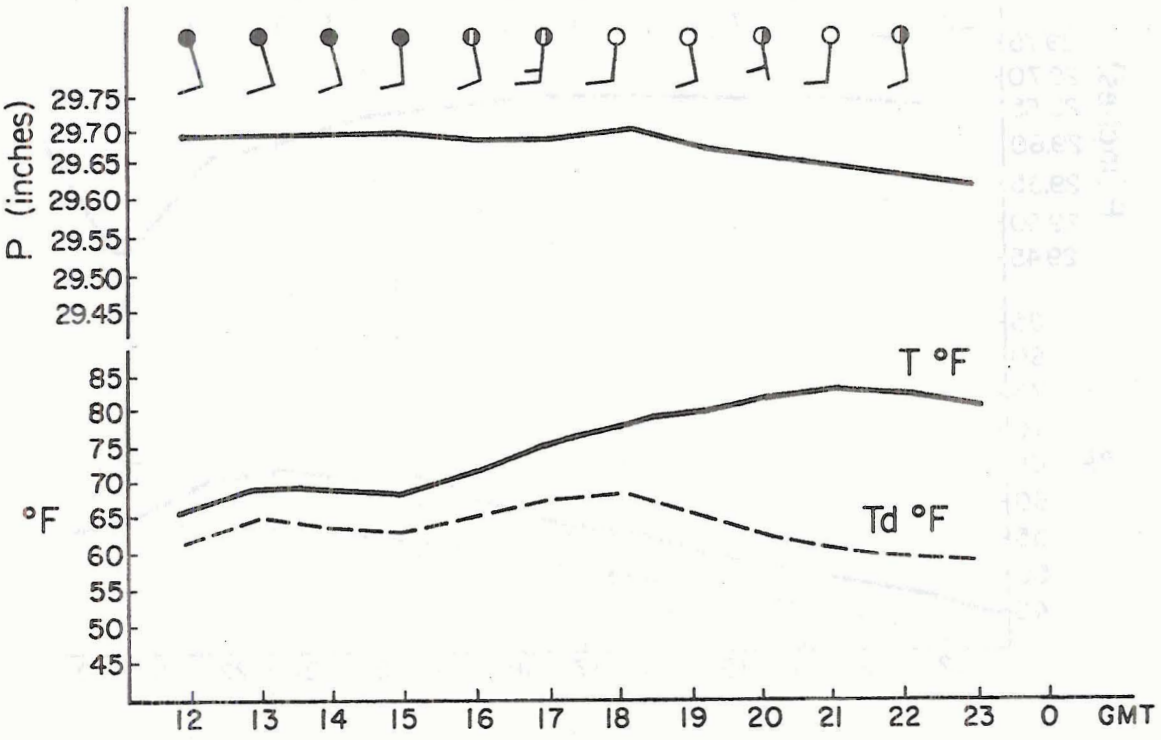

Figure 4.4-19. Time series for Lawton, Oklahoma (LTS).

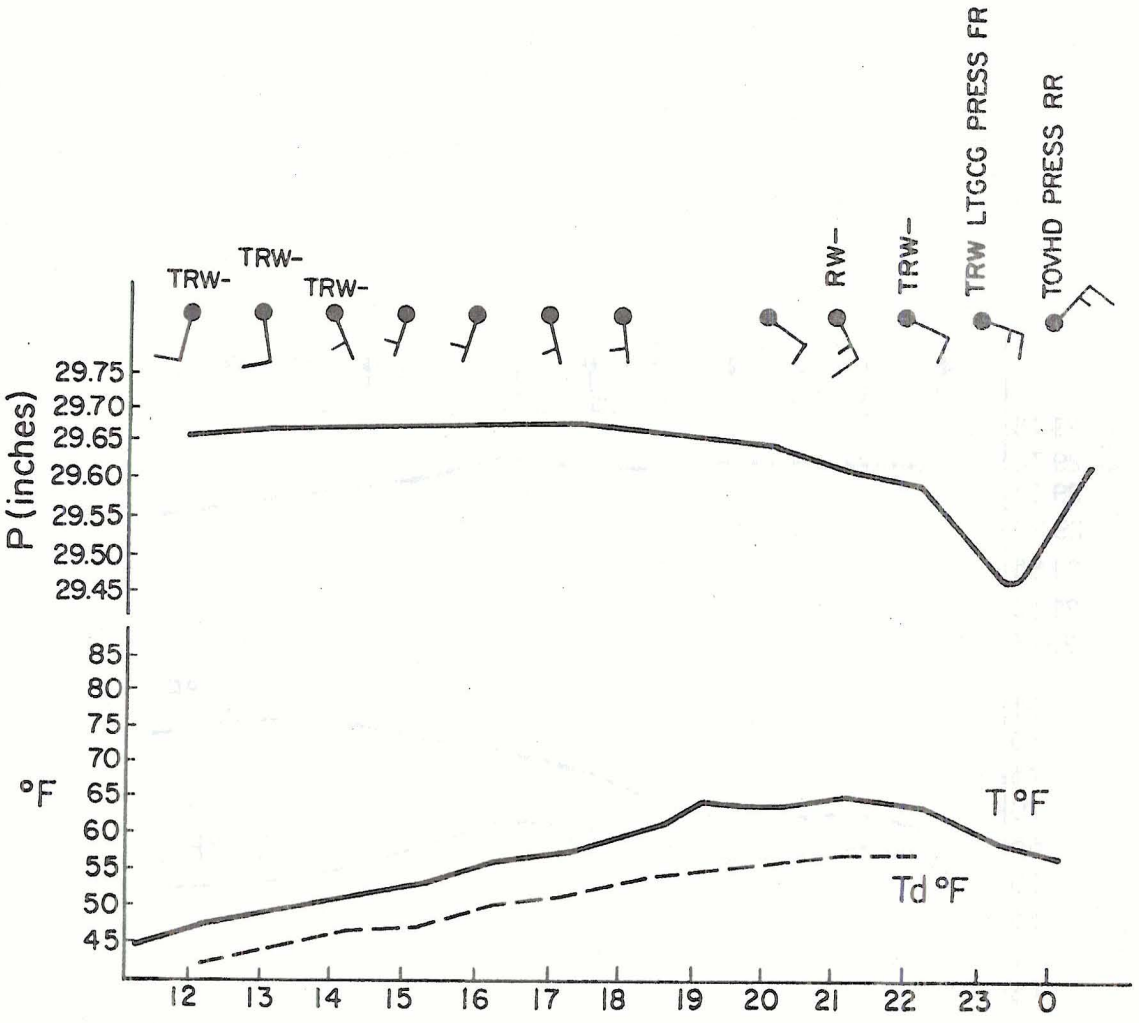

Figure 4.4-20. Time series for Enid, Oklahoma (END).

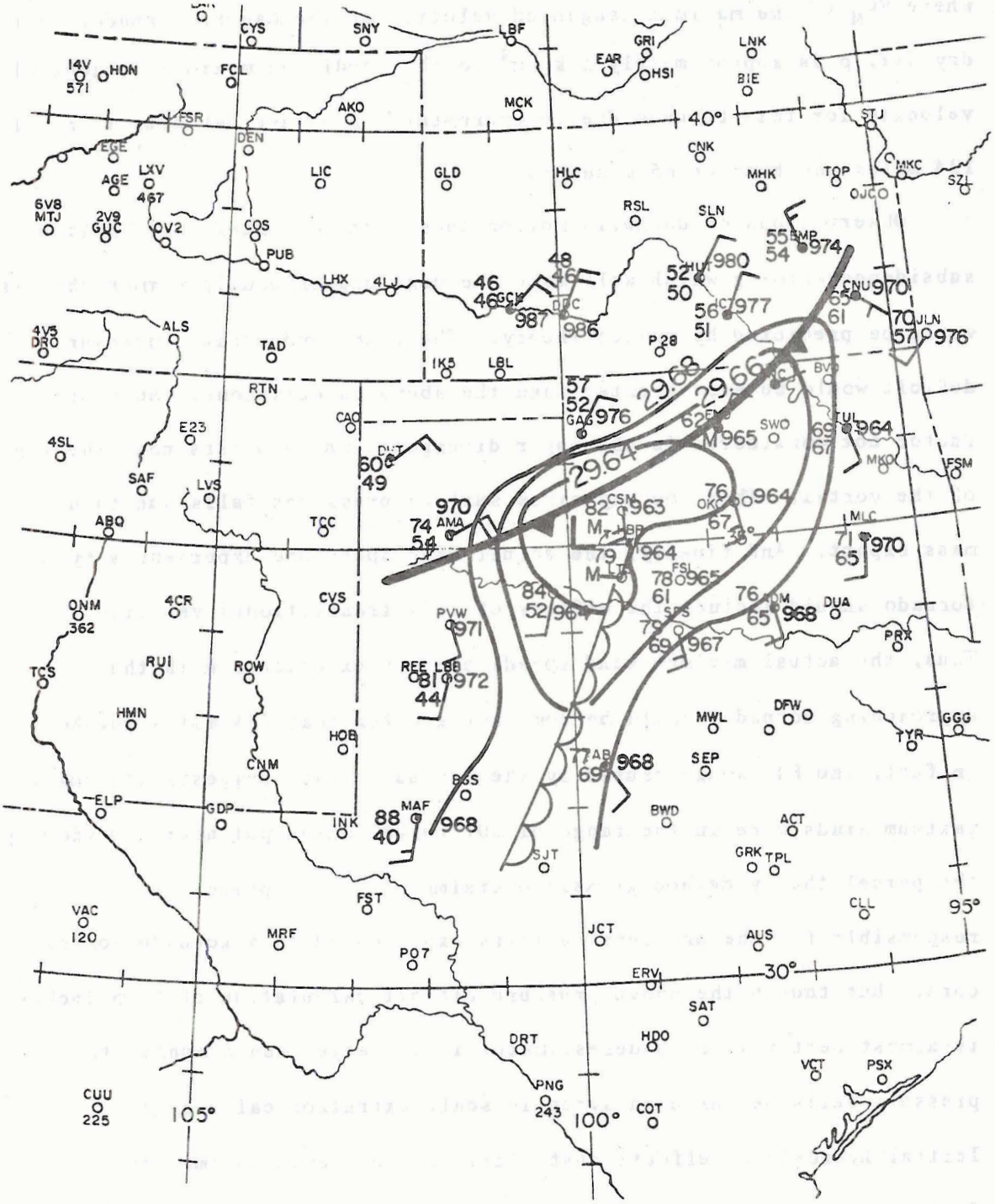

Figure 4.4-21. May 3, 0000Z surface analysis.

Equations 2.4.1, 2.4.2, and 2.4.3 produces the relationship $-\Delta p = \rho V\theta^2_M$ where $V\theta_M$ is the maximum tangented velocity of the Lahoma tornado. For dry air, ρ is approximately 1 kg/m^3 so the predicted maximum tangential velocity for this tornado due to hydrostatic pressure deficits is about 134 miles per hour or 65 m sec^{-1}.

Observations of downward motion in a tornado vortex core implies subsidence warming which will make the core significantly warmer than as would be predicted by parcel theory. Thus, the hydrostatic pressure deficit would be even greater than the above calculations. Another factor not considered is the upper divergence which exists near the top of the vortex. This too may cause surface pressures falls due to net mass export. And finally, the actual wind speed one experiences by a tornado should include the effects of it's translational velocity. Thus, the actual maximum wind speeds one may experience with the approaching tornado should be somewhat greater than 134 miles per hour. In fact, the F4 damage caused by the Lahoma tornado suggests its total maximum winds were in the range of 207 to 260 miles per hour. Obviously the parcel theory method grossly oversimplifies the processes responsible for the pressure deficits experienced in a tornado vortex core. But though the above pressure dificit calculation of 1.05 inches is almost certainly an underestimate, it is large when compared to pressure falls measured in synoptic scale extratropical cyclones. Initial hydrostatic effects must still be considered as important factors contributing to a tornado's low pressure.

Vertical velocity fields are not available for the Onienta storm while it possessed a tornado but motion pictures taken of it were viewed by the author and provide qualitative and quantitative information.

Figure 4.5-1 shows the earliest stages of tornadogenesis. By observing the motions within the condensation funnel on the movie films one can see rising motion in the feeder band under the wall cloud (Forbes, 1978) toward the forward side of the funnel. To the western or rear portion of the tornadocyclone, evaporation on the edge of the wall cloud demonstrates downward motion here (Golden and Purcell, 1978). This observational evidence supports the view that tornadoes form within the updraft core near the updraft-downdraft interface.

In Figure 4.5-2 two suction vortices are seen. The films show these vortices to be orbiting a common center. They subsequently decay while new vortices form ahead of them in the region where air is spiralling upward and inward toward the parent circulation center.

Finally, Figure 4.5-3 shows the tornado as a stable single vortex feature. Again, it is apparent that this tornado has formed near the updraft-downdraft transition boundary. The lowered darkened rain-free clouds have long been associated with updraft cores while in the background, the clouds are considerably less dense most likely due to the intrusion of cooler and relatively dryer air associated with flanking downdrafts (Golden and Purcell 1978). For the majority of its lifetime this system did consist of multiple vortices with individual vortices having wind speed estimates of 65 m sec^{-1} and translational speeds as high as 76 m sec^{-1} (Lee, 1981). As a result of this broad disorganized structure, the damage path for the Orienta tornado was up to two miles wide, but contained large areas within the path which were virtually unscathed.

Figure 4.5-1. Photograph of early stages of the Orienta tornado. Tornado's eastern or forward flank is to the left.

Figure 4.5-2. Twin suction vortices during early stages of Orienta tornado.

Figure 4.5-3. Orienta tornado as a well developed single vortex. (Courtesy of Dr. Howard Bluestein.)

CHAPTER V

DISCUSSION AND CONCLUSIONS

Three scales of cyclonic disturbances were involved in a severe weather outbreak in Oklahoma on May 2, 1979. The largest of these, the subsynoptic low experienced pressure falls and an increase in circulation despite morning mid level NVA and afternoon neutral vorticity advection. Surface and satellite image analyses reveals this dynamically weak system maintained its existence and intensified because of localized warm advection and infrared solar heating. Conventional forecasting techniques may not have expected the SSL to persist or deepen due to an absence of mid-level PVA (Petterson, 1956; Miller, 1972; Tegtmeier, 1974). Thus, lower tropospheric heating mechanisms should be given more emphasis (Maddox and Doswell, 1982).

Pressure falls from this differential heating combined with pressure rises to the north and northwest of the SSL increased the pressure gradient within the low center. This resulted in a rise of convergence and vorticity in northwest Oklahoma which triggered convection here by 2100Z. Furthermore certain factors in the warm sector of the SSL favored mesocyclogenesis after convection was initiated. This included convectively unstable air, large ambient vorticity partially due to the circulation around the SSL center and a veering of wind with height partially due to warm advection. Thus, once convection was triggered, the resultant intense updrafts could converge the ambient cyclonic vorticity in the larger scale environment plut tilt

the horizontal vortex tubes due to the ambient wind shear into the vertical. The vorticity produced from both convergence and tilting could spin up the updraft circulation to mesocyclone intensities within a relatively short time.

The mesocyclones evolved into two-celled structures as circulation centers were divided between an updraft and flanking downdraft. It is speculated that this marked the onset of the tornadic phase of the mesoscyclones. Maximum vorticity for the Lahoma tornadocyclone is of the order of 10^{-2} sec^{-1} and its largest values were measured by dual Doppler radar at the updraft-downdraft interface. Motion pictures of the Onienta storm indicate tornadogenesis occurred within the sector of the updraft immediately bordering the cool downdraft. It is inferred that tornadogenesis is favored in such locations because of enhanced convergence and vorticity. Flanking downdrafts may also intensify the tangential wind field around the mesocyclone and produce turbulent vortices from which tornadoes may evolve.

It is hoped that both the methodology and results of this project will be useful for future nowcasting methods. As weather service offices are presently modernizing, new real time computer products will become available. For example the McIdas system (Walsh and Whittaker, 1980) can produce a wind field based on cloud motion vectors derived from satellite image loops. Similarly the Prototype Regional Operational Forecasting System (PROFS) project in Boulder, Colorado has access to real time mesoscale weather station data which can be displayed with such fields as streamlines and vorticity with radar overlays (Reynolds and Smith, 1979). Vertical velocity profiles derived from rawinsonde data play an integral part of the nowcasting procedures

used in the PROFS project in Boulder, Colorado. As these products proliferate throughout the United States, many of the procedures used in this post-storm analyses could be used for short range severe weather prediction.

REFERENCES

Alberty, R. L., D. W. Burgess, C. E. Hare, and J. F. Weaver, 1979: Project Severe Environmental Storms and Mesoscale Experiment, U. S. Dept. of Commerce, NOAA, Environmental Research Laboratories, Boulder, Colorado, 253 pp.

Alberty, R. L., 1969: A proposed mechanism for cumulonimbus persistance in the presence of strong vertical shear. Mon. Wea. Rev., 27 33-57.

Anderson, R. K., J. P. Ashman, F. Bittnes, G. R. Farr, E. W. Ferguson, V. J. Oliver, and A. H. Smith, 1969: Application of Meteorological Satellite Data in Analyses and Forecasting. ESSA Tech. Rep. NESC 51, 226 pp.

Austin, J. M., 1951; Mechanism of pressure change. Compendium of Meteorology, Amer. Meteor. Soc., Boston, Mass, pp. 630-638.

Barnes, S. L., 1970: Some aspects of a severe, right-moving thunderstorm deduced from mesonetwork rawinsonde observations. J. Atmos. Sci., 27, 634-648.

Barnes, S. L., 1973: Mesoscale objective map analyses using weighted time series observations. NOAA tech. Memo. ERL NSSL-62, Norman, Okls., 60 pp.

Barnes, S. L., 1978a: Oklahoma thunderstorms on 29-30 April 1970. Part I: Morphology of a tornado storm. Mon. Wea. Rev., 106, 673-683.

Barnes, S. L., 1978b: Oklahoma thunderstorms on 29-30 April 1970. Part II: Radar-observed merger of twin hook echoes. Mon. Wea. Rev., 106, 685-696.

Baxter, T. L., 1971: A thunderstorm forecast technique derived from modeling considerations. Preprints, Seventh Conference on Severe Local Storms, Kansas City, Missouri, AMS., Boston, Mass., 13-16.

Beibe, R. G. and F. C. Bates, 1955: A mechanism for assisting in the release of convective instability. Mon. Wea. Rev., 83, 1-10.

Bluestein, H. B., E. K. Berry, J. F. Weaver, and D. W. Burgess, 1980: The formation of tornadic storms in northwestern Oklahoma on 2 May 1979. Preprints Eigth Conference of Analysis and Forecasting, Denver, Colo., Amer. Meteor. Soc., Boston, Mass., pp 63-69.

Bonner, W., 1966: Case study of thunderstorm activity in relation to the low level jet. Mon. Wea. Rev., 94, 167-178.

Brandes, E. A., 1977: Flow in severe thunderstorms observed by dual Doppler radar. Mon. Wea. Rev., 105, 113-120.

Brandes, E. A., 1978: Mesocyclone evolution and tornadogenesis: Some observatins. Mon. Wea. Rev., 106, 995-1011.

Brandes, E. A., 1981: Finestructure of the Del City - Edmund tornadic mesocirculation. Mon. Wea. Rev., 109, 635-647.

Brooks, E. M., 1949: The tornado cyclone. Weatherwise, 2, 32-33.

Brown, R. A., C. R. Safford, S. P. Nelson, D. W. Burgess, W. C. Bumgarnes, M. L. Weible, and L. C. Fortner, 1981: Multiple Doppler Radar analyses of severe thunderstorms: Designing a general analyses system. NOAA Tech. Memo. ERL NSSL-92, Norman, Okla. 21 pp.

Brown, R. A., L. R. Lemon, and D. W. Burgess, 1978: Tornado detection by pulsed Doppler radar. Mon. Wea. Rev., 106, 29-38.

Burgess, D. W. 1976: Single Dopple radar vortex recognition: Part I--mesocyclone signatures. Proceedings, 17th Conerence on Radar Meteorology, Seattle, Wash., Amer. Meteor. Soc., Boston, Mass, pp. 97-103.

Davies-Jones, R. P., 1973: The dependence of core radius on swirl ratio in a tornadic simulator. J. Atmos. Sci., 30, 1427-1430.

Davies-Jones, R. P., and E. Kessler, 1974: Tornadoes. Weather and Climate Modification, W. N. Hess, Ed.New York, John Wiley and Sons, pp. 552-559.

Davies-Jones, R. P., 1981: A new look at the vorticity equation with application to tornadogenesis. Preprints Twelfth Conference on Severe Local Storms, San Antonio, Tex., Amer. Meteor. Soc., Boston, Mass.

Forbes, G. S., 1978: Three scales of motion associated with tornadoes. Ph.D. Dissertation, Univ. of Chicago, Chicago, Ill., 359 pp.

Fujita, T. T., 1963: Analytical mesometeorology: A review. Meteorological Monographs, No. 27. Amer. Meteor. Soc., Boston, Mass., pp. 77-122.

Fujita, T. T., 1965: Formation and steering mechanisms of tornadocyclones and associated hook echoes. Mon. Wea. Rev., 93, 67-78.

Fujita, T. T., 1973: Tornadoes around the world. Weatherwise, 26, 56-83.

Fujita, T. T., G. S. Forbes, and T. A. Unenhofer, 1976: Close up of 20 March 1976 tornadoes: Sinking cloud tops to suction vortices. Weatherwise, 29, 117-131.

Golden, J. H. and D. Purcell, 1978: Airflow characteristics around the Union City tornado. Mon. Wea. Rev., 106, 22-27.

Haglund, G. T., 1969: A study of a severe storm of 16 April 1967. ESSA Tech. Memo. ERLTM NSSL 44, Norman, Olka., 54 pp.

Hasler, A. F., 1981: Stereograhic observations from geosynchronous satellites: An important new tool for the atmospheric sciences. Bull. Am. Meteor. Soc., 63, 194-212.

Heymsfield, G. H., 1978: Kinematic and dynamical aspects of the Harrah tornadic storm analyzed from dual Doppler radar data. Mon. Wea. Rev., 106, 233-250.

Holton, J. R., 1979: An Introduction to Dynamic Meteorology, Academic Press, New York, San Francisco, London, 319 pp.

Hoxit, L. R., C. F. Chappel and J. M. Fritsch, 1976: Formation of mesolows and pressure troughs in advance of cumulonimbus clouds. Mon. Wea. Rev., 104, 1419-1428.

Koch, S. and J. McCarthy, 1977: On the formation of tornadic storm systems in a dryline environment, Preprints, Tenth Conference on Severe Local Storms, Omaha, Neb., Amer. Meteor. Soc., Boston, Mass, pp. 479-486.

Lee, J. T., 1981: Summary of AEC-ERDA-NRC supported research at NSSL 1973-1979. NOAA Tech. Memo. ERL NSSL National Severe Storms Laboratory, Norman, Okla., 93 pp.

Lemon, L. R., D. W. Burgess, and R. A. Borwn, 1978: Tornadic storm airflow and morphology derived from single Doppler radar measurements. Mon. Wea. Rev., 107, 48-61.

Lemon, L. R. and C. A. Doswell III, 1979: Severe thunderstorm evolution and mesocyclone structure as related to tornadogenesis. Mon. Wea. Rev., 107, 1184-1197.

Maddox, R. A., D. W. Reynolds, T. H. Vonder Haar, 1979: Colorado State University Satellite Support to Sesame. Special Report, NSF Grant ATM-78-00530, Colorado State University, Fort Collins, Colo., 36 pp.

Maddox, R. A., L. R. Hoxit, and C. F. Chappel, 1979: Interaction between convective storms and their environment. Final report, NASA Contract S-40336B, Goddard Space Flight Center, Greenbelt, Md., 96 pp.

Maddox, R. A., and C. A. Doswell III, 1982: An examination of jet stream configurations, 500 mb vorticity advection, and low level

thermal advection patterns during extended periods of intense convection. Mon. Wea. Rev., 110, 184-197.

Magor, B. W., 1959: Mesoanalyses: Some operational analyses techniques utilized in tornado forecasting. Bull. Amer. Meterorol. Soc., 40, 499-511.

Marwitz, J. D., 1974: The structure and motion of severe hailstorms. Part I: Supercell storms. J. Applied Met., 11, 166-179.

McGinley, J. A. and Y. Sasaki, 1975: The role of symetric instabilities in thunderstorm development on dry lines. Preprints of the Ninth Conference on Severe Local Storms, Norman Okla., Amer. Meteor. Soc., 172-180.

McNultz, R. P., 1978: On upper tropospheric kinematics and severe weather occurrence. Mon. Wea. Rev., 106, 662-672.

Miller. R. C., 1972: Notes on analyses and severe storm forecasting procedures of the Air Force Global Weather Central. Air Weather Service Tech. Rep. 200 (rev.), Scott AFB, I11., 94 pp.

Moller, A. R., 1979: Mesoscale surface analyses of the 10 April 1979 tornadoes in Texas and Oklahoma. Proceedings, Eighth Conference on Analyses and Forecasting. Denver, Colo., Amer. Meteor. Soc., Boston, Mass., 36-42.

Negri, A. J. and T. H. Vonder Haar, 1980: Moisture convergence using satellite derived wind fields: A severe local storm case study. Mon. Wea. Rev., 108, 1170-1182.

Negri, A. J., 1976: Satellite observations of onset and growth of severe local storms. M.S. thesis, Colorado State University, Fort Collins, Colo., 89 pp.

Newton, C. W., 1963: Dynamics of severe convective storms, Meteorological Monographs, No. 27, Amer. Meteor. Soc., Boston, Mass., pp. 33-57.

Orlanski, I., 1975: A rational subdivision of scales for atmospheric processes. Bull. AMS, 56, 527-529.

Palmen, E. and C. W. Newton, 1969: Atmospheric Circulation Systems, Academic Press, New York and London, 603 pp.

Pelsen, C. A., 1977: A satellite interpretation of the dynamics of a severe local storm area using 5 minute interval S.M.S. data. Proceedings, Tenth Conferecence on Severe Local Storms, Omaha Neb., Amer. Meteor. Soc., Boston, Mass., pp. 1-7.

Petterson, S., 1956: Weather Analyses and Forecasting, Vol. I, McGraw Hill, New York, Toronto, London, 428 pp.

Purdom, J. F. W., 1973: Satellite imagery and the mesoscale convective forecast problem, Preprints, Eighth Conference on Severe Local Storms Denver, Colo., Amer. Meteor. Soc., Boston, Mass., pp 244-251.

Purdom, J. F. W., and J. Weaver, 1981: Nowcasting during the 10 April 1979 tornado outbreak: A satellite perspective. Proceedings, Twelfth Conference on Severe Local Storms, San Antonio, Tex., Amer. Meteor. Soc., Boston, Mass.

Ray, P. S., 1976: Vorticity and divergences within tornadic storms from dual Doppler observations. J. Appl. Met., 15, 879-890.

Reynolds, D. W., 1980: Observations of damaging hailstorms by geosynchronous satellite data. Mon. Wea. Rev., 108, 337-348.

Reynolds, D. A. and E. A. Smith, 1979: Detailed analyses of composited digital radar and satellite data. Bulletin, A.M.S., 60, 1024-1037.

Rhea, J. O., 1965: A study of thunderstorm formation along dry lines. J. Appl. Met., 5, 58-63.

Rotunno, R., 1981: On the evolution of thunderstorm rotation. Mon. Wea. Rev., 109, 577-586.

Rotunno, R., and J. B. Klemp, 1982: The influence of the shear induced pressure gradient on thunderstorm motion. Mon. Wea. Rev., 110, 152-158.

Scoggins, J. R. and J. E. Wood, 1971: Factors in the formation of convective clouds and thunderstorms. Proceedings, Seventh Conference on Severe Local Storms, AMS, Boston, Mass, 110-117.

Tegtmeier, S. A., 1974: The role of the surface subsynoptic low pressure system in severe weather forecasting, M.S. Thesis, University of Oklahoma, Norman, Okla., 66 pp.

Tidwell, S. G., 1981: A local simulation of the observed airflow with the 8 June 1974 Harrah Oklahoma tornadic thunderstorm. Preprints, Twelfth Conerence of Severe Local Storms, AMS, Boston, Mass.

Treqartha, G. T., and L. H. Horn, 1980: An Introduction to Climate, McGraw-Hill, New York, Toronto, London, 415 pp.

U. S. Dept. of the Air Force, 1969: Use of the Skew T_1 log P diagram in analyses and forecasting. Air Weather Service Manual 105-124, Scott A.F.B., Ill., 125 pp.

U. S. Dept. of Commerce, 1979: Storm Data, 21, No. 5

Ward, N. B., 1972: The exploration of certain features of tornado dynamics using a laboratory model. J. Atmos. Sci., 29, 1194-1204.

Weaver, J. F., 1979: Storm motion as related to boundary-layer convergence, Mon. Wea. Rev., 107, 612-619.

Weaver, J. F., and C. R. Safford, 1977: A case study of mesocyclone formation. Preprints, Tenth Conference on Severe Local Storms, Omaha, Nebr., AMS, Boston, Mas., 505-510.

Weaver, J. F. and S. P. Nelson, 1982: Multiscale aspects of thunderstorm gust fronts and subsequent storm development. Accepted for publication by Mon. Wea. Rev., 110, 707-718.

Wexler, R., 1977: Analyses of satellite imagery of clouds near mesocyclones. Preprints, Tenth Conference on Severe Local Storms, Omaha, Nebr., AMS. Boston, Mass., 177-180.

Wilhelmson, R. B., and J. B. Klemp, 1978: A numerical study of storm splitting that leads to long lived storms. J. Atmos. Sci., 35, 1974-1981.

APPENDIX A

LIST OF SYMBOLS

C_p Specific heat of dry air at constant pressure (1004 J deg^{-1} kg^{-1}).

f Coriolis parameter.

F_5 Wind speed at 500 mb.

F_8 Wind speed at 850 mb.

Γ_a Dry adiatic lapse rate with respect to pressure.

Γ Environmental lapse rate with respect to pressure.

g Accelleration due to gravity.

h Diabatic heating.

K_H Horizontal eddy exchange coefficient.

K_z Vertical eddy exchange coefficient.

p Atmospheric pressure.

q Liquid mixing ratio.

R Gas constant (287 J deg^{-1} kg^{-1}).

S Swirl ratio.

T Atmospheric temperature.

T_d Dewpoint depression.

T_v Atmospheric virtual temperature.

u Cartesian velocity component in the x direction.

$\underset{\sim}{V}$ Wind velocity.

$\underset{\sim}{V}_{LND}$ Wind velocity at level of nondivergence.

$\underset{\sim}{V}_o$ Lower tropospheric wind velocity.

$\underset{\sim}{V}_T$ Thermal wind velocity.

$\underset{\sim}{V}_s$ Surface wind velocity.

V_θ Tangential wind speed of a tornado vortex

$V\theta''$ Tangential wind speed of tornadocyclone updraft

v Cartesian velocity component in the y direction.

w Cartesian velocity component in the z direction.

ω Vertical speed of an air purcel with respect to an isobaric coordinate system $(\frac{dP}{dt})$

ξ_o Vertical component of earth relative vorticity in the lower troposphere.

ξ_{LND} Vertical component of earth relative vorticity at the level of nondivergence.

ξ_T Vertical component of earth relative vorticity from the thermal wind.

ρ Atmospheric mass density.

APPENDIX B

An estimation of surface heating rate difference between clear and cloudy regions may be obtained by applying the first law of thermodynamics to data obtained from the Nimbus Satellite Earth Radiation Budget Scanner. Consider first a region under a cloud free sky in Oklahoma during the late afternoon of May 2, 1979. Average incident irradiance at the top of atmosphere as measured by satellite was 450 W m^{-2}. Surface albedo for this region, which is composed mainly of grasslands may be taken to be .20. Atmospheric albedo was detected to also be about .20. Nearly 15% of this incoming radiation was absorbed by the mid troposphere and by water vapor. Thus of the 450 W m^{-2} of incoming radiation, approximately (450 W m^{-2}) (1 - .2) (1 - .2) (1 - .15) or 245 W m^{-2} struck the earth's surface. Of this, 30% or 74 W m^{-2} was converted to sensible heat (see Trewartha and Horn, 1980). If we consider the surface sensible heat flux from the ground as being absorbed by the lower 100m of the earth's atmosphere and if we assume a hydrostatic atmosphere with no significant vertical motion occurring then from the first law of thermodynamics we have

$$\frac{dT}{dt} = \frac{1}{\rho C_p \Delta Z} \frac{dh}{dt}$$

$$= \frac{73.5 \mathrm{Wm}^{-2}}{(1.25 \mathrm{kgm}^{-3})(1004 \mathrm{Jkg}^{-1}\mathrm{deg}^{-1})(100\mathrm{m})}$$

$= 3.8^{o}F$ per hour.

For a cloudy sky in this same region, the atmospheric albedo was measured to be .8 while the atmospheric absorbtivity is at least .2. Therefore, the net radiation striking the earth's surface had an irradiance of only 58 W m^{-2} of which 30% or 17 W m^{-2} was available for sensible heating. The resulting heating rate for a surface beneath an overcast sky was only $.9^{o}F$ per hour. Thus, surface heating due to solar radiation in an environment with clear skies was roughly four times greater than that with overcast skies.